Integrated Structural Health Management Of Complex Carbon Fiber Reinforced Composite Structures

by

Yingtao Liu

A Dissertation Presented in Partial Fulfillment
of the Requirements for the Degree
Doctor of Philosophy

Approved March 2012 by the
Graduate Supervisory Committee:

Aditi Chattopadhyay, Chair
Lenore Dai
Hanqing Jiang
John Rajadas
Antonia Papandreou-Suppappola

ARIZONA STATE UNIVERSITY

May 2012

ProQuest LLC.
789 East Eisenhower Parkway
P.O. Box 1346
Ann Arbor, MI 48106 - 1346

ABSTRACT

Structural health management (SHM) is emerging as a vital methodology to help engineers improve the safety and maintainability of critical structures. SHM systems are designed to reliably monitor and test the health and performance of structures in aerospace, civil, and mechanical engineering applications. SHM combines multidisciplinary technologies including sensing, signal processing, pattern recognition, data mining, high fidelity probabilistic progressive damage models, physics based damage models, and regression analysis. Due to the wide application of carbon fiber reinforced composites and their multiscale failure mechanisms, it is necessary to emphasize the research of SHM on composite structures.

This research develops a comprehensive framework for the damage detection, localization, quantification, and prediction of the remaining useful life of complex composite structures. To interrogate a composite structure, guided wave propagation is applied to thin structures such as beams and plates. Piezoelectric transducers are selected because of their versatility, which allows them to be used as sensors and actuators. Feature extraction from guided wave signals is critical to demonstrate the presence of damage and estimate the damage locations. Advanced signal processing techniques are employed to extract robust features and information. To provide a better estimate of the damage for accurate life estimation, probabilistic regression analysis is used to obtain a prediction model for the prognosis of complex structures subject to fatigue loading. Special efforts have been applied to the extension of SHM techniques on aerospace and spacecraft

structures, such as UAV composite wings and deployable composite boom structures. Necessary modifications of the developed SHM techniques were conducted to meet the unique requirements of the aerospace structures. The developed SHM algorithms are able to accurately detect and quantify impact damages as well as matrix cracking introduced.

This dissertation is dedicated to my parents,

Hebin Liu and Gairong Liu,

and my wife, Jingrui Li,

for their unfaltering love and support.

Without you, none of these would be possible.

ACKNOWLEDGMENTS

First and foremost, I would like to express my gratitude and deep appreciation for Prof. Aditi Chattopadhyay who supported me and provided me with her guidance both in my academic endeavors and my personal life. I consider her to be both my academic advisor and a life-long friend that I can trust and count on.

I also would like to express my gratitude to my dissertation committee, Prof. Antonia Papandreou-Suppappola, Prof. Hanqing Jiang, Prof. John Rajadas, and Prof. Lenore Dai who provided me with their guidance throughout my academic life in Arizona State University. I especially appreciate their patience and kindness when providing directions towards the correct path to the solution.

I would like to give a special thank you to Kay Vasley, the executive assistant of AIMS center, for all her help and support. Without you, all of us would be buried by paper work.

I would like to appreciate Dr. Mark Seaver from Naval Research Laboratory for providing UAV composite wings, consulting in impact tests and damage quantification techniques, and priceless suggestions on the future research and proposals.

Last but not least, I also would like to thank Dr. Masoud Yekani Fard, Dr. Kuang C. Liu, Dr. Chuntao Luo, Dr. Clyde Coelho, Dr. Dallas Kingsbury, Dr. Jun Wei, Dr. Seung Bum Kim, Dr. Sunilkumar Soni, Dr. Subhasish Mohanty, Albert Moncada, Anthony Vizzini, Jinjun Zhang, Joel Johnston, Luke Borkowski, Chase

Hrdina, Kevin Hensberry, and Ryan Lawson for their support and friendship that created a pleasant work environment.

I acknowledge the support from the Army Research Laboratory and Air Force Research Laboratory. The contract number is: FA94530910316. The program manager is Derek Doyle.

TABLE OF CONTENTS

LIST OF TABLES

LIST OF FIGURES

Chapter 1

INTRODUCTION

1.1. Motivation for Structural Health Management

Research in structural health management (SHM) has been highly motivated by safety and expense concerns in the last twenty years. SHM systems have found interesting applications in two types of structures: innovative new structures and aging structures. It has been applicable to instrument SHM system in new structures that present novel aspects in terms of design or materials. On the other hand, aging structures with known problems can benefit from SHM systems to extend the useful lifespan. The basic premise of an SHM system is that damages alter stiffness, mass or damping of a structure and in turn cause changes in its dynamic response. The complete health state of a structure can be determined based on presence, location, type and severity of damages and estimation of remaining useful life (RUL). Four key aspects are usually related to SHM: (i) environmental influence and operational load for components or systems; (ii) understanding of damage characterizations; (ii) monitoring and modeling of the growth of damage; and (iv) future performance of components or systems during the accumulation of damage. Development of SHM in these four aspects has impact on the entire product life cycle, from the design criteria to the decision making for maintenance strategy. Most in-service structures require maintenance to optimize their operation conditions and lifespan. These procedures prolong the useful life and prevent catastrophic failure. Recent development in advanced sensing techniques, material characterizations, pattern recognition, and data management allows improvement of SHM at various levels

of structures and systems. Recently, due to the rapid development of computing capabilities, real time damage state monitoring has become available for specific applications. Prognosis and the prediction of RUL also turn out to be a popular research area. However, there is no general SHM methodology that can be widely used in various conditions for different structures. Most developed SHM techniques only focus on special load conditions and pre-designed components. The *in-situ* diagnostic and prognostic technologies are in great demand for the real time detection of damage in both existing and new structures with minimum human involvement.

The performance of complex engineering systems can gradually degrade due to fatigue, high operation temperature, and extreme environments, as shown in Figure 1. Current maintenance methods include schedule based maintenance (SBM) and maintenance triggered after failure. The goal of SBM is to prevent structural failure by following a planned maintenance schedule. If failure occurs prior of the scheduled maintenance, emergency repair is required. These methods have several drawbacks including high cost, unnecessary or unintended maintenance, and labor intensiveness. To address these issues, condition based maintenance (CBM) has been proposed. Instead of scheduling maintenance to a fixed time table, CBM uses SHM technologies to provide service according to the condition of structures. The working conditions of structures will be monitored and reported in real time. A key requirement for CBM is a thorough understanding of the ways in which system condition is degenerated. It is also important for the CBM system to keep abilities to detect, identify, and communicate all conditions that require maintenance immediately. Therefore, the integration of SHM and CBM has

opened a new research area for complex engineering structures and systems.

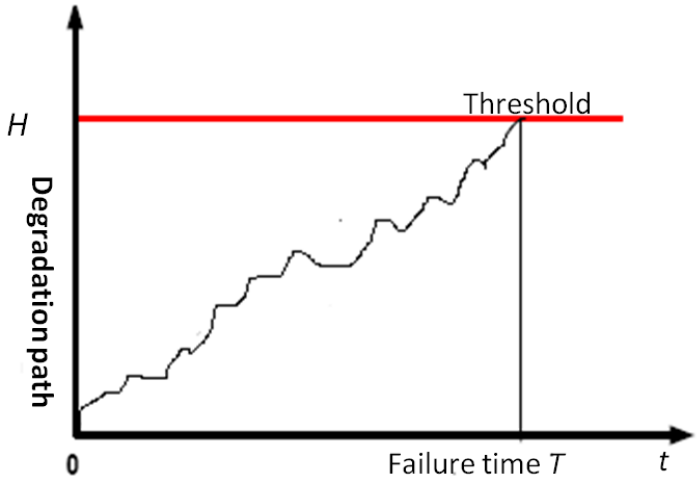

Figure 1. Structural degradation process

1.2. SHM for Composite Structures

Carbon fiber reinforced plastic (CFRP) composite materials are on the cutting edge of engineering, with performance and costs suitable to applications including mechanical, aerospace and civil engineering. Advantages of CFRP materials include light weight, high strength to weight ratio, corrosion resistance, long life expectancy, etc. As shown in Table 1, the strength and stiffness of fibers used in modern CFRP composites are much higher than the traditional bulk materials.

Table 1. Properties of composite reinforcing fibers

Material	E (GPa)	σ_b (GPa)	ϵ_b (%)	ρ (Mg/m^3)	E/ρ (MJ/kg)	σ_b/ρ (MJ/kg)	cost ($/kg)
E-Glass	72.4	2.4	2.6	2.54	28.5	0.95	1.1
S-Glass	85.5	4.5	2.0	2.49	34.4	1.8	22-33
Aramid	124	3.6	2.3	1.45	86	2.5	22-33
Boron	400	3.5	1.0	2.45	163	1.43	330-440
HS Graphite	253	4.5	1.1	1.80	140	2.5	66-110
HM Graphite	520	2.4	0.6	1.85	281	0.951.3	220-660

Compared to traditional metallic material systems, CFRP composites have special requirements for SHM techniques. The technical challenges come from the nature of materials as well as their unique structural degradation mechanisms. Matrix material systems impregnate fibers in CFRP composites. They also transfer load to fibers and protect fibers from abrasion and environmental corrosion. Since fiber orientation can be optimized in order to carry the highest load in the designed directions, this makes composite materials to be heterogeneous due to their different mechanical properties in different directions. Inappropriate manufacturing process, unsatisfactory maintenance, and harsh operational environment can cause invisible damage in composites and may result in catastrophic structural failure. In addition, the failure mechanisms of composite structures are complicated comparing to traditional metallic materials. Multiple types of damage, such as delamination, matrix cracking, and fiber breakage, often occur simultaneously. The structural failures of composites are usually caused by a combination of several damage types. Due to the addressed reasons, researchers are facing significant challenges to integrate novel SHM systems in composite structures and components.

1.3. Key Issues of SHM in Composites

The monitoring of composites can be performed at the material level, component level, and the structural level. At the material level, information related to the material behavior is provided. At the component level, the working conditions among multiple elements are studied. At the structural level, the global structure behavior and performance are investigated. The biomimetic approach can clearly explain the core procedure of SHM. If a human body is hurt, the pain is detected by the nervous system

and communicated to the brain. Once a patient realizes his illness and goes to see a doctor, the doctor will examine the patient and prescribe a cure, as shown in Figure 2. The concept can also be applied to the SHM system for composites. When the malfunction of composites is detected, several key issues need to be addressed to determine the state of damage. These key issues include: (i) whether there is damage (detection), (ii) where is the damage (localization), (iii) how severe is the damage (quantification), (iv) how long can the structure can be safely used (RUL/prognostics). The service and repair will be provided when the RUL reaches a critical level, as shown in Figure 2. These key issues will be further addressed in details.

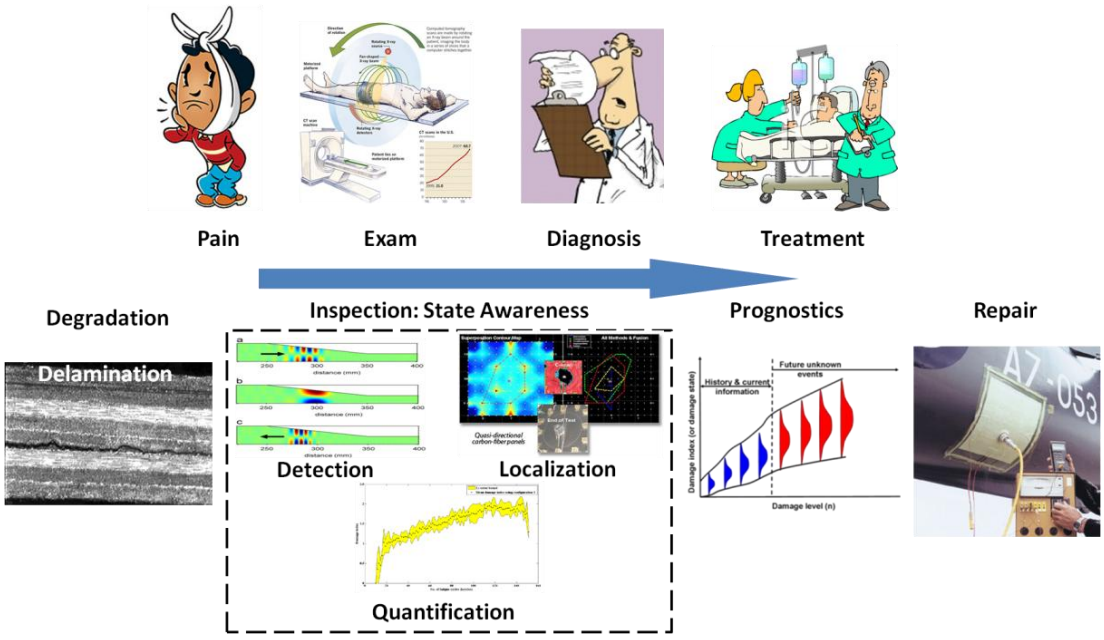

Figure 2. Explanation of SHM using biomimetic approach

1.3.1. Damage Detection

The first key issue of SHM is to identify the existence of damage in composite structures to prevent catastrophic failure. Many NDE methodologies can be extended for the

application of SHM. In fact, they are similar in many aspects. For example, both methods seek to detect the damage state, localize the damage position, and assess the damage severity. A variety of NDE techniques, such as ultrasonic scanning, acoustic emission, X-ray, and infrared thermography, have been used to validate the SHM techniques for damage identification in composites (Amaro et al., 2012, Aymerich et al., 2010, Salamone et al., 2011, Liu et al., 2009, 2011a, 2011b). Typical NDE methodologies rely on off-line implementation for assessing the damage state without accelerating it. This may require the disassembly of components or structures for inspection. However, the goal of SHM is to complete the damage identification and state awareness on-line. In addition, SHM systems also investigate the load history and predict the RUL. For composite structures, due to their special assembly requirements, it is impossible to disassemble the components in-service. Therefore, unique SHM techniques are necessary for the *in-situ* application in composites.

To date, the most useful SHM techniques developed for composites include vibration based approaches and guided wave (GW) propagation based approaches (Sohn and Farrar, 2001, Su et al., 2006). Montalvão et al., (2006) reviewed the development of vibration based SHM and damage detection techniques. Raghavan et al. (2007) reviewed the GW approaches on SHM in complex engineering structures. Typical vibration based approaches use modal analysis to estimate the state of structure based on the changes in modal properties, such as natural frequencies and modal shapes. The limiting issue with this approach is that modal properties are not sensitive to damage precursor and even small scale damage, such as matrix cracks and small delaminations. Other influences,

such as temperature, can also change the modal properties. For example, Balmes et al. (2008) reported the temperature effects on vibration monitoring and a nonparametric damage detection algorithm was developed. It is difficult to estimate the structural state with high fidelity using the vibration approach for real applications. The GW propagation approach has been a hot research area in the last decade. Both active and passive sensing using the GW propagation has been used to address multiple damage types in composites including impacts and fatigue. Since the sensors are either surface mounted or embedded in composites, this approach can be used for structures with complex geometries. Passive sensing is appropriate for the online monitoring of fatigue and impact damage due to the energy efficiency and integrated sensing system. However, active sensing may result in better detection accuracy and fidelity since the excitation signal and frequencies can be optimized according to the structural geometry, material, and boundary conditions (Giurgiutiu et al., 2005). It is noted that the GW propagation approach requires advanced signal processing techniques to interpret sensing signals and extract appropriate features representing the damage. The signal processing techniques developed for GW include time series analysis, time-frequency analysis, statistical signal processing, etc (Mallet et al., 1993, Sohn, 2001a, Liu et al., 2012).

1.3.2. Damage Localization

Localization is an extension of damage detection in the process of SHM. In a large composite structure, it is necessary to localize the damage position when it is desirable to predict its growth rate and path. The location of existing damage determines how quick the damage will grow under certain internal or external loading conditions.

For example, the growth of delaminations in a composite unmanned aerial vehicle (UAV) wing is completely different when the delamination locates at the end of the wing as opposed to the tip of the wing, even if the applied load is the same (Seaver et al. 2010).

Since the fiber orientation of CFRP composites can be optimized based on design criteria, the heterogeneous material properties make it difficult to localize damage. The methods to estimate the damage positions vary for different damage types, such as impact damage and delaminations. To locate impact damage in real time, acoustic emission and principal strain methods are the two popular approaches reported in literature (Meo et al., 2005, 2010, Hiche et al., 2010, Salamone et al., 2011). The available sensors include fiber Bragg grating (FBG), lead zirconate titanate (PZT) and macro fiber composite (MFC). For existing delaminations, the ultrasonic active sensing approach has been proven useful (Liu et al., 2011c, Vizzini et al. 2011). The vibration approach which studies the curvature of modal vibration deflection shapes has been reported in literature (Staszewski et al., 2009). However, all of these techniques utilize the sensing data recorded from more than one sensor or spatial position to localize the damage. In addition, most developed techniques cannot localize multiple damages in structures.

1.3.3. Damage Quantification

Damage quantification provides an assessment of the severity and operating risks of existing damage. In SHM, the damage can be described as the change of material properties (Young's modulus, shear modulus), geometric parameters (delamination size, shape), mechanical properties (stiffness, damping), and sensing features (damage index). When quantifying the damage, the objective is to use a physically meaningful parameter

to characterize the damage level. Therefore, the first step of damage quantification is to decide a quantification criterion for the composite structures.

Quantification using material properties, geometries and mechanical properties requires the assistance of NDE technologies. For example, to measure the delamination size in composite panels, flash thermography, C-scan, or X-ray is required (Park et al., 2006, Aktas et al., 2009, Soma Sekhar et al., 2006). To quantify the change of material properties such as modulus, strain gages or digital image correlation systems are necessary. The development of advanced sensing and signal processing techniques uses novel damage index/metrics to represent the damage propagation in composites. The counts and energy from acoustic emission systems can be used to represent the growth of delamination in composites under fatigue loading (Liu et al., 2009). The amplitude of ultrasonic waves can be used to quantify the damage in composite UAV wings (Matt et al. 2005). The combination of traditional physical measurement of damage using NDE technologies can validate the quantification results of the advanced sensing approaches, which has been a common approach to validate the novel quantification metrics and methods.

1.3.4. Prognostics

Estimation of RUL and prediction of future states are the next logical step in SHM. Prognostic methodologies are crucial to avoid catastrophic failure, provide issuance of timely service and maintenance, and made decision for the employment of auxiliary systems to extend the structural service life. Prognosis systems attempt to forecast structural performance by assessing the current damage state, estimating the

future loading environments, and predicting the RUL and structural degradation process through simulation and/or prior knowledge. The successful development of a prognosis system will require the integration of many technologies including advanced sensing, signal processing, development of novel damage metrics, physics based modeling, and deterministic and probabilistic predictive modeling (Inman et al., 2005, Farrar et al., 2003, Mohanty et al., 2009a, 2009b, 2010). Farrar and Lieven (2007) reviewed the previous work on prognosis, addressed its unique requirements, and predicted the future research directions in details.

Prognosis algorithms can be classified as physics based and data driven approaches. A combination of these two is also employable. Physics based models are useful for the prediction involving new loading conditions, environments and structural configurations. However, high computational load is always involved in the physics based approach. The data driven approach relies on the previous measurements and sensing features to assess the current damage conditions. Usually pattern recognition methods and system identification techniques are involved with this approach. Once the current damage condition is cleared, the prognosis goal will be specified. The most desirable objective of prognosis is to estimate how much time remains for the structures to be used safely. By training a mathematical predictive model, the future state can be estimated. Since the structural failure is expressed through specific indices as functions of the previous and current states, when any of these indices exceeds a predefined critical value, the structure at that point is considered to be failed.

1.4. Sensors and Sensing Techniques for SHM in Composites

The development of SHM depends on the damage features extracted from sensing signals. Therefore, the capabilities of sensors significantly influence the application of SHM in complex engineering structures. The most popular sensors used in SHM include PZT wafers, MFC, optical FBG sensors, accelerometers, strain gages, acoustic emission sensors, etc. The recent development of smart particles and nano materials also lead to the integrated sensing capabilities in composites, which are also referred to as the self-sensing materials (Liu et al., 2012b).

1.4.1. Ceramic PZT Transducers

Manufactured from piezoceramic elements, ceramic PZT transducers can be customized in a wide range of shapes and sizes. Typical ceramic PZT transducers are shown in Figure 3. They can be used as actuators and sensors. To serve as an actuator, the PZT converts an electrical signal into mechanical motion or force. When serving as a sensor, the PZT converts mechanical motion or force back into an electrical signal. Several approaches including elastic wave propagation, time-frequency analysis, impedance-based sensing method and wave energy analysis method have been developed for active sensing with ceramic PZT transducers. The advantages of ceramic transducers widen their applications. First, optimized excitation signals can be designed based on the geometry, shape, materials and even environmental influences. The designed excitation signals work in the most sensitive frequency range for composite structures which assist in identifying damage. Second, point-to-point measurements between actuators and sensors provide information to locate damage. Third, active sensing can combine several

different sensors into one sensing step. For example, Takeda et al. (2005) have reported the combination of PZT actuators and FBG sensors for active sensing. The main drawback of ceramic PZT is that they are fragile and cannot be applied to flexible structures.

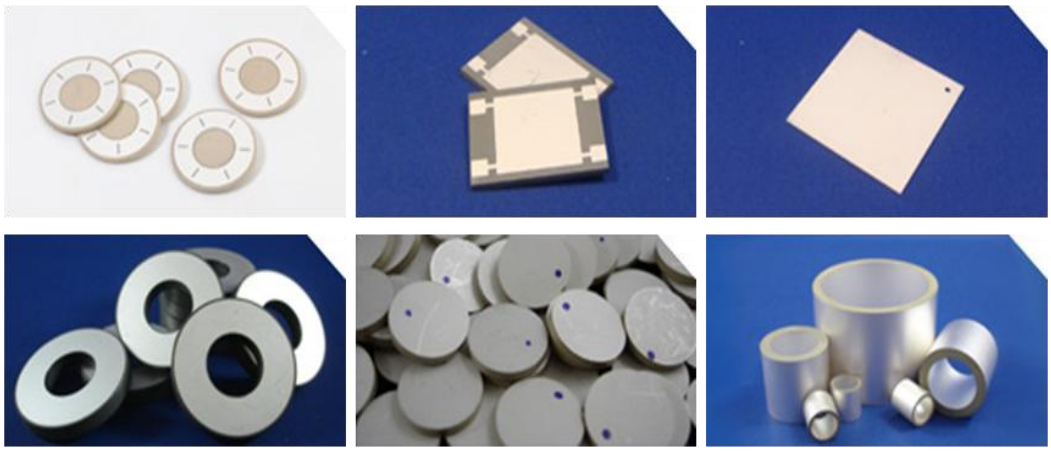

Figure 3. Ceramic PZT transducers (Figures from APC Ltd.)

Windowed cosine waves and chirp waves are two important excitation wave forms for GW based analysis of SHM. The two wave forms are introduced respectively as follows. Figure 4 shows an example of windowed cosine wave, which is also called burst wave. Properly designed windowed cosine wave has several important advantages. First, it has a centered peak in the time domain, as showed in Figure 4. Most energy of windowed cosine wave is concentrated near the peak. The damage features are indicated in this relatively small central region. Second, the symmetric feature of windowed cosine waves helps to minimize the noise in the sensing signals. Errors in data collection can be easily recognized in the time domain. One traditional windowed cosine signal can be written in the form as below:

$$S_T(t) = s_0(t)\cos(2\pi f_c t) \tag{1}$$

where f_c is the center of the carrier frequency, $s_0(t)$ is the short-duration smoothing window and $S_T(t)$is the designed windowed cosine wave form.

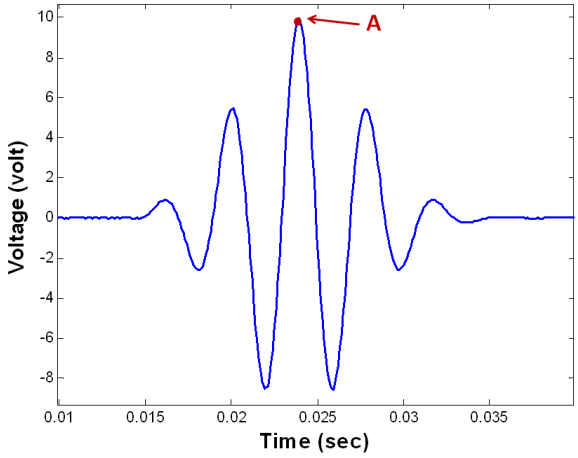

Figure 4. 4.5-cycle windowed cosine signal

One example of the chirp signal is showed in Figure 5. Chirp signal can be generated from a linear swept-frequency cosine signal. Mathematically, a chirp wave signal can be described as follows

$$f_i(t) = f_0 + \beta t \tag{2}$$

$$\beta = \frac{f_1 - f_0}{t} \tag{3}$$

where $f_i(t)$ is the instantaneous frequency, f_0 is the default frequency at the initial time, f_1 is the default frequency at the end time, and t is the swept time. Compared with burst signals, chirp signals cover a wide frequency range. The average signal energy of chirp signal is much higher than that of a burst signal with the same amplitude. The stronger signal energy allows a higher signal to noise ratio. The second advantage of chirp signal is the signal can be designed to cover the exact frequency range needed. When excitation

signals sweep cross the damage area, the sensing signal will cover all sensitive frequencies. The damage features extracted from different frequency ranges can be fused into a critical index to clearly represent the degradation process.

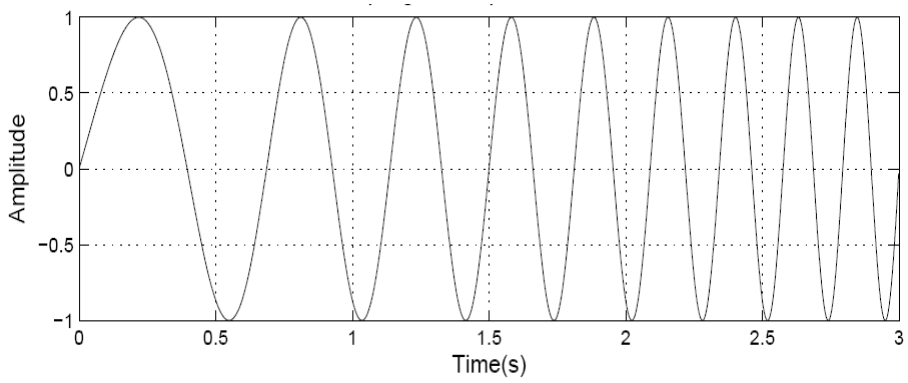

Figure 5. A chirp signal from 1 to 3 Hz

1.4.2. Flexible MFC Transducers

Flexible MFC transducers were first developed at NASA Langley Research Center. Active piezoceramic fibers are aligned in a unidirectional manner with interdigitated electrode patterns on polyimide film. Structural epoxy is used to host the MFC layers, as shown in Figure 6a). It is noted that the cross section of macro fibers is in the rectangular shape due to the method used to form the fibers, as shown in Figure 6b). The fibers are cut from piezoceramic wafers using a CNC controlled dicing saw. The interdigitated electrode patterns are made from copper-clad polyimide film using a photo resist and etch process. The macro piezoceramic fibers are mounted on the bottom electrode film using structural epoxy. The fibers are properly fixed and aligned when the epoxy is slightly heated. Then the top electrode film is applied. Finally all the MFC layers are placed in a vacuum hot press to prevent the voids in the epoxy matrix. The advantages of MFCs include extreme flexibility, durability and high electromechanical

coupling coefficients.

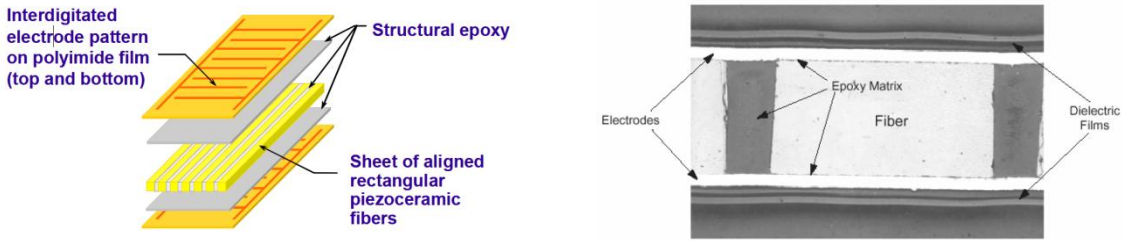

(a) MFC structure (b) Cross section of macro fiber

Figure 6. The structures of MFC actuator (Wilkie, 2000)

MFCs have been used for dynamic testing and control, vibration sensing and actuation, and energy harvesting. For example, Ruggieroa et al. (2004) presented an experimental investigation of the vibration testing of an inflated, thin-film torus using MFCs as both actuators and sensors. Multiple actuators were used to properly excite the global modes of the structure and distinguish between pairs of modes at nearly identical resonant frequencies. In addition, MFCs can be applied to replace ceramic PZT transducers on flexible structures. Sodano et al. (2005) compared the energy harvesting capabilities of ceramic PZT wafers, MFCs, and bimorph Quick Pack actuators. Batteries are recharged to determine the charge time and maximum chargeable battery capacity. The experiments identified the feasibility of their use in practical applications. In this dissertation, the application of MFCs as both actuators and sensors is introduced in details in Chapters 6 and 7.

1.4.3. Optical FBG Sensors

Optical FBG sensors have made a significant entrance in the sensor panorama in the last ten years. FBG sensors are made from optical fibers which are thin glass fibers that are usually protected by a polymer coating or even a metal coating in extreme

conditions, as shown in Figure 7. Multiple gratings can be etched into a single fiber and multiple FBG optical fibers can be inserted in one cable for targeted application. The grating in FBG typically has a sinusoidal refractive index variation over a defined wavelength. The reflected wavelength is called the Bragg wavelength. When a laser is sent into the optical fiber in FBG sensors, the light at designed wavelength is reflected. When the grating is compressed or stretched under mechanical or thermal load, the wavelength of reflected laser light changes slightly. By measuring the shift in laser wavelength, the mechanical or thermal load can be identified.

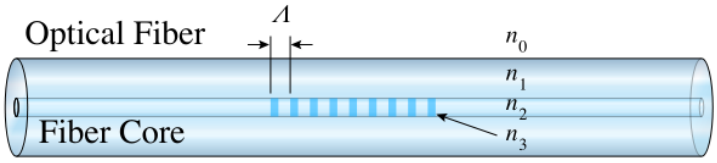

Figure 7. FBG structure

The application of FBG in CFRP composites can be classified into two categories: the surface mounted approach and the embedded approach. The surface mounted approach has been applied to detect and localize impact damages in composites. For example, Frieden et al. (2012) reported a damage localization method to predict the impact position based on interpolation of a reference data set. A high rate interrogation method based on intensity modulation of the Bragg wavelength shift was used to acquire the FBG signals. The localization method was found to have good prediction accuracy. The embedded approach is harder to achieve than the surface mounted approach due to the fabrication difficulties. Yashiro et al. (2005) developed an approach to predict multiple damage states in composite laminates using embedded FBG sensors. The

proposed approach is useful to explain the results of a quasi-static tensile test for a notched CFRP cross-ply laminate. Takeda et al. (2005) developed a damage detection method by combining PZT actuators with FBG sensors for embedment inside a lamina of composite laminates without strength reduction. PZT actuators generated Lamb waves in a CFRP laminate and the transmitted waves were received by an FBG sensor attached on or embedded in the laminate using a high-speed optical wavelength interrogation system. This system was able to detect interlaminar delamination in CFRP cross-ply laminates.

1.4.4. Acoustic Emission Sensing Techniques

Acoustic emission is well known in both the SHM and NDE communities. In ASTM standard acoustic emission is defined as "the class of phenomena whereby transient elastic waves are generated by the rapid release of energy from localized sources within a material, or the transient waves so generated" (ASTM E1316). In composite materials, acoustic emission sources can be from matrix cracking, fiber breakage, debonding and movement between fiber and matrix, delamination and fiber pullout. External noises can interfere with the acoustic emission signal and introduce background noise to sensing data. Background noise is commonly minimized with the establishment of appropriate test and evaluation thresholds. Remaining background noise can be filtered prior to analysis of the AE data.

There are two types of acoustic emission signals, continuous and burst types. The waveform of continuous acoustic emission signals is similar to Gaussian random noise. However, the amplitude keeps changing with the released energy. Burst type acoustic emission signals are short duration pulses that are caused by the release of high amplitude

strain energy. They are used to indicate fast and large damage growth in structures. The monitoring of continuous acoustic emission signals relate to the continuous degradation process in structures. The combination of these two types of acoustic emission signals can be used to monitor the damage degradation process in composite structures. As shown in Figure 8, the commonly extracted acoustic emission parameters include peak amplitude, duration, rise time and counts. It has been found that using a fixed threshold just above the background noise level allows monitoring of the damage processes efficiently.

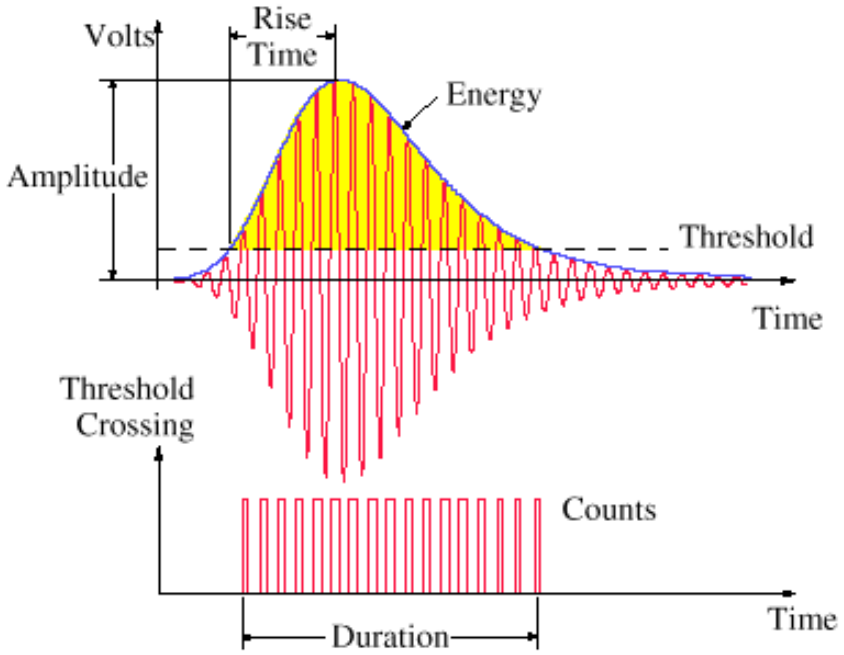

Figure 8. Typical acoustic emission signal and available features (Huang, 1998)

There are several advantages of the acoustic emission sensing technique. It can be used to detect and localize damage in structures in real-time. It is also sensitive to damage compared to other passive sensing techniques. Acoustic emission can be used to monitor both large structures and small structures. When used on small structures, acoustic

emission sensors can be concentrated around the critical components and areas. Acoustic emission sensing techniques require very little operator involvement once the experiment has been set up. The disadvantage is that acoustic emission sensing can be severely influenced by loading conditions. In addition, if the load or damage does not create a sufficient amount of energy, the specimen cannot generate detectable acoustic emission signals.

1.5. Objectives

The objectives of this dissertation are as follows:

- Develop a general SHM frame work to detect, localize, quantify and estimate the RUL of CFRP composites. The developed methodologies are able to identify multiple damage types including matrix cracking, fiber breakage, and delaminations caused by fatigue and impact.
- Develop robust damage detection methodology that integrates GW approach and time-frequency analysis algorithms. Define novel damage index/metrics to represent the severity of damage for quantification.
- Expand damage detection method for localization in CFRP composites. The developed localization algorithm is able to estimate the confidence range of the damage position.
- Develop a prognosis and RUL estimation algorithm to predict the future states of composites structures under fatigue loading. The developed prognosis RUL should be robust on different composite structures and loading conditions.
- Validate the developed methodologies using complex composite structures,

such as flat and stiffened composite panels, UAV wings and deployable satellite booms. Provide necessary modification of the developed SHM algorithm for aerospace requirements. The SHM algorithms should be robust to fiber orientation, lay-up sequences, and environmental noise.

1.6. The Outline of Dissertation

This dissertation contains seven chapters and is organized as follows:

Chapter 2 presents damage assessment methodology using GW approach and a time-frequency signal processing technique. Matching pursuit decomposition (MPD) algorithm is used for extracting wavelets from the Lamb wave signals in the time-frequency domain. A small time-frequency atom dictionary is defined to avoid the exhaustive search over the time-frequency domain and to reduce the computation costs. A two-step damage detection approach, which uses both pulse-echo and pitch-catch active sensing schemes, is developed for the identification of delaminations. The delamination is quantified using a signal energy based damage index. The results show that the MPD algorithm can be used to identify the seeded delaminations in composite structures with complex geometries and material properties. The results of this chapter have been published in Journal of Intelligent Materials and Structures (Liu et al. 2012).

Chapter 3 investigates the development of a new approach for SHM and damage localization using a guided wave based active sensing system. This approach uses time-frequency analysis to calculate the difference between the time-of-flights (ToFs) of the converted modes for each sensor signal. The damage location and the group velocity are obtained by solving a set of nonlinear equations. The proposed method can be used for

composite structures with unknown lay-up and thickness. To validate the proposed method, experiments were conducted on both composite plates and stiffened composite panels. The locations of the delaminations in the composite specimens were validated using a flash thermography system. The accuracy of the developed localization method was experimentally examined.

Chapter 4 presents a condition based prognosis approach to estimate the RUL of composite specimens in real time. On-line damage states are estimated with real time sensing information and are fed to an off-line predictive model to update future damage states and RUL. The on-line damage index or damage state at any given fatigue cycle is estimated using correlation analysis. The condition based prognosis model is used to estimate the cumulative fatigue damage in composite test structures under constant amplitude fatigue loading. Based on the on-line and past history state information, an off-line model is developed to predict the future state and the RUL. The off-line model is a stochastic model which is developed based on a Gaussian process approach. The procedure is validated against uniaxial fatigue loading as well as biaxial fatigue loading. Experimental validations demonstrate that the prediction capability of the prognosis algorithm is effective in predicting the RUL even under complex stress states. The results of this chapter have been published in Journal of Nondestructive Evaluation (Liu et al. 2010).

Chapter 5 extends the developed SHM algorithm before to a composite UAV wing. A novel damage detection methodology is demonstrated for monitoring and quantifying the impact damage propagation. Statistical feature matrices, composed of

features extracted from the time and frequency domains, are developed. Kernel Principal Component Analysis (KPCA) is used to compress and classify the statistical feature matrices. Compared with traditional principal component analysis (PCA) algorithms, the KPCA method demonstrates better feature clustering and damage quantification capabilities. A new damage index, formulated using Mahalanobis distance, is defined to quantify impact damage. The developed methodology has been validated using low velocity impact experiments with a sandwich composite UAV wing.

A novel SHM methodology based on system identification techniques is presented to identify the damage in laminated composite booms in Chapter 6. NDE techniques, frequency response analysis and Auto-Regressive with eXogenous (ARX) input models are used to approximate the transfer functions between input and output sensing signals. Structural degradation is identified by examining the change of transfer functions at different damage states. A single-input-single-output (SISO) approach is adopted in this chapter. System identification techniques allow characterizing of structural degradation without the need for acquiring excessive training data. The proposed methodology is verified through experimentation where damage is gradually induced by flattening and wrapping the deployable boom samples around a circular hub. The results of this chapter have been published in Journal of Spacecrafts and Rockets (Liu et al. 2011d).

Chapter 7 summarizes the research work of this dissertation, emphasizes the important original contributions and findings of this dissertation. The future research directions and recommendations are also discussed.

Chapter 2

GUIDED WAVE BASED DAMAGE DETECTION IN COMPOSITES

2.1. Introduction

In composites, imperfections such as delaminations, fiber breakage, and matrix cracks can significantly alter the mechanical characteristics and eventually affect the life of the structure. The first objective of SHM is to detect the presence of defects and imperfections close to the nucleation stage so that proper steps can be taken to avoid system or sub-system level failure. The general purpose of damage detection using active sensing in SHM is to find the change of sensing features before and after structural degradation. Robust damage features can represent the damage initiation and monitor the damage propagation. Different techniques have been investigated in literature, such as vibration-based approach and piezoelectric impedance analysis (Doebling, et al., 1998; Park, et al., 2003). Multiple types of sensors including strain gages and FBG sensors have been used. However, due to the material complexity and structural requirement, most of these techniques are not sensitive enough to detect damage initiation in composites structures.

Among various damage detection technologies under investigation, one of the most popular approaches for composite structures is the GW based techniques. These techniques involve exciting the structures with high frequency stress waves and processing the different structural response to detect and characterize *in-situ* damage within structures. Since mechanical, aerospace, and civil structures are composed of typical beam, plate, and shell structures, GW based techniques are applicable in

developing damage detection framework for such systems. Compared with traditional detection approaches, the advantage of GW is that an actuator-sensor pair has a high sensitivity to damages and a large coverage area. This allows the GW based techniques to be used for monitoring damage initiation in large scale structures. When stress waves are forced to follow a path by the two traction free surface boundaries, such as for thin plates and beams, GW is usually specified as Lamb wave. Surface-bonded/embedded piezoelectric wafer transducers are typically used as sensors and actuators for Lamb wave approach (Raghavan and Cesnik, 2007; Zhao, 2007). More details into the propagation of the Lamb waves can be found in (Kessler et al., 2002; Kim and Sohn, 2007; Giurgiutiu, 2005; Su et al., 2006; Liu et al., 2012). Due to the superposition of shear wave and longitudinal wave, Lamb wave signals are also complex in nature. More than one Lamb wave mode can be generated simultaneously at any excitation frequency and each mode has a unique dispersion curve. Therefore, it is important to develop efficient analysis techniques to study the Lamb wave signals and isolate different Lamb wave modes. The motivation of this chapter is to investigate the GW based damage detection and related feature extraction techniques.

2.2. Lamb Wave Based Damage Detection

Due to the dispersive and multimode characteristics, Lamb wave is complicated in nature. The dispersion and multimode of Lamb wave can be theoretically analyzed by solving Rayleigh-Lamb equations defined for the symmetric and anti-symmetric modes on an infinite plate with a thickness of 2h

$$(k^2 + s^2)^2 \cosh(qh) \sinh(qh) - 4k^2 qs \sinh(qh) \cosh(qh) = 0 \quad (4)$$

$$(k^2 + s^2)^2 \sinh(qh)\cosh(qh) - 4k^2 qs\cosh(qh)\sinh(qh) = 0$$

where $q^2 = k^2 - k_l^2$, $s^2 = k^2 - k_s^2$, k is a wave mode, and k_l is the wave number for longitudinal wave and k_s is the wave number for shear wave. The dispersion curve can be expressed by the excitation frequency and plate thickness. The group velocity C_g can be defined as

$$C_g = \frac{d\omega}{dk} \tag{5}$$

where ω denotes an angular velocity.

Typically, two types of Lamb wave modes, the symmetric (S mode) and the anti-symmetric (A mode), are generated during wave propagation in thin plates. The Lamb wave modes with the lowest order are called S_0 and A_0 modes. The S and A modes convert into new modes when discontinuity such as thickness change is present in the plates. As shown in Figure 9, the S_0 mode is first generated by the actuator. When the S_0 mode reaches the delamination, the wave mode converts into S_0/S_0 and A_0/S_0 modes above and below the delamination. The notation S_0/S_0 implies S_0 mode converted from the S_0 mode and A_0/S_0 denotes A_0 mode converted from the S_0 mode. When the S_0/S_0 and A_0/S_0 modes travel through the delamination zone, these two modes convert again into $S_0/S_0/S_0$, $A_0/S_0/S_0$, $S_0/A_0/S_0$, and $A_0/A_0/S_0$ modes. For small delamination size, the $S_0/S_0/S_0$ and $S_0/A_0/S_0$ modes combine together in the time domain, and are displayed as the S_0 mode recorded by the sensor. The $A_0/S_0/S_0$ and $A_0/A_0/S_0$ modes combine together, and manifest as the converted mode recorded by the sensor. This phenomenon, indicating the generation of an additional Lamb wave, is called mode conversion (MC), and the associated mode is referred to as the MC mode. When a delamination exists in a thin

composite plate, there is a jump discontinuity in thickness at the delamination zone; as a result, the Lamb wave converts into the MC mode. The mode conversion of Lamb waves propagating in a composite plate with a single delamination is shown in Figure 9. The delamination can be detected by identifying the MC mode in a Lamb wave propagation signal.

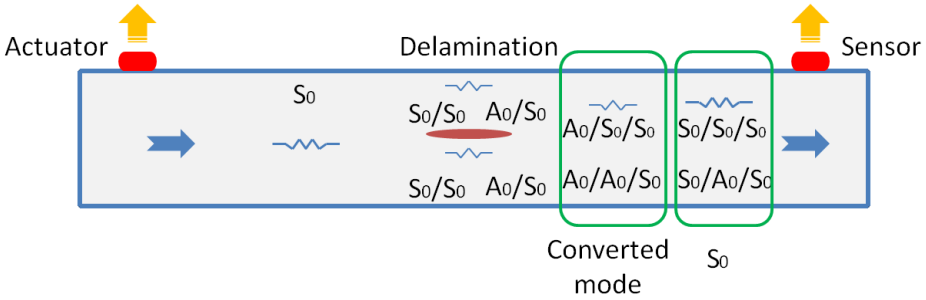

Figure 9. Schematic of Lamb wave propagation with an embedded delamination

2.3. Feature Extraction Using Matching Pursuit Decomposition

Feature extraction plays a significant role in Lamb wave based SHM system. The goal of feature extraction is not only to extract information to detect potential damage, but also to provide information for the characterization, quantification, and localization, which is used for RUL estimation. Traditionally, the well-known Fourier transform provides the 'global' information about the frequency content, and it is suitable for signals with stationary frequency content. However, the frequencies of Lamb wave signals vary in the time domain. This type of signals can be better represented in the time-frequency domain to extract time-varying frequency information. To analyze the time-varying sensor response effectively, the time and frequency domain characteristics must be considered simultaneously. These time-frequency representations (TFRs) characterize a given signal over the time-frequency plane by combining the time and

frequency domain information to yield more revealing information about the temporal localization of a signal's spectral components. The MPD is a time-frequency based technique that decomposes a signal into highly localized time-frequency atoms and can provide a highly concentrated TFR (Mallat and Zhang, 1993; Qian and Chen, 1994; Das et al., 2009). It is an iterative algorithm that decomposes any signal into a linear expansion of waveforms that belong to a redundant dictionary. The dictionary of the MPD consists of a collection of time-frequency atoms which are the dilated (time-scaled), translated (time-shifted) and modulated (frequency-shifted) versions of a single basic atom. The basic atom is often chosen to be a Gaussian signal as Gaussian signals are the most concentrated signals in both time and frequency.

For Lamb wave signals, the signal with finite energy $x(t)$ can be decomposed into a linear combination of time-frequency atoms. This type of infinite approximations can be written as

$$x(t) = \sum_{i=0}^{\infty} \propto_i g_i(t) \tag{6}$$

where $g_i(t)$ is the time-frequency atom (sub-waveform) selected from the MPD dictionary D and $\propto_i$ is the corresponding expansion coefficient. The finite linear combination of these time-frequency atoms can be used to provide an approximation of the signal with arbitrary accuracy. After N iterations, the resulting expansion can be expressed as

$$x_N(t) = \sum_{i=0}^{N} \propto_i g_i(t) \tag{7}$$

The residual signal $Rx_N(t)$ with N iteration is

$$Rx_N(t) = x(t) - x_N(t) = x(t) - \sum_{i=1}^{N} \propto_i g_i(t) \tag{8}$$

Because the signal has finite energy, the energy of the approximated signal is also preserved. The energy conservation can be expressed as

$$\|x(t)\|^2 = \sum_{i=0}^{N} \|x_N(t)\|^2 + \|Rx_N(t)\|^2 \tag{9}$$

In order to find the best match between the signal and time-frequency atoms, the inner product of the signal and each time-frequency atom is calculated. Let $g(t) \in D$, the signal $x(t)$ can be decomposed into

$$x(t) = \langle x(t), g(t) \rangle\, g(t) + Rx \tag{10}$$

where Rx is the residual signal after approximation using the time-frequency atom $g(t)$. To minimize the energy of Rx, the proper $g(t)$ is selected from the dictionary D and $g(t)$ satisfies

$$|\langle x(t), g(t) \rangle| \geq \alpha \sup|\langle x(t), g(t) \rangle| \tag{11}$$

where α is an optimality factor that satisfies $0 < \alpha \leq 1$, $\sup|\langle x(t), g(t) \rangle|$ is the least upper bound of the inner product of $\langle x(t), g(t) \rangle$. The decomposition of signal $x(t)$ is completed by successive calculation with time-frequency atoms from the dictionary. Let $g_i(t)$ be the time-frequency atom of the i_{th} iteration, the approximated signal at this iteration is

$$x_i(t) = \langle Rx_i(t), g_i(t) \rangle \tag{12}$$

when i=0, let $Rx_0 = x(t)$. According to Equations 7, 10 and 12, the approximated signal with a total of N iterations is

$$x_N(t) = \sum_{i=1}^{N} \langle Rx_i(t), g_i(t) \rangle \tag{13}$$

and the original signal can be expressed as

$$x(t) = \sum_{i=1}^{N} \langle Rx_i(t), g_i(t) \rangle + Rx_N \tag{14}$$

where Rx_N is the residual signal at the Nth iteration. Although a redundant dictionary can provide flexible decomposition of the signal, the calculation cost is also high. To reduce the number of unnecessary time-frequency atoms, a modified MPD algorithm is used. The time-frequency dictionary of the MPD algorithm is optimized based on the features of the Lamb wave signals from the structures being interrogated. Limited sub-waveforms which can best represent the original signal are included in the dictionary. By using the optimized atom dictionary, the original signal can still be efficiently decomposed with high local time-frequency resolution.

In this dissertation the actuation signal studied is a cosine windowed tone burst wave. According to the Lamb wave theory, only S_0, A_0 and the related converted modes exit as sub-waveforms. All the S_0, A_0 and the related converted modes can be obtained by the dilation and translation of the basic sub-waveform. This procedure reduces the size of the MPD dictionary significantly. It must be noted that the MPD algorithm efficiently yields a compact representation of the burst wave signals in terms of selected basic atoms in the dictionary. Therefore, it reduces the computational cost significantly. In addition, the unwanted noise is filtered out because the noise waveforms are typically orthogonal to the selected atoms.

2.4. Experimental Setup

Experiments were carried out using both in-house fabricated composite flat plates and stiffened panels. The damage type investigated was embedded delaminations. The composite flat plates were fabricated with the dimensions of 330×330 mm^2 and $(0°/90°)_3$ lay-up. Plain weave carbon fiber fabrics were used as the fiber system. The epoxy FS-A23 (resin) and FS-B412 (hardener) (from Epoxy System Inc.) were used as the matrix system. Nine composite plates were fabricated in-house, one without delamination, and the other plates, each with at least one seeded delamination (5×5 mm^2). Teflon patches were inserted during lay-up to generate the delamination. The dimensions of the plate and the PZTs are shown in Figure 2. The distance between the PZT pair was 127 mm, and the delamination was placed centrally between the two PZTs. The flash thermography was used to visualize the delaminations, and the images are presented in Figure 10.

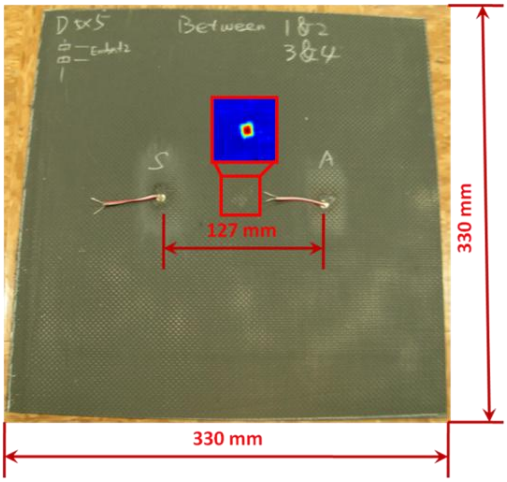

Figure 10. Composite flat plate sample with surface mounted PZTs

Stiffened composite panels with $(0°/90°)_3$ layup were fabricated in-house. Each panel has two co-cured blade stiffeners on its surface, as illustrated in Figure 11. The

same carbon fiber fabrics system and epoxy system were used. A total of nine PZT wafers and one PZT ring were surface bonded on the stiffened side of the panel surface. The dimensions of the structure and the locations of the PZTs are shown in Figure 12. Two composite panels were fabricated with seeded delaminations. Teflon patches were inserted during lay-up to simulate delaminations. The other two composite panels were fabricated without delaminations to study the healthy state of the composite panels.

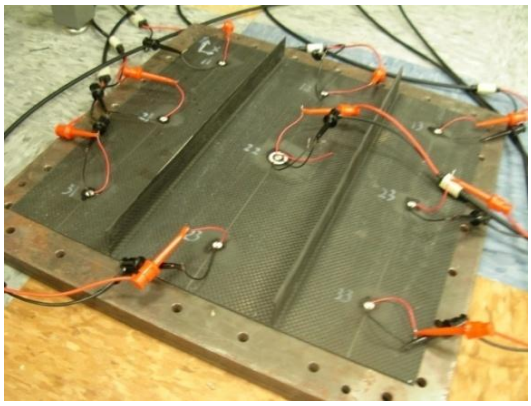

Figure 11. Stiffened composite panel with bonded PZT patches

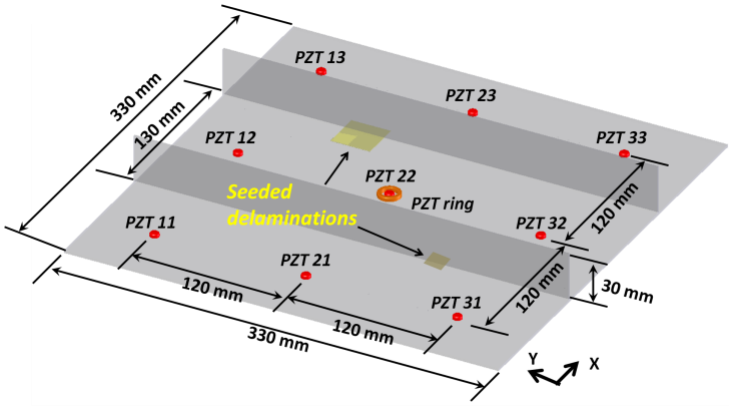

Figure 12. Dimensions of composite panel and PZT patches

A 4.5-cycle windowed cosine burst wave was generated using a NI 5412 waveform generator, and the Lamb wave signals were captured by a NI 5105 digitizer at a sampling frequency of 20 MHz. In order to optimize the central frequency of the

actuation signal, several actuation signals were generated using central frequencies varying from 50 to 300 KHz in 10 KHz increments. Ten observations were recorded at each frequency, and the sensor signal was averaged from the ten observations to reduce the sampling error. By studying the sensor signals as well as the dispersion curves of the S_0 and A_0 modes, it is noted that the Lamb wave signals with the central frequency of 180 kHz is optimal for the present case and is used to excite the actuators.

2.5. Results and Discussion

2.5.1. Detection of Delamination in Composite Flat Plates

The developed delamination detection technique by identifying MC mode in GWs is first studied in flat composite plates. The sensor signal recorded from the healthy plate is used as the baseline data and analyzed using the MPD algorithm. The TFR of the sensor signals collected from various composite samples with seeded delamination can be compared with the baseline TFR features. New Lamb wave modes (MC modes) can be identified to represent the existence of delaminations. The time of flight (ToF) information can also be easily obtained from the TFR and validated by the MPD signal approximation in the time domain. Based on the energy in each time-frequency atom, the signals are decomposed in descending energy order. The signal and the first six atoms associated with the healthy plate, plotted in the time domain, are shown in Figure 13 (a). The first six atoms containing 96.3% of the signal energy were decomposed from the sensor signal and rebuilt as the approximated signal, as shown in Figure 14. The residual signal is considered as the noise. Therefore, the approximated signal rebuilt from the six signal atoms can reasonably represent the sensor signal. The TFR of the signal is shown

in Figure 13 (b). Each Lamb wave mode needs to be identified after the signal decomposition. Based on the Lamb wave theory and the dispersion curves associated with each Lamb wave mode, the S_0 mode has the highest velocity. Since the dimensions of the composite plate and PZT transducers are known, the S_0 reflection mode can be identified. The group velocity of the S_0 mode and the A_0 mode are computed as 5.71 m/ms and 2.03 m/ms, respectively. The S_0, A_0 and reflected S_0 modes are distinctly displayed without any overlap, as shown in Figure 13 (b). In this TFR figure the brighter the time-frequency atom, the higher is signal energy contained in the local MPD atom. Comparing the results shown in Figure 13 (b) and Figure 14, it is noted that the S_0 mode contains 62.8% of the signal energy, the reflected S_0 mode contains 19.3% of the signal energy and the A_0 mode contains 2.9% of the signal energy.

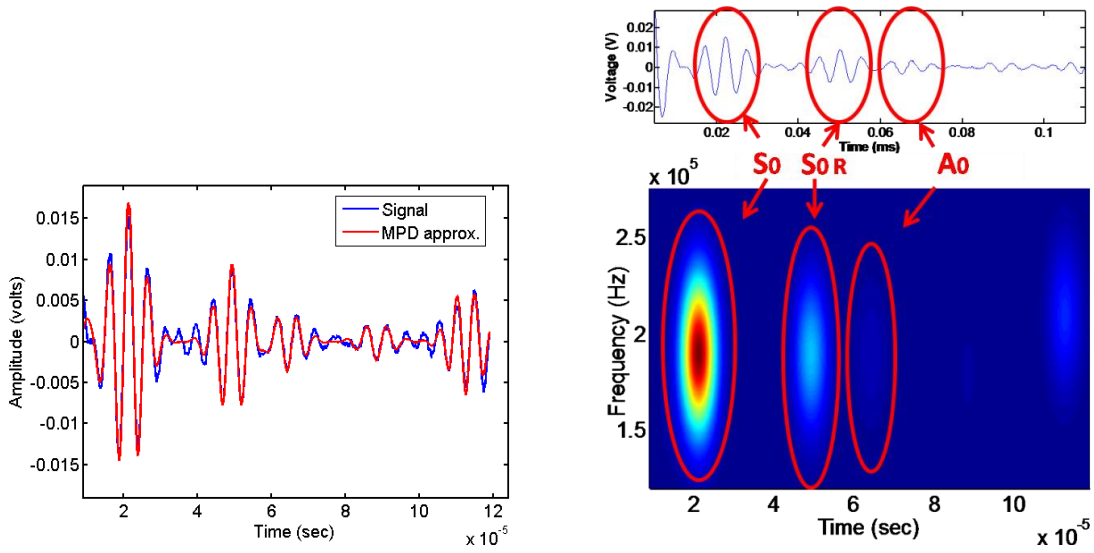

(a) Sensor signal and MPD approximation (b) Time-frequency representation of sensor signal

Figure 13. MPD time-frequency representation of sensor signal

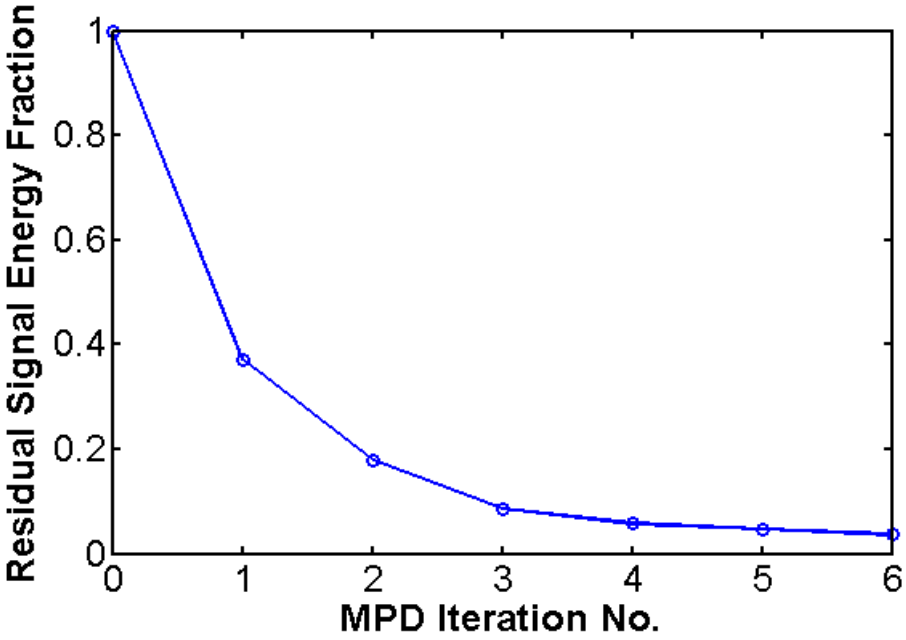

Figure 14. Residual energy of MPD analysis for composite plate without delamination

Eight composite plates with different seeded delamination patterns were tested, as shown in Figure 15. Using the MPD algorithm, the MC mode can be detected and represented in the time-frequency domain. Damage detection is conducted by identifying the MC mode in the sensor signal, which is generated by a stiffness change in the plate. Comparing the TFRs of the sensor signals collected from the healthy plate and from the plate with a 5×5 mm^2 delamination, the MC mode is clearly detected between the S_0 and S_0 reflection mode, as shown in Figure 13. The TFRs for each delamination pattern and time domain signals are shown in Figure 16. For all the damage patterns studied in this section, the delamination can be clearly detected. This shows that the proposed methodology has reasonable reliability for detecting delaminations varying in size, location and number. Because the delamination is embedded during the fabrication, the influence of fabrication variation is insignificant in the detection of delamination. It is

noted that the ToF of the MC mode varies between different composite samples. This is caused by the variation in fabrication, and the different distances between the PZT actuator and the seeded delaminations in each sample. Because the 5×5 mm^2 delamination size is fairly small compared with the distance between PZTs, the energy of the MC mode is relatively low when compared with the energy of S_0 and S_0 reflection mode. After 6×10^{-5} s, there are several noticeable time-frequency atoms. These atoms are the superposition of several reflected and converted modes, but it is hard to identify the mode sources. Therefore, these reflection modes were not studied. The MC mode has clearer TFR with a larger delamination size. The advantages of using the MPD algorithm are clearly depicted in the results presented. The experimental results clearly demonstrate the efficiency of the developed approach to detect seeded delaminations with varying distribution through the composite test specimens. The time-frequency dictionary of the MPD algorithm is optimized based on the features of the Lamb wave signals obtained from the structure being interrogated. Limited sub-waveforms which can best represent the original signal are included in the dictionary.

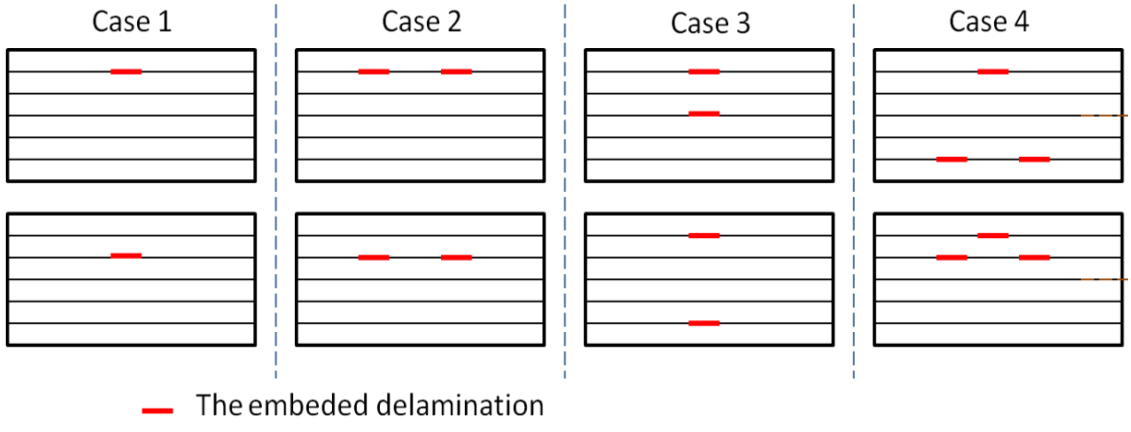

Figure 15. Different embedded delamination patterns

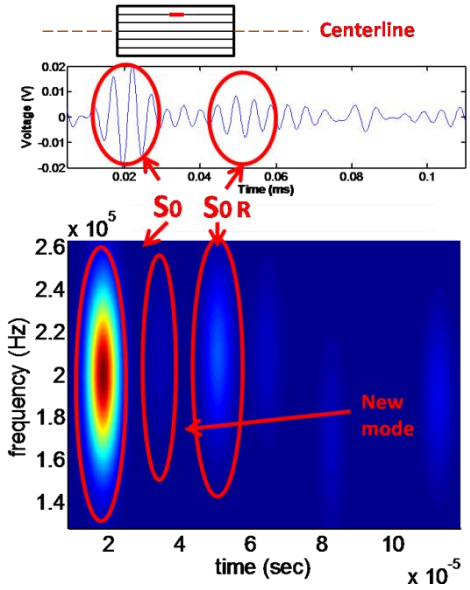

(a) Case 1, in-plane delamination at interface 1

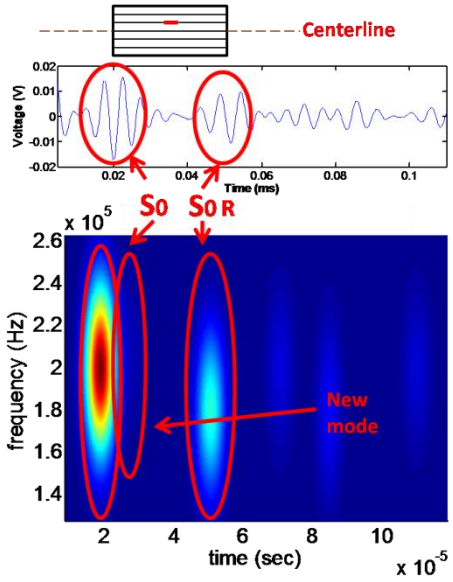

(b) Case 1, in-plane delamination at interface 2

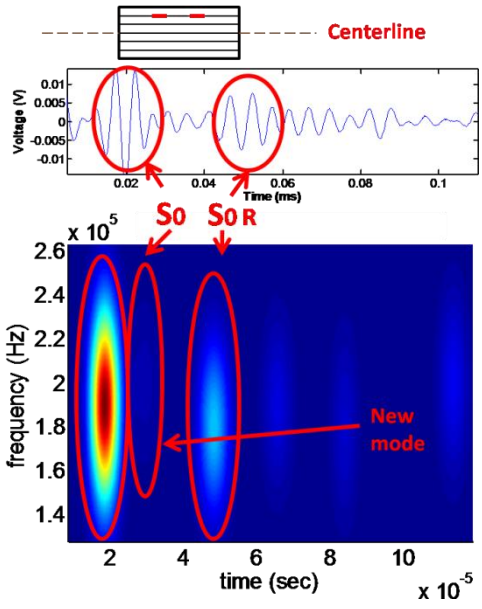

(c) Case 2, in-plane delaminations at interface 1

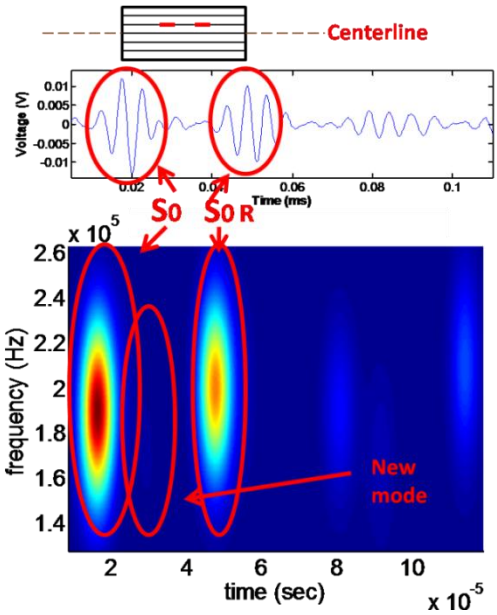

(d) Case 2, in-plane delaminations at interface 2

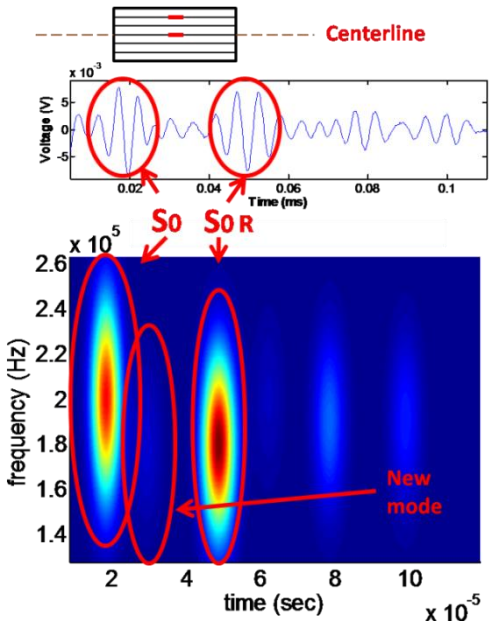

(e) Case 3, through-thickness delaminations at interface 1 & 5

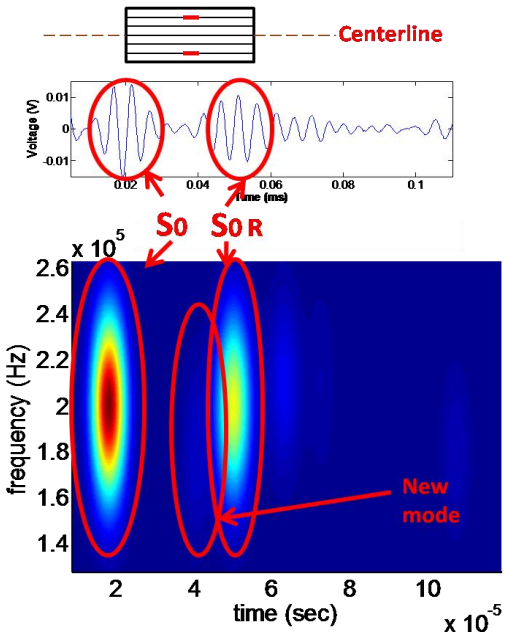

(f) Case 3, through-thickness delaminations at interface 1 & 5

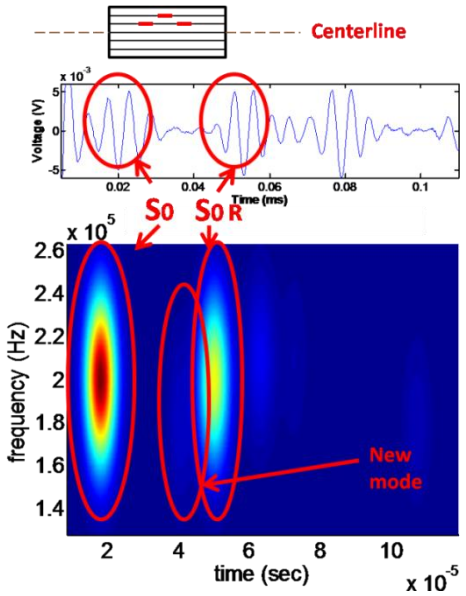

(g) Case 4, through-thickness delaminations at interface 1 & 2

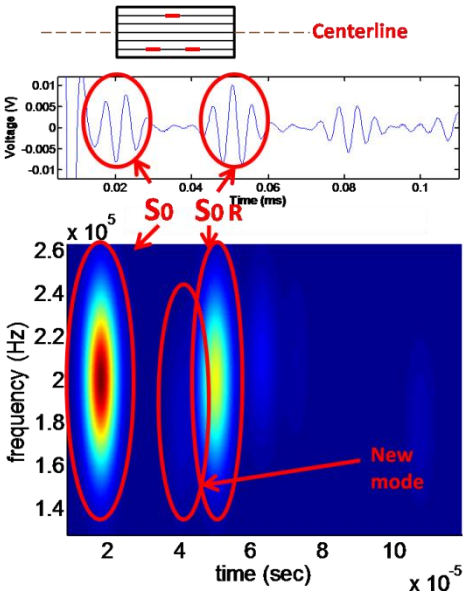

(h) Case 4, through-thickness delaminations at interface 1 & 5

Figure 16. Time-frequency representation of different delamination patterns

2.5.2. Detection of Delamination in Composite Stiffened Panels

For structures with large and/or complex geometries, two-step damage detection methodology using the pulse-echo and pitch-catch schemes can identify the existence of delamination damage. Further damage location information can be estimated following the same strategy. Using only one sensor and one actuator, pulse-echo approach can quickly detect the existence of damage in a large composite structure. A single PZT ring actuator with strong excitation signals is sufficient to interrogate the entire composite panel. The pulse-echo scheme can provide quick damage estimation at the global level. Once the delamination is detected, the pitch-catch approach will provide detailed information of damage location and severity using a PZT array with eight PZT wafer sensors. The detailed local detection information can be used for future prognosis and RUL estimation. The concept of the two-step global and local damage detection strategy can be applied to the SHM of large engineering structures such as aircraft wings and fuselages. Global detection can examine the structural integrity in a short time. Once potential structural damage is detected, local damage detection can identify the detailed location, severity, and damage type for the further maintenance.

Pulse-echo scheme is first used to detect the existence of delamination. The complex geometry of the stiffened panel introduces reflection modes to the sensor signals when the pulse-echo scheme is used for damage detection. To successfully detect delamination, the different reflection modes need to be isolated and identified. When the S_0 mode arrives at the T-section of the blade stiffener, the mode scatters into three components, one propagating in the plate, one propagating in the blade stiffener and a

reflection in the plate, as shown in Figure 17 (a). Similarly, when the component of the S_0 mode that is transferred into the blade stiffener reflects back to the T-section, this mode also scatters into another three components. Two of these propagate along different directions in the plate and the third is reflected back into the stiffener, as shown in Figure 17 (b).

Due to the Lamb wave scattering at the T-section, the S_0 and A_0 modes generated by the actuator propagate along different possible paths and finally are recorded by the PZT ring sensor. The eight shortest possible Lamb wave propagation paths are shown in Figure 17(c). Both the propagation distance and the group velocities of S_0 and A_0 modes are known, therefore the theoretical ToF along each propagation path can be calculated, as shown in Tables 2 and 3. Since PZT 22 is placed in the center of the panel, path 6 is the same in both the X and Y directions. Therefore, path 6 will contain Lambs waves from both the X direction and Y directions, which results in an increase in magnitude.

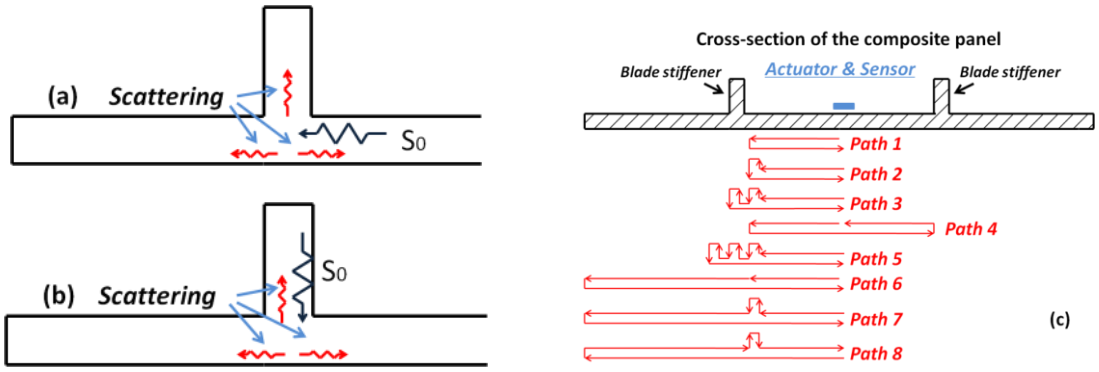

Figure 17. (a) Lamb wave mode scattering into T-section; (b) Lamb wave mode scattering from T section; (c) Different paths of Lamb wave propagation in stiffened composite panel using the pulse-echo approach

Table 2. ToF analysis for S_0 mode

	Path Distance (m)	Group Velocity of S_0 mode (m/ms)	Time of Flight (ms)
Path 1	0.13	5.25	0.0248
Path 2	0.19	5.25	0.0362
Path 3	0.25	5.25	0.0476
Path 4	0.26	5.25	0.0495
Path 5	0.32	5.25	0.0610
Path 6	0.33	5.25	0.0629
Path 7	0.39	5.25	0.0743
Path 8	0.39	5.25	0.0743

Table 3. ToF analysis for A_0 mode

	Path Distance (m)	Group Velocity of A_0 mode (m/ms)	Time of Flight (ms)
Path 1	0.13	1.47	0.0884
Path 2	0.19	1.47	0.1292
Path 3	0.25	1.47	0.1700
Path 4	0.26	1.47	0.1768
Path 5	0.32	1.47	0.2176
Path 6	0.33	1.47	0.2240
Path 7	0.39	1.47	0.2653
Path 8	0.39	1.47	0.2653

In Figure 18, the S_0 mode conversion is considered when an S_0 wave mode arrives at the stiffener. Mode conversion occurs at the T-section because of the thickness change. The original S_0 mode converts into A_0 and S_0 modes and propagate along the 3 possible directions. Due to the low group velocity of the A_0 mode, only the converted A_0 mode reflected back to the PZT ring sensor was recorded in the experiment. However, the

reflected converted A_0 mode cannot be clearly displayed in the TFR because of the low energy caused by wave scattering and attenuation.

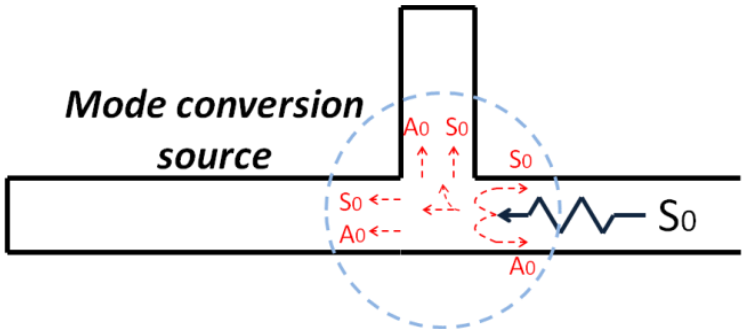

Figure 18. Mode conversion at T section

The healthy composite panel is used to identify each Lamb wave mode for the echo signal. A burst wave with a central frequency of 180 kHz was used to generate the Lamb wave. The Lamb wave echo signal was recorded from the PZT ring sensor. The TFR of the echo signal is shown in Figure 19. The first two atoms can be easily identified as the S_0 mode propagates along paths 1 and 2, respectively. The experimental ToF of the two atoms matches with the theoretical calculation. Since paths 3 and 4 have close path lengths, the S_0 modes propagating along the two paths overlap together in the time-frequency domain and represent as the third atom in Figure 19. Similarly, the S_0 modes propagating along paths 5 and 6 merges and is seen as the forth atom in Figure 19. The fifth atom is identified as the A_0 mode since the experimental ToF of this mode matches with theoretical calculation shown in Table 3. The theoretical and experimental results for ToF are compared in Table 4. Due to the signal attenuation and multiple reflections and scatterings, it is noted that the S_0 mode propagating along paths 7 and 8 lose most of the signal energy. There is no clear TFR for this mode in the time-frequency domain. It

can be reasonably concluded that the S_0 mode, which propagates longer than path 7 and 8, can be ignored.

Table 4. ToF comparison for S_0 modes

	Theoretical Time of Flight (ms)	Measured Time of Flight (ms)
Path 1	0.0248	0.0248
Path 2	0.0362	0.0365
Path 3	0.0476	0.0499
Path 4	0.0495	0.0499
Path 5	0.0610	0.0615
Path 6	0.0629	0.0615

Delamination was detected in the damaged composite stiffened panel. Using the MPD time-frequency analysis algorithm, the TFR of the echo signal can be demonstrated, as shown in Figure 20. Compared to the TFR shown in Figure 19, the S_0 mode propagating along path 1-6 and the A_0 mode can be identified at the same time instance. In addition, one more atom is detected in this TFR. When the S_0 modes propagate through the delamination of the composite panel, the two modes convert into a new mode, which can be named as the MC mode. In fact there are several MC modes due to multiple delaminations. After several reflections of the stiffeners and boundaries, the MC modes overlap and combine with each other. This combined MC mode is recorded by the PZT ring sensor. The new atom correlates with the delaminations in the composite panel. Using the global pulse-echo scheme, the delaminations can be quickly detected by one single PZT ring sensor. However, the pulse-echo approach cannot provide more

information about the location, number of delaminations, etc. A local pitch-catch active sensing scheme is necessary to obtain these details.

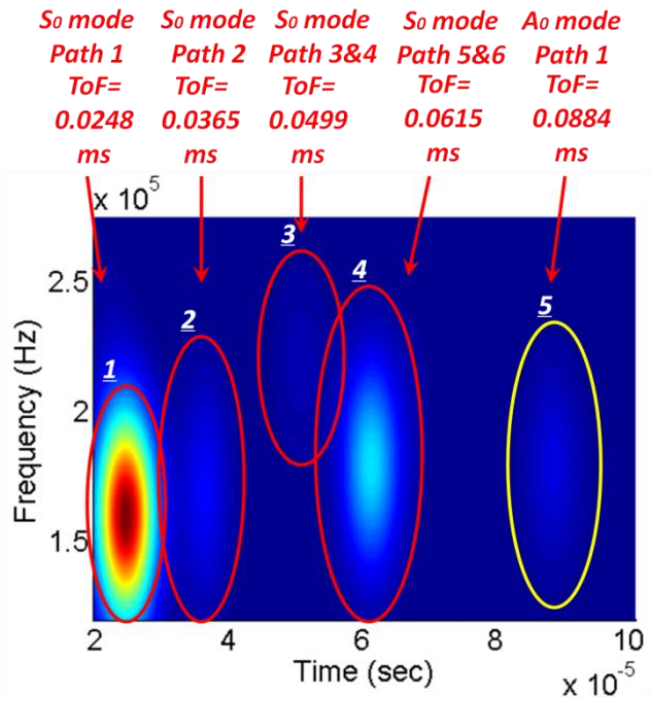

Figure 19. TFR and mode identification of echo Lamb wave using healthy stiffened panel

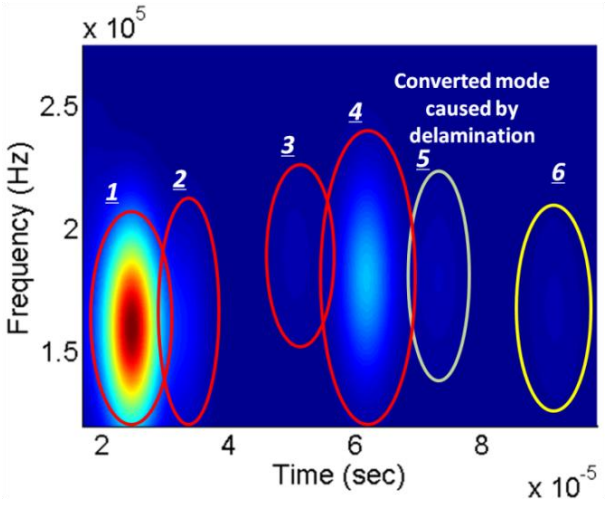

Figure 20. TFR and mode identification of echo Lamb wave using stiffened panel with delamination

Once delamination is detected using the global scheme, local damage detection approach is used to find more detailed damage information. The pitch-catch scheme uses a sensor array with nine PZT wafers to detect the local delamination between the actuator and sensors. PZT 22, which is located at the center of the composite panel, is used as the actuator. A burst signal with a central frequency of 180 kHz is used as the excitation signal. The PZT sensor signal recorded from the healthy panel is used as the baseline data. The first five Lamb wave atoms in the TFR are identified using the baseline data. Delamination is detected by identifying the new MC modes in the signal recorded from the panel with delaminations, which is similar to the pulse-echo approach.

Using the healthy composite panel, the sensor signal collected from PZT 21 is used to study the influence of the stiffened panel on the sensor signal. The first four possible propagation paths for PZT 21 are shown in Figure 21, and the associated TFR is shown in Figure 22. The first S_0 and the following reflection of S_0 modes are illustrated. The arrival of the A_0 mode was recorded at 0.086 ms. The experimental ToF results matches with theoretical analysis. Similar time-frequency atoms with more attenuation and time shift can be identified in the signal collected from the other PZT sensors.

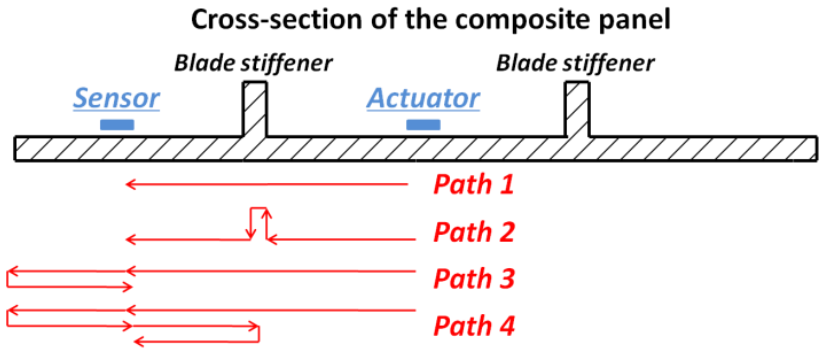

Figure 21. Possible propagation paths for PZT 21

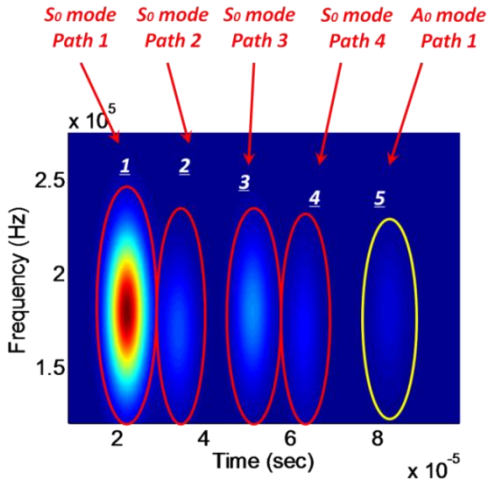

Figure 22. TFR of Lamb wave collected from PZT 21 using healthy panel

Two delaminations were detected between PZTs 22 and 31 and PZTs 22 and 13, respectively. The TFR of the sensor signal recorded from PZT 31 using the healthy panel is shown in Figure 23. Each Lamb wave mode can be represented as a time-frequency atom in the TFRs. The location of each atom in the TFR can be verified by studying the ToF of each Lamb wave mode. As shown in Figure 23, the first time-frequency atom is identified as the first arrived S_0 mode, the second and the third atoms are the S_0 reflection modes due to the boundary and the stiffener. The fourth atom is the A_0 mode. Similar atoms can be identified in the sensor signals recorded using the composite panels with seeded delaminations. However, using the damaged composite panel, the fifth atom in the TFR of the PZT 31 signal is identified as the converted mode caused by the delamination, as shown in Figure 24. Due to the delamination between PZTs 22 and 13, the converted mode is also detected in the signal recorded from PZT 13. However, in the sensor signals of PZTs 11 and 33, there is no such converted mode introduced by delamination. These results demonstrate that the two seeded delaminations are detected by the local PZT

sensor using the pitch-catch active sensing scheme. Using the proposed methodology, multiple delamination damages can be detected.

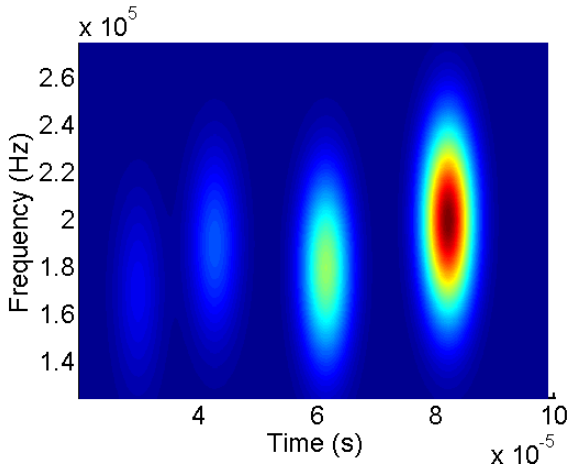

Figure 23. TFR of Lamb wave collected from PZT 31 using healthy composite panel

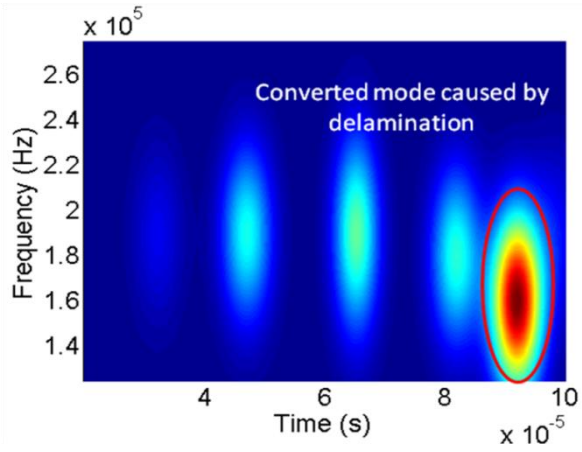

Figure 24. TFR of Lamb wave collected from PZT31 using composite panel with delaminations

Although the developed damage detection schemes are validated using composite structures, the method can be extended to metallic and complex engineering structures. The mode conversions and signal energy reduction of Lamb wave due to damage are also true in metallic materials. The two-step global and local damage detection schemes

provide the quick damage detection option as well as the detailed damage awareness option. This is important especially for the SHM of complex engineering structures and systems. Therefore the developed global and local detection schemes using the MPD algorithm has potential application to detect different damage scenarios.

2.6. Concluding Remarks

In this chapter, damage detection method in carbon fiber reinforced composites using guided wave approach has been investigated. The guided wave propagation theory and MPD algorithm are introduced. Using the MPD algorithm, the Lamb wave signal can be represented in the time-frequency domain for the identification of different Lamb wave modes. Therefore, the sensing features can be extracted to represent the existence of delamination in composites. The developed method is experimentally validated using composite plates with seeded delaminations at difference interfaces. A two step strategy for detection and characterization of delaminations in stiffened composite panels is presented. A pulse-echo scheme rapidly detects the existence of delamination in the composite panels by identifying the converted modes caused by delaminations. Only one PZT ring sensor is required to detect the studied structure with a complex geometry. However, further damage state information, such as the location and number of delaminations, cannot be obtained. A pitch-catch scheme can detect the delamination in the area between PZT actuator and sensors. By studying the signal energy of the converted mode, the severity of the signal can also be estimated. Other useful diagnosis features for damage diagnosis and prognosis can be obtained using proper feature extraction algorithms. The results are significant because they demonstrate effective

damage detection and characterization in a composite structure with both a complex geometry and orthotropic material properties.

Chapter 3

DAMAGE LOCALIZATION IN COMPOSITES

3.1 Introduction

The location of damage is necessary for further quantification and prognosis analysis when the existence of damage is detected. Damage localization techniques can be classified as either an active sensing approach or a passive sensing approach. Active sensing approaches can be used to localize the existing damage in composites. In passive sensing approaches, impact damage or propagating damage caused by fatigue can be monitored and the damage positions identified.

Damage localization in composite structures requires accurate guided wave information and features. Most previous work focused on locating impact damage in composite structures using passive sensing approaches (Meo et al., 2005; Staszewski et al., 2009; Hiche et al., 2010). The traditional damage localization method is to use the triangulation method and the time of flight (ToF) information to obtain three ellipses requiring at least three active sensors. The intersection point of the three ellipses is considered to be the damage spot. Knowledge of group velocities of the guided wave in all directions is required for this approach (Gorman and Ziola, 1991; Coverley and Staszewski, 2003; Reynold et al., 2009). Neural network algorithms have been used to obtain the angle dependent group velocity profile (Moll et al., 2010). Other damage localization approaches include direct wave paths analysis between an actuator and multiple sensors (Sohn et al., 2005), the energy decay model (Wang and Yuan, 2006), principle stress directions for impact locations (Salamone et al., 2011), smart sensors and

sensing techniques, such as Laser Doppler Vibrometer (LDV) (Staszewski et al., 2009) and Fiber Bragg Grating (FBG) sensors (Hiche et al., 2010; Adewuyi and Wu, 2010). These approaches have been validated using isotropic and quasi-isotropic plates with simple geometries. However, limited work has addressed the extension of damage localization to general anisotropic composite structures with complex geometries.

In this chapter, an active sensing based damage localization method is presented. The proposed methodology used a PZT sensor array to detect the delamination location. The MPD algorithm was used to compute the differences of ToF of the converted modes between master and slave sensors. To assess the delamination location in composite structures, the sensor locations and differences of ToF were used to create three nonlinear equations. The nonlinear equations were converted into an unconstrained optimization problem and solved using Newton's method. Due to the redundancy of the PZT sensor array, a probabilistic location estimation algorithm was used to provide the confidence range of the delamination in the composite structures. Experiments were conducted using the composite structures with three types of layups and two types of carbon fiber fabrics. The proposed method does not require any information about the material properties, layup or thickness information. A confidence range for the estimated delamination is provided using the proposed methodology.

3.2 Damage Localization Algorithm

The delamination localization algorithm for composites is based on the difference of ToF of the converted modes caused by delamination. A piezoelectric based active sensing method is used to localize delamination in composites. The actuator and sensor

placement is shown in Figure 25. Providing that the center of the delamination in the composite plate is (x_d, y_d) and the sensor positions are (x_i, y_i) (i=1, 2,…, 6). The distance between the delamination and each PZT sensor is D_i and expressed as

$$D_i^2 = (x_d - x_i)^2 + (y_d - y_i)^2 \tag{15}$$

For this technique, a Lamb wave is first generated by the actuator. When the Lamb wave propagates through the delamination area, mode conversions and reflections can scatter the Lamb wave in all directions in the composite. The ToF, T_i, from the delamination to the sensor, S_i, combines with the group velocity, V_i, to yield a new expression for distance,

$$D_i = T_i V_i \tag{16}$$

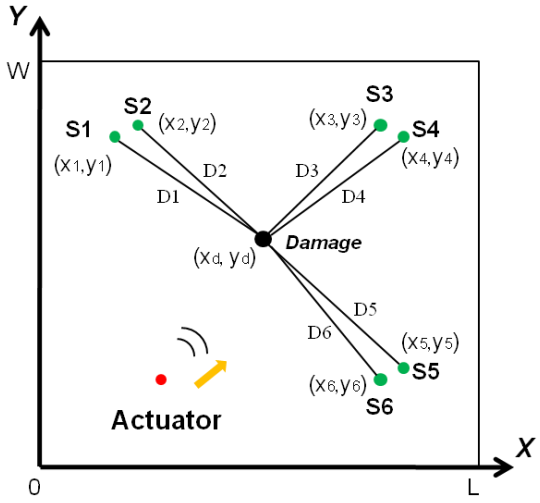

Figure 25. Actuator and sensor placement on composite samples

The group velocity of a Lamb wave is a function of fiber orientation, material properties, thickness, etc. As most composite structures are anisotropic materials which have different material properties in different directions, the group velocity is different for each direction. In short, V_i (i = 1, 2,…, 6) have unique values for various directions.

However, as shown in Figure 26 when two sensors S1 and S2 are placed close to each other but far from the delamination, we have $D_1, D_2 \gg d_{12}$.

$$\frac{d_{12}}{D_1} \approx \frac{d_{12}}{D_2} \approx \sin(\propto) \approx 0 \tag{17}$$

where d_{12} is the distance between sensors S1 and S2. We can assume $\propto \approx 0$. The group velocities from the delamination to the sensors can be assumed to be the same.

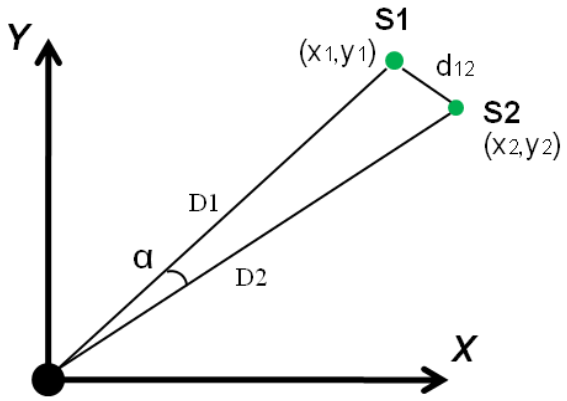

Figure 26. Scheme of optimized sensor arrangement

$$V_i \approx V_{i+1} \quad (i= 1,3,5) \tag{18}$$

Based on Equations 15, 16 and 18, three equations with eight unknowns are present and can be consolidated to yield a generic equation for comparing the two velocities,

$$\frac{\sqrt{(x_d - x_i)^2 + (y_d - y_i)^2}}{T_i} = \frac{\sqrt{(x_d - x_{i+1})^2 + (y_d - y_{i+1})^2}}{T_{i+1}} \tag{19}$$

where i= 1,3,5. The unknown variables are x_d, y_d, and T_i (i=1,2,…,6) associated with delamination location and the ToF of propagated mode conversions resulting from wave interaction with the delamination. The nonlinear equations condensed in Equation 19 cannot be solved because there are more unknown variables than equations. In order to provide additional information, one sensor is picked as the master sensor, and the other

sensors are used as slave sensors. The differences of ToF of the converted modes between the master sensor and each slave sensors can be written as,

$$T_{s,j} = T_m + \Delta T_{j,m} \tag{20}$$

where $T_{s,j}$ is the ToF of the converted mode for the slave sensor j (j=1,…5), T_m is the ToF of the converted mode for the master sensor, and $\Delta T_{j,m}$ is the difference of ToFs between master sensor and slave sensor j. Using the time-frequency analysis approach, $\Delta T_{j,m}$ can be solved by identifying the converted modes of the Lamb wave signal in the time-frequency domain. The selection of the master sensor is random. If sensor S1 is chosen as the master sensor, the nonlinear Equation 19 can be written as,

$$\begin{aligned}
&\frac{\sqrt{(x_d - x_1)^2 + (y_d - y_1)^2}}{T_1} - \frac{\sqrt{(x_d - x_2)^2 + (y_d - y_2)^2}}{T_1 + \Delta T_{2,1}} = 0 \\
&\frac{\sqrt{(x_d - x_3)^2 + (y_d - y_3)^2}}{T_1 + \Delta T_{3,1}} - \frac{\sqrt{(x_d - x_4)^2 + (y_d - y_4)^2}}{T_1 + \Delta T_{4,1}} = 0 \\
&\frac{\sqrt{(x_d - x_5)^2 + (y_d - y_5)^2}}{T_1 + \Delta T_{5,1}} - \frac{\sqrt{(x_d - x_6)^2 + (y_d - y_6)^2}}{T_1 + \Delta T_{6,1}} = 0
\end{aligned} \tag{21}$$

In Equation 21, there are three unknown variables in these three nonlinear equations. The unknowns are x_d, y_d, and T_1. Theoretically, these equations can be solved. More Lamb wave propagation information, such as group velocities in different directions can also be calculated after solving Equation 21.

Using the refined MPD algorithm, the guided wave signals from different sensors can be represented in the same time-frequency domain. The difference of ToFs between sensors can be compared and accurately calculated. This ToF information is used as input information for the damage location objective equations.

To efficiently solve the nonlinear equations, they are combined and solved using an unconstrained Newton's method. Newton's method has been proven to be an efficient iterative method for finding roots of equations (Rao, 1996). In optimization, Newton's method is equivalent to iteratively minimizing a local quadratic approximation to the objective function.

The localization objective Equation 21 can be written as,

$$F(x) = 0 \tag{22}$$

where F is the vector of the equations F_i (i=1,2,3) and x is the vector of the unknowns. For vector x, we have,

$$x_1 = x_d;\ x_2 = y_d;\ x_3 = T_1; \tag{23}$$

Assume at x*, we have F(x*)=0. Newton's method converges to x* by computing the Jacobian matrix of the function F. The Newton's iteration can be expressed as,

$$x^{n+1} = x^n + \delta x^n = x^n - J(x^n)^{-1}F(x^n) \tag{24}$$

where x^n is the current point, x^{n+1} is the iteration point after x^n, and $\delta x^n = J(x^n)^{-1}F(x^n)$. The Jacobian matrix $J(x)$ can be expressed as,

$$J(x) = \frac{\partial F(x)}{\partial x} = \begin{bmatrix} \frac{\partial F_1(x)}{\partial x_1} & \frac{\partial F_1(x)}{\partial x_2} & \frac{\partial F_1(x)}{\partial x_3} \\ \frac{\partial F_2(x)}{\partial x_1} & \frac{\partial F_2(x)}{\partial x_2} & \frac{\partial F_2(x)}{\partial x_3} \\ \frac{\partial F_3(x)}{\partial x_1} & \frac{\partial F_3(x)}{\partial x_2} & \frac{\partial F_3(x)}{\partial x_3} \end{bmatrix} \tag{25}$$

For unconstrained optimization, the merit function measures the agreement between the function value and the ideal optimized value. Generally, the merit function can be written as a scalar valued function,

$$f(x) = \|F(x)\|^2 \tag{26}$$

The solution x* of nonlinear equations F(x) = 0 are also the global minimum of the objective function f(x). Newton's method is used to find the global minimum solution for the objective function.

3.3 Probabilistic Estimation of Delamination Location Range

Assuming that the same group velocities for the two nearby PZT sensors on the composite specimen introduces system estimation error to the proposed algorithm and increases uncertainty of the estimated delamination location. Probability based location estimation can provide a certain location range and improve the damage awareness in composite structures.

Redundant PZT sensors are used in the proposed localization method. Four pairs of sensors are bonded on each composite sample. For every composite sample, round robin experiments were conducted. Each PZT transducer was used as an actuator once in the eight experiments. Based on Equation 26, eight delamination positions can be estimated. They are ($x_{d,i}$, $y_{d,i}$) (i=1,2,…8). Since a different actuator is used in each experiment, the experiments can be considered independent. The final delamination position (x_d, y_d) is defined as,

$$x_d = \frac{\sum_{i=1}^{i=n} x_{d,i}}{n}, \quad y_d = \frac{\sum_{i=1}^{i=n} y_{d,i}}{n} \tag{27}$$

where (x_d, y_d) is the final estimated delamination position and n is the total amount of experiments conducted for each composite sample. For the cases studied in this chapter, n is equal to 8.

The delamination positions in the x and y axes are also independent to each other. To define the estimated data vector D, the following equation can be used,

$$D = \{d_m\} = [x_{d,1}, \dots x_{d,8}, y_{d,1}, \dots, y_{d,8}] \tag{28}$$

The confidence range of the delamination can be estimated by calculating the standard deviation, α, of vector D (Papoulis and Pillai, 2002),

$$\alpha = \sqrt{\frac{\sum_{i=1}^{i=m}(d_m - \bar{d})}{m}} \tag{29}$$

where $\bar{d}$ is the mean of vector D. For the case studied in this chapter, m is equal to 16.

3.4 Experimental Setup

Three experiments were conducted to validate the proposed localization methodology. In experiment 1, composite plates with a $[0°/90°/0°]_s$ layup were fabricated in-house. Plain weave fiber fabrics were used as the fiber system to simulate composites with quasi-isotropic material properties. In experiment 2, composite plates with $[(0° /90° /0°)_{pw}/90°_{uni}/(0° /90° /0°)_{pw}]$ layup were fabricated. Both plain weave fiber fabrics and unidirectional fiber fabrics were used to obtain orthotropic material properties. In experiment 3, stiffened composite panels with two stiffeners were fabricated using $[0°/90°/0°]_s$ layup. Plain weave fiber fabrics were used as the fiber system. A two-part epoxy, FS-A23 (resin) and FS-B412 (hardener) from Epoxy System Inc., was used as the matrix system for all composite coupons. Delaminations were seeded in the composite plates and panels during fabrication using Teflon patches. Flash thermography (Echo Therm System) was used to validate the position and size of the delaminations. The

composite plates and stiffened panels with flash thermographic images are shown in Figure 27.

(a) Composite plate (b) Stiffened composite panels

Figure 27. Composite plates and stiffened panels used in experiments

A PZT array using eight PZT transducers were bonded on the surface of the composite samples in four pairs, as shown in Figure 27. In each PZT pair, the two transducers were placed close to each other. One PZT was used as the actuator and other three PZT pairs were used as sensors. A waveform was generated using a NI 5412 waveform generator, and the Lamb wave signals were captured using an NI 5105 digitizer at a sampling frequency of 20 MHz. In order to optimize the central frequency of the actuation signal, several actuation signals were generated using central frequencies varying from 10 kHz to 300 kHz in 10 kHz increments. A 4.5-cycle cosine windowed burst signal with a central frequency of 180 kHz was chosen as the actuation signal. Ten observations were recorded at each measurement and the sensor signal was averaged from these observations to reduce the sampling error. Round robin tests were conducted to improve the localization accuracy.

3.5 Results and Discussion

In experiment 1, the composite plate with quasi-isotropic material properties was tested. Baseline data was collected from the healthy composite sample. Guided wave sensor data was collected from the sample with seeded delamination. The Lamb wave signals were analyzed using the MPD algorithm. The Lamb wave modes recorded from both the healthy sample and the sample with seeded delamination were represented in the time-frequency domain. By comparing the two time-frequency representations (TFRs) in the time-frequency domain, the first converted mode caused by the delamination can be identified, as shown in Figure 28. From the TFRs of the master sensor and the nearby slave sensor, the difference of the ToF of the converted mode can be calculated, as shown in Figure 28.

The delamination localization results are shown in Figure 29. The real delamination position is 10.2 mm away from the estimated delamination position, but still in the 95% confidence range of the estimated delamination area. The detailed real and estimated delamination positions are shown in Table 5.

Experiment 2 validated the proposed methodology using the composite plates with orthotropic material properties. Both plain weave and unidirectional fiber fabrics were used. The ToF difference between PZT sensors were computed using the MPD algorithm. The delamination localization results show that the real delamination is 12.6 mm off the estimated delamination position, as shown in Figure 30 and the detailed real and estimated positions are shown in Table 5.

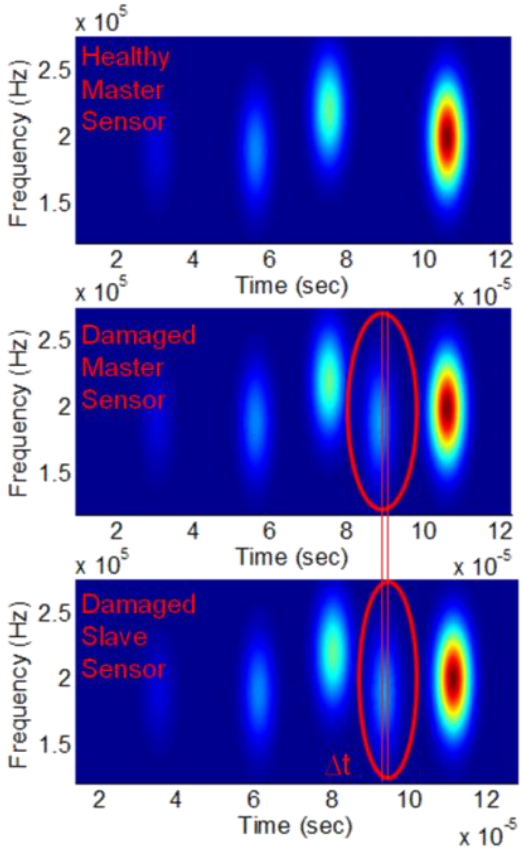

Figure 28. TFRs of the Lamb wave signals collected from master sensor in healthy plate, master and slave sensors from damaged plate

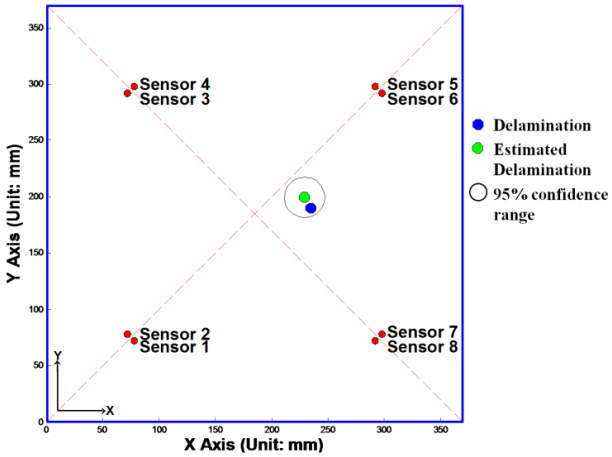

Figure 29. Estimated delamination position and confidence range for quasi-isotropic composite materials

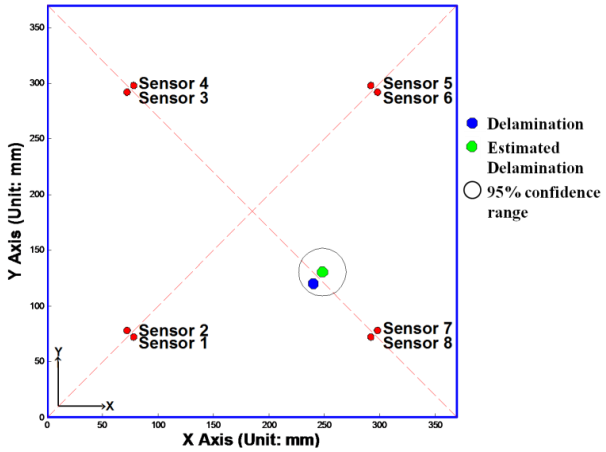

Figure 30. Estimated delamination position and confidence range for orthotropic composite materials

Experiment 3 validated the proposed methodology using the composite plates with two stiffeners. Similar to the approach used previously, the MPD algorithm was used to calculate the ToF difference between sensors. The delamination location was calculated by solving the optimization objective function. Localization results show that the real delamination position is 12.2 mm away from the estimated position, as shown in Figure 31. The detailed real and estimated delamination positions are shown in Table 5.

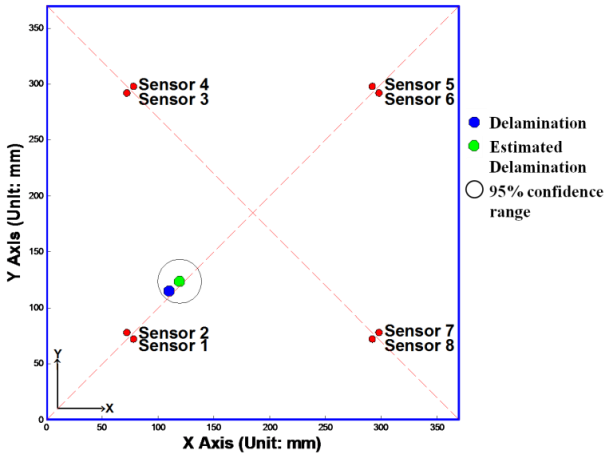

Figure 31. Estimated delamination position and confidence range for stiffened panels

Table 5. Real and estimated delamination positions

	Real Position (unit: mm)	Estimated Position (unit: mm)	95% confidence range (unit: mm)
Experiment 1	(235.4,190.7)	(229.3, 199.5)	18.3
Experiment 2	(240.1,120.9)	(248.3, 130.5)	21.5
Experiment 3	(110.2, 115.6)	(119.3, 123.7)	19.8

3.6 Concluding Remarks

In this chapter, a delamination localization methodology using a guided wave based active sensing technique is presented. Due to the complexity associated with the interrogated composite structures, guided wave information and composite material properties are difficult to obtain. By solving an optimization function subject to three nonlinear objective equations, the delamination position can be estimated without knowing the group velocity or ToF for each wave mode. Information required for the proposed methodology includes the sensor position, and the difference of ToF of the converted modes caused by delamination between master sensor and slave sensors. By comparing the sensor data with the baseline data collected from the healthy samples, converted modes caused by the seeded delamination can be identified. Using the MPD algorithm, the guided wave signals are represented in the time-frequency domain, and the difference of the ToF of the converted modes between master and slave sensors can be calculated. The group velocities from the delamination to the two nearby PZT sensors are assumed to be the same. Redundant sensors are placed on the surface of composite samples. Probabilistic confidence range estimation provides the 95% confidence range for the estimated delamination positions.

The developed localization methodology is experimentally validated using in-house fabricated composite plates and stiffened panels. Both healthy and damaged composite samples were fabricated using plain weave fiber fabric system and unidirectional fiber fabric system. The experimental results demonstrated that the real delamination positions can be accurately located in the 95% conference range of the estimated positions.

Chapter 4

PROGNOSIS AND RUL ESTIMATION USING GAUSSIAN PROCESS

4.1. Introduction

Although the study of fatigue behavior in composites has been a popular research subject over the years, SHM and prognosis of composite structures is still at its infancy. The estimation of the reliability and remaining useful life (RUL) is important for condition-based system maintenance of composite structures because the composite structural components can be repaired or replaced in time prior to catastrophic failures. Generally, two approaches have been applied to the prognosis of composite structures. They are either physics based or probabilistic data driven based approaches. Physics based approaches model the degradation progress with tuned fatigue parameters. In literature, most research work about physics based fatigue models has been focused on developing phenomenological/empirical models to predict the mechanical properties of composites. Typically, these models describe strength or stiffness degradation during constant amplitude fatigue loading (Philippidis and Passipoularidis, 2007; Boerstra, 2005). A detailed review is presented by Delgrieck and Paepegem (2001). However, a major drawback is that extensive experimental data is required to describe these models. In addition, most theoretical models developed for a particular material system need further investigation and evaluation when a different material system is used (Filis et al., 2004; Epaarachchi, 2006). Furthermore, even for the same material system, damage mechanisms are different under static loading and fatigue loading (Bond and Farrow, 2000). These reasons make the physics based models lack confidence in real-life

applications. It is noted that currently available, physics based propagation approaches are in general based on initial assumption of damage size. However, the composite degradation process is so complex that it is difficult to assume a damage state for developing a damage propagation model. Recently, Gobbato et al. (2008, 2009) published a probabilistic and mechanics based model to stochastically propagate the damage throughout the joints of unmanned aerial vehicles (UAVs). Real time monitoring of damage states using the state of the art SHM techniques is required to update the initial condition of the damage propagation model in real-time. Such condition based damage state forecasting will help to reduce the uncertainty in residual useful life estimation of composite structures. A condition based integrated prognosis model applied to metallic structure is presented by Mohanty, et. al (2009).

In this chapter the above mentioned condition based prognosis approach is further extended to estimate the residual useful life of composite structures subject to constant fatigue loading in real-time. On-line damage states, which are estimated using real time sensing information, are fed to an off-line predictive model to update future damage states and RUL. The on-line damage index or damage state at any given fatigue cycle is estimated using correlation analysis. Based on the on-line information of the previous and current damage states, an off-line model is developed to predict the future damage state and estimate the RUL. The off-line model is a stochastic model which is developed based on the Gaussian process approach. The condition based prognosis model is used to estimate the cumulative fatigue damage in composite test structures under constant amplitude fatigue loading. The developed procedure is validated under uniaxial fatigue

loading as well as biaxial fatigue loading. Experimental validations demonstrate that the prediction capability of the prognosis algorithm is effective in predicting the RUL under complex stress states.

4.2. Damage States Estimation and Prognosis Model

The prognosis model comprises of two primary components: (1) on-line damage state estimation, (2) off-line damage state prediction. The on-line damage state is estimated based on real-time sensor measurements. Once the on-line state information becomes available, it is recursively fed to the off-line damage state predictive model to assess the future damage states and to calculate the associated residual useful life.

The degradation process of composite structures is a complex phenomenon. Both damage types and sizes are time varying in nature, as they change with the loading spectra and the operational life. However, for any composite degradation system, the time varying transfer function or input-output relation can be described as shown in Figure 32. The transfer function represents the time degrading system at any damage state. As the damage grows in the composite structure, the parameters of the transfer function also change.

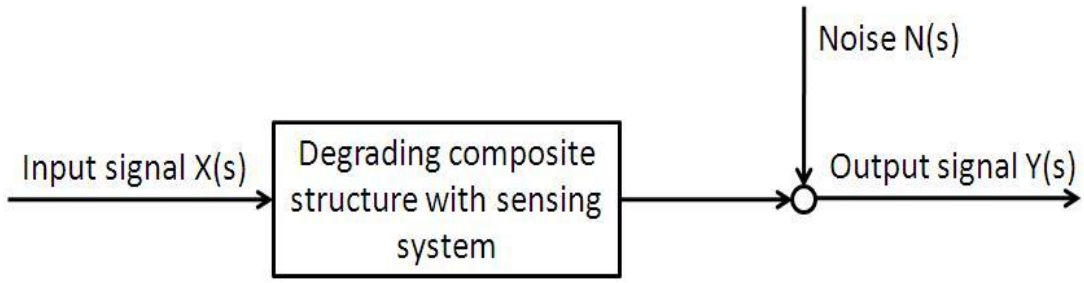

Figure 32. Transfer function for a general composite degrading system

The transfer function H(s) can be written as,

$$Y(s) = H(s)X(s) + N(s) \tag{30}$$

where, X(s), Y(s) and N(s) are the input, the output and the noise at state s.

For discrete-time systems, the transfer function in Equation 30 can be written as,

$$Y(z) = b_0X(z) + b_1X(z-1) + \cdots + b_MX(z-M) + N(z) \tag{31}$$

where b_m $(m = 0,1,2,\cdots,M)$ are the finite impulse response coefficients. At any damage state, according to Equation 31, the lagged cross-correlation coefficients between two sensor signals can be expressed as,

$$\gamma_{XY}(m) = b_0\gamma_{XX}(m) + b_1\gamma_{XX}(m-1) + \cdots + b_M\gamma_{XX}(m-M); \quad m = 0,1,2,\cdots,M \tag{32}$$

where m is the correlation lag number, $\gamma_{XY}(m)$ is the cross correlation coefficient and γ_{XX} is the auto correlation coefficient. With the known time series input X(t) and output Y(t), the cross-correlation coefficients at different damage states can be obtained. Rather than explicitly finding all the FIR coefficients and hence the transfer function H(s) based on the cross-correlation coefficient, a damage index is evaluated. The damage index, which is based on the real-time input output measurements, equivalently estimates the damage state of the composite structure. The damage index is expressed as follows:

$$a_n = \sqrt{\frac{\sum_{m=0}^{m=M}(\gamma_{XY}^n(m) - \gamma_{XY}^0(m))^2}{\sum_{m=0}^{m=M}\left(\gamma_{XY}^0(m)\right)^2}} \tag{33}$$

where n is the damage level indicator, γ_{XY}^n represents the nth level cross-correlation coefficients and γ_{XY}^0 represents cross-correlation coefficient at healthy condition, which is used as reference.

As mentioned earlier, once the real-time damage state is estimated, the information is sent to a predictive model to forecast the future states of the structure even though no real-time information is available. The predictive model developed is based on Gaussian process (GP) which is the generalization of Gaussian distribution over a function space of infinite dimension (Büche, 2005). It is parameterized by a mean and a covariance function. With state information available up to nth damage level, the predictive distribution at (n+1)th damage level can be given as:

$$P(a_{n+1}, a_n) = \frac{1}{Z}\exp\left(-\frac{(a_{n+1} - \hat{a}_{n+1})^2}{2\sigma^2_{\hat{a}_{n+1}}}\right) \tag{34}$$

$$\hat{a}_{n+1} = k^T K_n^{-1} a_n \tag{35}$$

$$\sigma^2_{\hat{a}_{n+1}} = \kappa - k^T K_n^{-1} a_n \tag{36}$$

where $\hat{a}_{n+1}$ is the predictive mean at the (n+1)th damage level, and $\sigma_{\hat{a}_{n+1}}$ is the associated error variance of the prediction, K_n is the $n \times n$ kernel matrix for the vector a_n, κ and k^T are the partitioned components of kernel matrix.

For the future damage state prediction, the GP model given by Equations 34-36 recursively predicts the future damage states based on the last on-line data available. The training data set D and test input vector $a_{n+\tilde{n}}$ can be written as,

$$D = \left[\begin{array}{ccccc|c} \overbrace{a_0 & a_1 & a_2 & \cdots & a_{d-1}}^{\text{training data matrix}} & \overbrace{a_d}^{\text{target vector}} \\ a_1 & a_2 & a_3 & \cdots & a_d & a_{d+1} \\ \vdots & \vdots & \vdots & \cdots & \vdots & \vdots \\ a_{n-d} & a_{n-d+1} & a_{3n-d+2} & \cdots & a_{n-1} & a_n \\ a_{n-d+1} & a_{n-d+2} & a_{3n-d+3} & \cdots & a_n & a^p_{n+1} \\ a_{n-d+1} & a_{n-d+2} & a_{3n-d+3} & \cdots & a^p_{n+1} & a^p_{n+2} \\ \vdots & \vdots & \vdots & \cdots & \vdots & \vdots \\ a^p_{n-d-1+\tilde{n}} & a^p_{n-d+\tilde{n}} & a^p_{n-d+1+\tilde{n}} & \cdots & a^p_{n-2+\tilde{n}} & a^p_{n-1+\tilde{n}} \end{array}\right] \tag{37}$$

$$a_{n+\tilde{n}} = \left[\overbrace{a^{p}_{n-d-1+\tilde{n}} \quad a^{p}_{n-d+\tilde{n}} \quad a^{p}_{n-d+1+\tilde{n}} \quad \cdots \quad a^{p}_{n-2+\tilde{n}}}^{\text{test input data vector}}\right] \tag{38}$$

where in Equations 37 and 38, the subscript n is the damage level to which the last on-line data is available, the subscript ñ is the damage level after the availability of the last on-line data and the superscript p indicates the predicted damage index.

4.3. Experimental Setup

4.3.1. Uniaxial Loading Fatigue Tests and Experimental Validation

To experimentally validate the prognosis model, a uniaxial tensile fatigue test was performed on a composite beam. The composite specimen loaded on the test frame can be seen in Figure 33. A four-ply composite beam was selected as the test specimen and was manufactured in-house with unidirectional carbon fiber/epoxy matrix composite materials. The matrix used was HEXION EPON 863 and EPI-CURE 3290. The specimen had a stacking sequence of $[0°/90°]_S$ and its dimensions are shown in Figure 34 (a). Three strain gages were mounted on the surface of the specimen, two on the top side and one on the back side of the specimen, as shown in Figure 34 (b). The specimen was subjected to constant amplitude fatigue loading with maximum amplitude (σ_{max}) of 11 kN and load ratio $R = 0.1$ on a MTS uniaxial fatigue frame operating at a frequency of 10 Hz. It is noted that a 0.75 inch wide notch in the center of the specimen was made to create an initial damage. An Omega OM2-163 strain gage amplifier was used to amplify the strain signals and a 48 channel NI PXI system was used to acquire the strain gage signals. In addition, the initial healthy state and final damaged state of the composite specimen was estimated by using flash thermography (Echo Therm) system.

The flash thermographic images of the healthy and damaged states are shown in Figure 35. The developed real-time MATLAB based prognosis algorithm was synchronized with the NI data acquisition system to estimate the current damage states and to predict both the future damage states and the residual useful life in real-time.

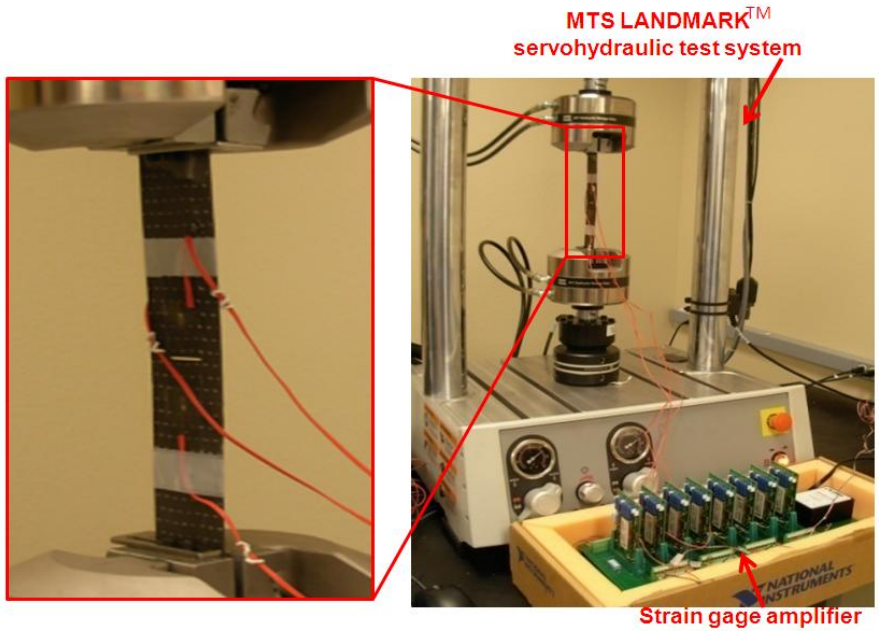

Figure 33. Four-ply composite plate loaded in a MTS servo hydraulic test frame

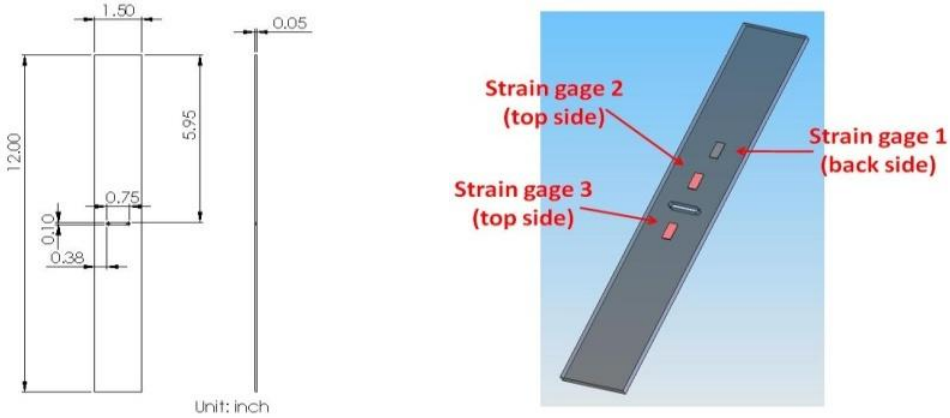

(a) Configuration of specimen (b) Test specimen with strain gages

Figure 34. Unidirectional composite specimen

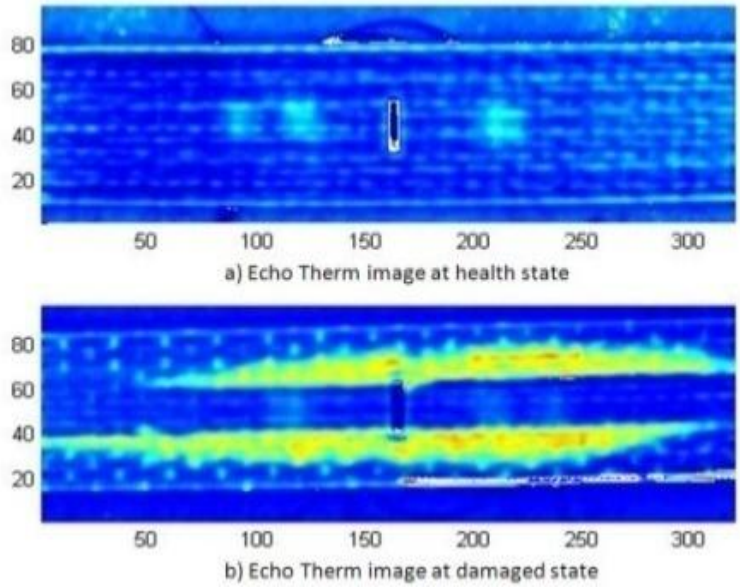

Figure 35. Echo therm images at health and damage states

4.3.2. Biaxial Loading Fatigue Tests

To validate the prognosis model under complex biaxial loading, another set of fatigue test was performed by applying bi-axial loading on a composite cruciform specimen. The composite cruciform specimen and the experimental setup can be seen in Figure 36. To uniformly distribute the load in the web area of the cruciform specimen, two interface areas were machined by CNC machine at both front and back sides of the specimen. The dimensions of the specimen are shown in Figure 37. The final failure of the cruciform specimen occurred due to the interface delamination in the web area. The specimen was subjected to a constant amplitude fatigue loading with maximum amplitude (σ_{max}) of 5 kips and load ratio R = 0.1. It is noted that based on an uniaxial tensile tests with dog bone specimens, the yield stress is approximated as $\sigma_Y = 8$ kips. The specimen was loaded at a frequency of 10 Hz. It should be noted that both the x-axis and y-axis actuator of the biaxial frame were subjected to in-phase fatigue loading.

Similar to uniaxial testing condition, for on-line state estimation, strain gage signals were used. One strain gage rosette was mounted in the web area of the cruciform specimen (gage area), and another strain gage rosette is mounted in the flange area (arm area). The strain gage signals were conditioned by an Omega OM2-163 strain gage amplifier and acquired using a 48 channel NI PXI DAQ system.

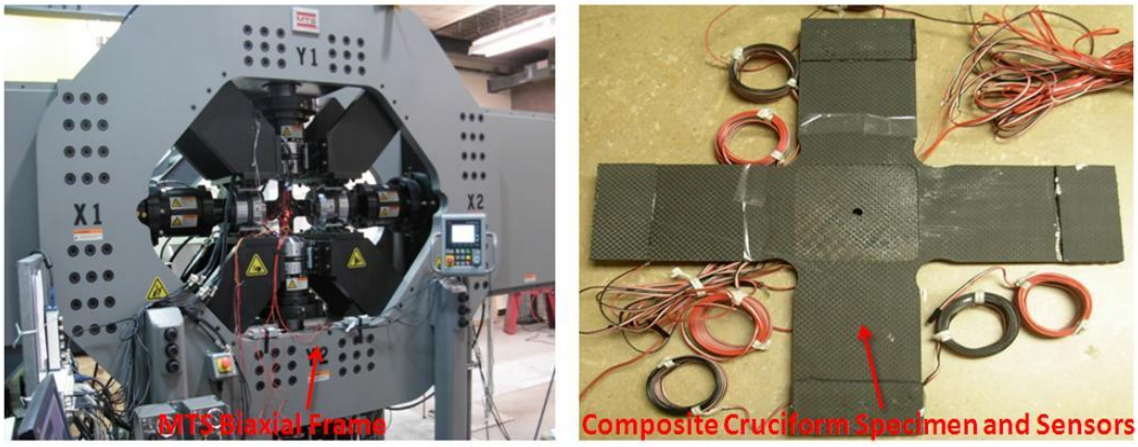

Figure 36. Composite cruciform specimen and experimental setup

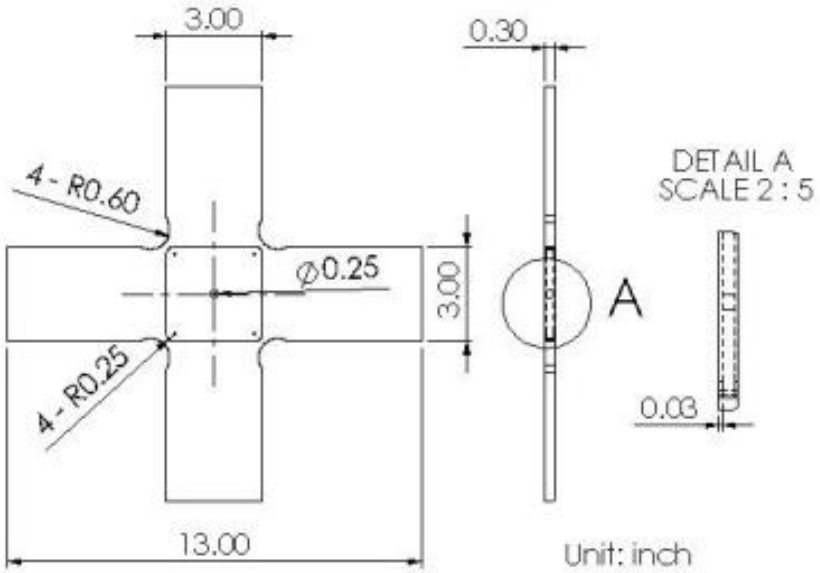

Figure 37. Configuration of composite cruciform specimen

4.4. Results and Discussion

4.4.1. Prognosis Validation Using Unidirectional Fatigue Tests

In order to evaluate the damage index in Equation 33, strain signals are mapped as input and output. For this purpose, three strain gages are mounted at different locations of the specimen. As shown in Figure 34 (b), strain gage 1 is furthest from the possible damaged area (i.e. area near the notch) compared to both strain gages 2 and 3. This causes the sensitivities of all three strain gages to be different. Strain gages 2 and 3, symmetrically placed around the pre-cut notch, are more sensitive to the damage compared to the strain gage 1. It is noted that the input strain gage should be ideally placed away from the damage area, such that the strain measurements from this gage will be least affected by the damage. To experimentally evaluate the proposed damage index, two different cases of input-output mapping, such as case I: input from sensor 1 and output from sensor 3 and case II: input from sensor 2 and output from sensor 3, are considered. The estimated time-series damage index at different fatigue cycles is shown in Figure 38. It is noted from Figure 38 that both the time-series features show clear trends for damage growth during the entire fatigue process. However, it is seen that the time-series features with measurements from strain gages 1 and 3 is more sensitive compared with measurements from strain gages 2 and 3. The reason is that signals from strain gage 1 remain nearly uniform during the fatigue process whereas strain gages 2 and 3 capture more local strain changes due to fatigue. The damage indices calculated from the correlation between strain gages 1 and 3 are used in the future damage state prediction and RUL estimation. It

is noted that the actual damage is equivalent to the damage indices that are estimated from the real-time sensor measurements.

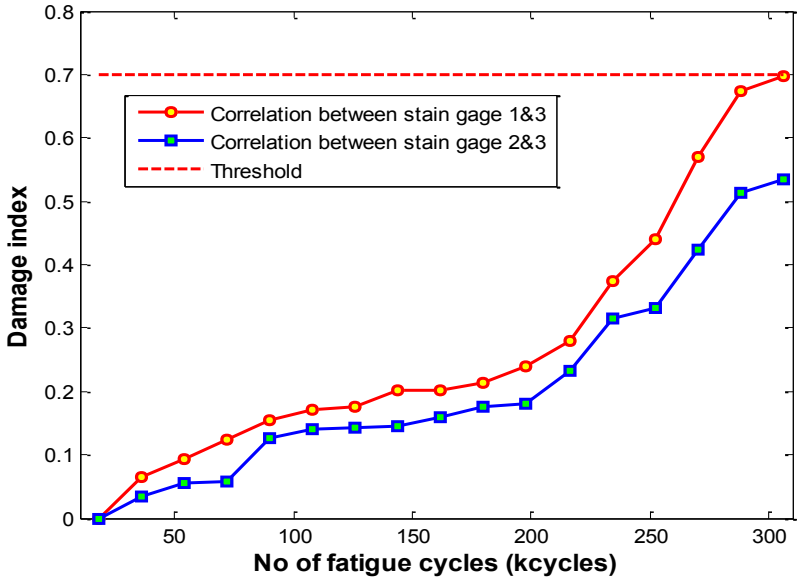

Figure 38. On-line damage states estimations

Based on Equations 34 to 38, a multi-step ahead prognosis strategy is followed recursively to forecast the future damage state. The prognosis algorithm initiates after a certain damage level (six damage levels in the present case) to collect sufficient previous damage state information. The mean damage index for the next damage level is predicted using Equations 34 and 35. The predicted mean damage index is fed back to the prognosis model to update the training data matrix and the test input vector. The feedback process is continued recursively until the predicted damage index reaches its critical failure value. In the present case the critical damage index is chosen to be 0.7. However, it depends on the user to choose the critical damage index value based on the safety and application requirements. It is noted that damage index value of '1' indicates complete failure. Figure 39 shows the predicted future damage states and RUL information. A

good correlation can be seen between the predicted and experimental damage states. It can be also seen that the accuracy of future damage state prediction improves as more and more experimental information (such as strain measurements and the corresponding estimated damage states) is available.

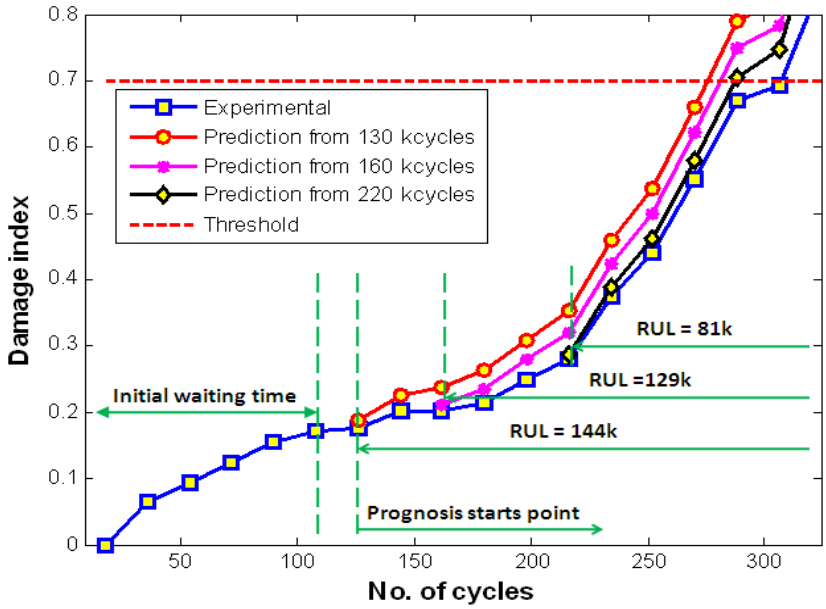

Figure 39. Future damage state and RUL prediction

4.4.2. Prognosis Validation Using Biaxial Fatigue Tests

In the previous section it is found that the proposed prognosis model is capable of predicting the future damage states and remaining useful life under uniaxial fatigue loading. This section focuses on the experimental validation for biaxial fatigue loadings. The damage state prediction for the composite biaxial loading test is performed recursively with multi-step ahead prediction method discussed before. The predicted damage states with on-line data available up to certain fatigue instances are shown in Figure 40. It is noticed that unlike the uniaxial case where first six damage states were sufficient to start the prediction algorithm correctly, for biaxial loading case the

prediction algorithm waits several damage levels to forecast reasonably correct damage states. This is because damage state information (as estimated from on-line model) from the first several damage levels is not able to capture the complex damage growth dynamics of the structure. It is noted, that the ideal waiting time is equivalent of 'd' damage levels (ref. Equations 37 and 38), where 'd' is the input dimension of Gaussian process predictive model. Three prediction time-series are shown in Figure 40. They start from 164k cycles, 191k cycles and 218k cycles, respectively. The predicted damage states correlate well with the actual damage states. The residual useful life at a given damage level up to which the on-line data was available is also forecasted. Figure 41 shows the comparison of predicted RUL and actual RUL calculated from the 160k cycles to the failure of cruciform specimen. It can be seen that there is a good correlation between predicted and actual RUL. From Figure 40 and Figure 41, it is also noticed that both the state prediction and RUL predictions are improved (i.e. close to actual) when more and more on-line information is available.

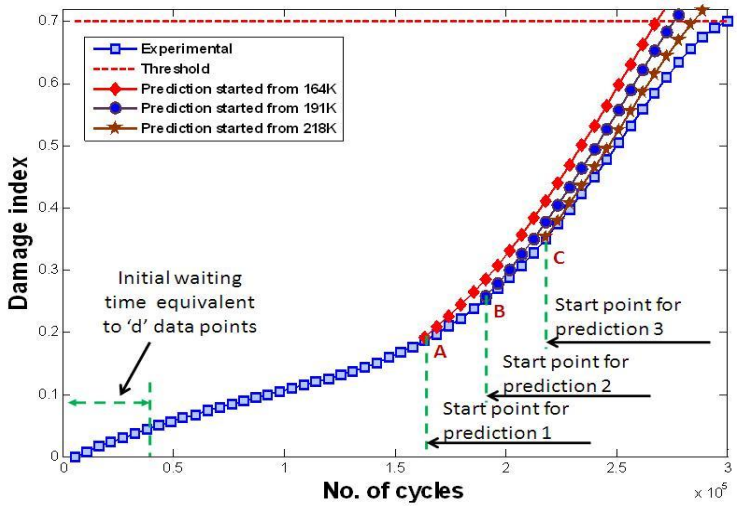

Figure 40. Damage states and RUL prediction for composite cruciform specimen

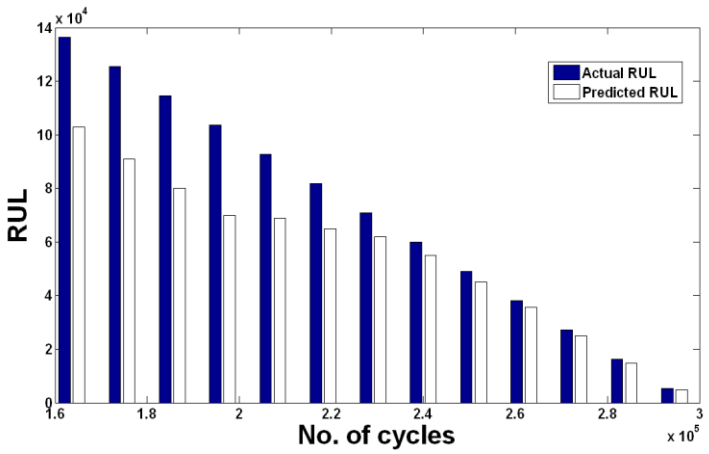

Figure 41. Comparison of predicted RUL and actual RUL

4.5. Concluding Remarks

An integrated prognosis algorithm has been developed to forecast damage state and estimate RUL of composite test structures. The prognosis model combines two modules: (i) on-line damage state estimation module, (ii) off-line damage state and RUL prediction module. A damage index formulation has been evaluated and used to extract fatigue damage states from real-time strain gage measurements. Based on the on-line estimated damage states the second stage Gaussian process predictive model is used to forecasts the future damage states and the corresponding remaining useful life. It is found that there is a good correlation between the predicted damage states and actual damage states. The accuracy of predicted states and RUL improved at the later stages of fatigue life as more on-line information or states became available to the predictive model. The prognosis model is validated for both uniaxial tensile fatigue test and biaxial fatigue test with carbon fiber epoxy matrix composite specimens manufactured in house.

Chapter 5

LOW VELOCITY IMPACT DAMAGE MONITORING

5.1. Introduction

Impact has been the subject of many experimental and analytical investigations. Sources of low-velocity impacts include tool drop, runway debris, collision with vehicles, etc. The internal damage state after a low velocity impact in CFRP composites can be complex and multimodal, including matrix cracking, delaminations and fiber breakage. The impact damage can propagate under service loading leading to catastrophic structural failure. Therefore, it is critical to develop accurate and robust SHM methodologies to detect and monitor the damage initiation due to low velocity impacts. Advanced sensing and associated signal analysis/interpretation approaches have been well-developed to monitor impacts on composite structures with simple geometries. Meo and Zumpano, (2005) developed an *in-situ* impact damage detection and identification methodology using piezoelectric sensors and guided wave propagation approaches. Moll et al. (2010) developed a multi-site impact damage localization approach applicable to anisotropic wave propagation which did not assume any simplifications regarding to anisotropic wave propagation. Hiche et al. (2011) developed a strain amplitude-based algorithm for impact localization on composite laminates using FBG sensors. However, due to the complex damage mechanisms, most of the published data driven approaches only validated the methodologies on plate-like or sandwich composite structures. Due to the associated challenges, very limited work has been reported on application to complex geometries and real applications.

Obtaining a proper feature representation of the damage state from the sensing data is a fundamental problem in SHM. Generally, not all of the original features are beneficial for damage detection and classification. Some of the features include a significant amount of noise and will negatively influence the performance of SHM system. Therefore it is essential to remove the noisy features or derive some new features from original data space, so that only the necessary information is retained for damage classification, quantification and prognosis. Traditionally, linear feature extraction and selection are conducted in the original input space. Therefore nonlinear relationships cannot be extracted from the original dataset. For example, only features from time domain or frequency domain are considered in some of the PZT based active sensing approaches (Sohn et al. 2001; Su, et al., 2006; Tang, et al. 2011). However, the nonlinear structural degradation process may not be fully represented by time or frequency domain features. It is necessary to develop robust feature extraction/selection methodologies to represent the multiscale structural damage in heterogeneous material systems.

This chapter extends the damage quantification work on composite wing sections using FBG sensors initiated by Seaver et al. (2010). A new feature selection methodology for impact damage detection and quantification using kernel method and a guided wave based active sensing approach is developed. The effects of statistical feature selection using KPCA from the time and frequency domains are studied. A robust SHM feature is extracted using KPCA to represent the low velocity impact damage on a composite sandwich wing structure. A damage index based on Mahalanobis distance is used to quantify the damage. The methodology is applied to a composite wing of an UAV.

5.2. Statistical Feature Extraction

Selection of appropriate features, which are sensitive to damage but robust to noise, is a key issue in SHM. Statistical features have been demonstrated to be useful to represent damage in complex engineering structures (Sohn et al., 2001). A PCA based multivariate statistical technique integrated with Q- and T^2- measures was able to distinguish cracks in a steel plate and identify an added mass on an aircraft turbine blade (Mujica et al., 2011). The method has been proven to be useful in both the low frequency range using vibration based approaches and high frequency range using guided wave based active sensing approaches. However, PCA can only extract linear features. Because most complex engineering systems are associated with nonlinearity, nonlinear features can be more useful for damage detection and quantification. A nonlinear statistical feature extraction method is used in this work to identify and quantify low velocity impact damage in a composite wing.

5.2.1. Statistical Analysis Using KPCA

KPCA is a nonlinear extension of PCA and can be used to extract the nonlinear relation among variables (Scholkopf et al., 2000; Cao et al., 2007). In KPCA, a nonlinear kernel function is used instead of a linear function; the PCA can now be performed in a high-dimensional space which is nonlinearly related to the input space. Assuming the input data is mapped into the centered feature space Φ, we have

$$\sum_{j=1}^{N} \Phi(x_j) = 0 \tag{39}$$

The covariance matrix is defined as

$$\bar{C} = \frac{1}{N}\sum_{j=1}^{N} \Phi(x_j)\,\Phi(x_j)^T \tag{40}$$

The eigenvalues λ and eigenvectors V satisfy

$$\lambda V = \bar{C}V \tag{41}$$

It must be noted that the solutions for V which satisfy Equation 41 lie in $\Phi(x_j)$ (j=1…N). Therefore we can write

$$\lambda\big(\Phi(x_j)\cdot V\big) = \big(\Phi(x_j)\cdot \bar{C}V\big) \tag{42}$$

and

$$V = \sum_{j=1}^{N} \propto_j \Phi(x_j) \tag{43}$$

where $\propto_j$ (j=1,…,N) are the coefficients. The Kernel matrix K can be defined as

$$k_{ij} = \Phi(x_i)^T\Phi(x_j) = \Phi(x_i)\cdot\Phi(x_j) \tag{44}$$

Based on the application, different kernel functions, such as sigmoid kernels and polynomial kernels, can be selected to get the best performance. A Gaussian kernel function is used to nonlinearly map the input data to the high dimensional space. The N dimensional Gaussian kernel is defined as

$$K_N(\vec{x},\sigma) = \frac{1}{\left(\sqrt{2\pi}\sigma\right)^N} e^{-\frac{|\vec{x}|}{2\sigma^2}} \tag{45}$$

where σ determines the width of the Gaussian kernel. The new eigenvalues obtained from the KCPA analysis are used as the new feature vectors for the impact damage quantification.

5.2.2. Mahalanobis Distance Based Damage Index

The low velocity impacts are quantified using a Mahalanobis distance based damage index. The use of Mahalanobis distance has been demonstrated as a useful parameter for feature classification and quantification (Sohn, 2007). Two feature vectors $\vec{x}$ and $\vec{y}$ are assumed to have $\vec{x}\vec{y}$ the same distribution with the covariance matrix S. The Mahalanobis distance D^{M} is expressed as

$$\mathrm{D}^{\mathrm{M}} = \sqrt{\mathrm{D}} = \sqrt{(\vec{x} - \vec{y})^{\mathrm{T}} \mathrm{S}^{-1} (\vec{x} - \vec{y})} \tag{46}$$

where S^{-1} represents the inverse of the covariance matrix S. The Mahalanobis distance is used to define a new damage index for impact damage quantification in this paper. Denoting the KPCA feature vector at the i^{th} damage state $\overrightarrow{F_i}$ and the KPCA feature vector at the healthy state $\overrightarrow{F_h}$, the damage index DI_i corresponding to the i^{th} damage state can be defined as

$$DI_i = \frac{\mathrm{D}^{\mathrm{M}}(\overrightarrow{F_i}, \overrightarrow{F_h})}{\mathrm{D}^{\mathrm{M}}(\overrightarrow{F_h}, \overrightarrow{F_h})} \tag{47}$$

5.3. Experimental Setup

A sandwich composite UAV wing was used as the test article to assess the damage propagation due to multiple impacts. The wing is composed of four layers of carbon fiber fabrics; two layers were made from woven fiber fabrics (C282 carbon fabrics) and two layers were made from unidirectional fiber fabrics (3K T300 5" uni tape). The lay-up of the composite skin is [±45º woven /0º uni /0º uni /±45º woven]. The epoxy resin used is MGS L285 with MGS H287S hardener. There is an aluminum core at the center which can be used to connect the wing to the UAV fuselage. The rest of the wing has a foam

core made from Last-A-Foam. The cross-section of the wing has an airfoil shape. The geometry and cross-section of the wing is shown in Figure 42.

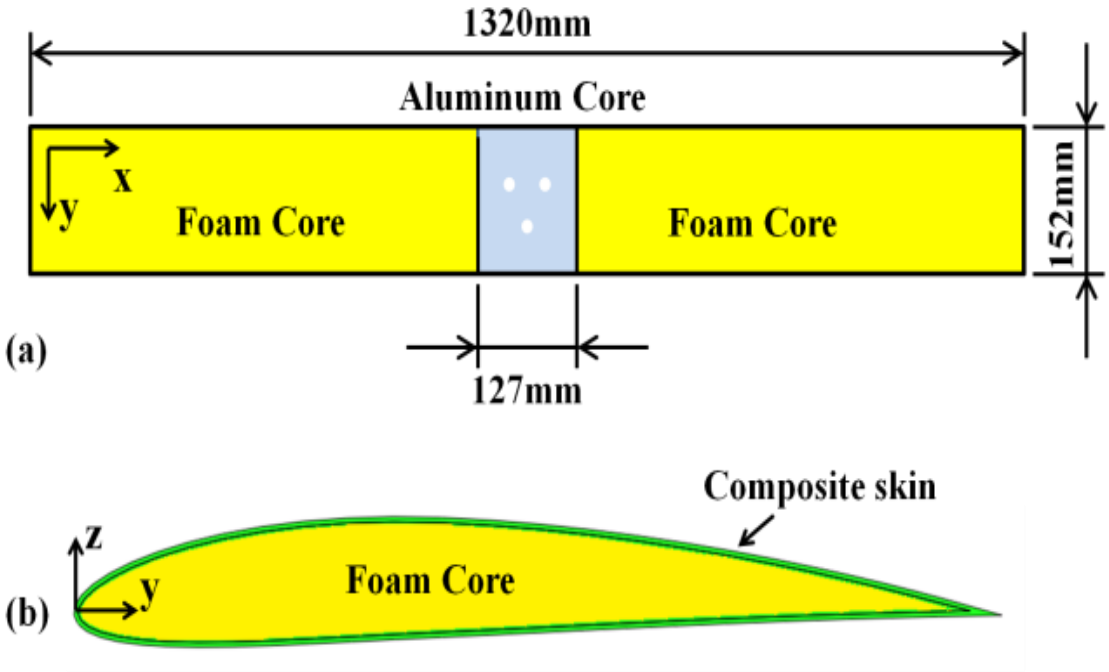

Figure 42. Geometry and cross-section of composite wing

A series of impact tests were conducted to investigate the effects of low velocity impacts on the composite wing. A pair of customized wing fixtures was fabricated to clamp the wing. The experimental setup is shown in Figure 43 (a). A swing arm impact system is used in the experiment. The diameter of the impactor head is approximately 32mm. Both the impact force and velocity were recorded to estimate the impact energy deposited in the test article. The impact force was measured using a dynamic load cell (Model: Dytran 1061V4), and the velocity and position of the swing arm was measured using a rotary encoder. By running several trial tests, an appropriate initial height of the impact head was determined to ensure damage of the foam core but not the composite skin. The impact energy is about 11J for each impact test.

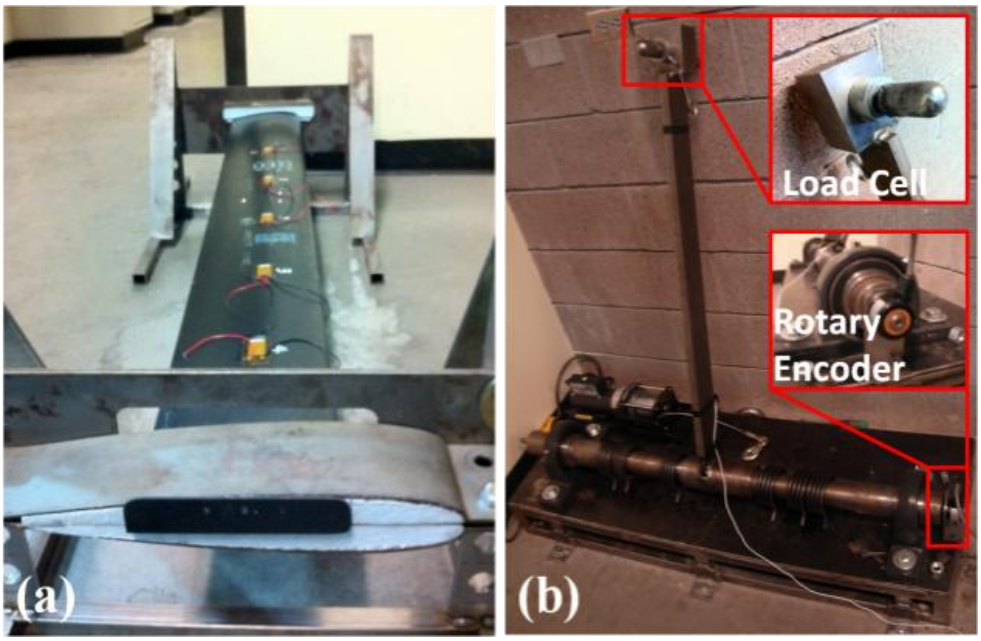

Figure 43. a) Experimental setup: composite wing in the fixture; b) Low velocity impact system

The impact area was divided into eight sections. A total of ten impact tests were conducted. The exact impact locations are shown in Figure 44. No visible damage was observed on the composite skin during the first eight impacts. However, the ninth and tenth impacts introduced sever visible dents on the composite skin, as shown in Figure 45.

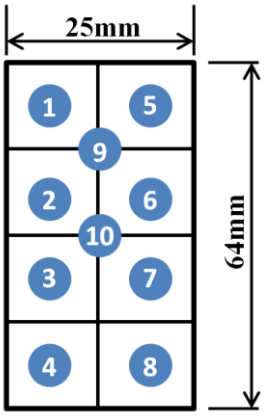

Figure 44. Impact sequence during experiment

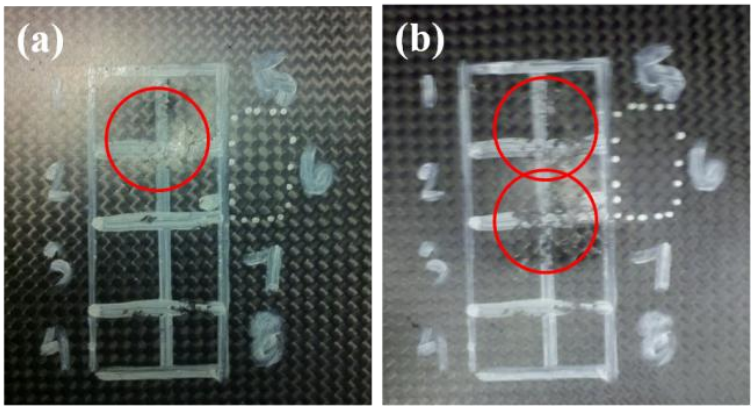

Figure 45. Visible damages in composite skin after impacts 9 and 10; a) Damage after impact 9; b) Damage after impact 10

Nondestructive tests using the flash thermography (Thermal Wave Imaging Inc., Model: EchoTherm) were conducted to visualize the extent of damage. Flash thermography utilizes high density flash heat generated by infrared heat lamps to excite the specimen with thermal radiation. Two infrared cameras record the thermal images with respect to time to evaluate the change in temperature field over time. Structural damage and imperfections can be differentiated from undamaged material due to their difference in local thermal diffusivity. Flash thermography images were taken before and after each impact, as shown in Figure 46. Prior to impact testing, no structural defect was detected because the temperature in the test field decays at a constant rate. However, after each impact, the red spots in the flash thermography images demonstrate the varying thermal diffusivity at the impact area. This indicates damage propagation and structural degradation caused by the series of low velocity impacts.

A wing autopsy test was conducted after the tenth impact to diagnose the exact nature of the damage in the composite wing. Multiple types of damage including foam

cracking, debonding between foam core and composite skin, and fiber breakage and delaminations in the composite skin were detected, as shown in Figure 47.

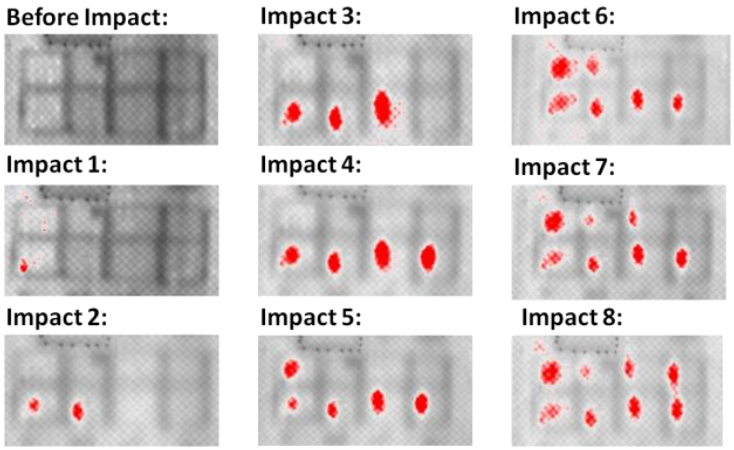

Figure 46. Flash thermography images of the damage area before and after impact tests 1-8

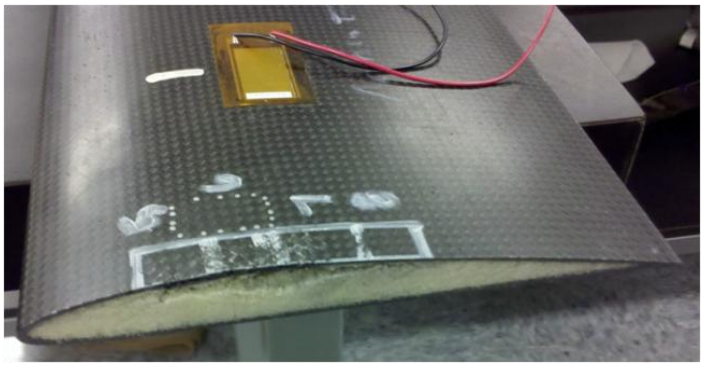

Figure 47. Composite wing autopsy after impact test 10

To detect and quantify the impact damage, a guided wave based active sensing approach using MFC transducers is used in this paper. Two MFC transducers were surface instrumented on the composite wing. The positions of MFCs are shown in Figure 48. A 4.5-cycle cosine windowed tone burst wave was used as the excitation signal. The excitation waveform was generated using the NI 5412 waveform generator, and the Lamb

wave signals were captured using the NI 5105 digitizer at the sampling frequency of 20 MHz. In order to optimize the central frequency of the excitation signal, several signals were generated using central frequencies varying from 10 to 300 kHz in 10 kHz increments. Ten observations were recorded at each frequency and the sensor signals were averaged from these observations to reduce the sampling error. After preliminary tests and signal processing, the optimal frequency selected was 100 kHz. The sensor signals were collected at the healthy state and following the fifth and tenth impacts, as shown in Figure 49.

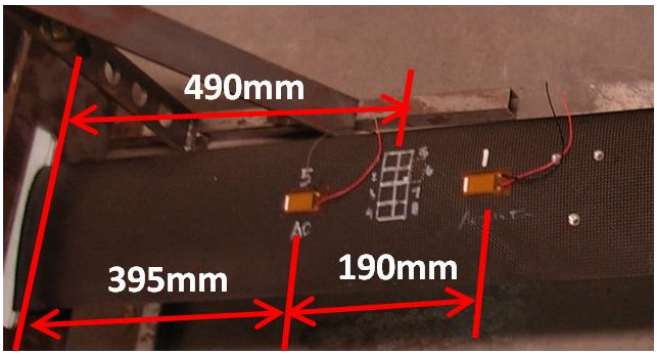

Figure 48. Surface instrumented MFC transducers for active sensing

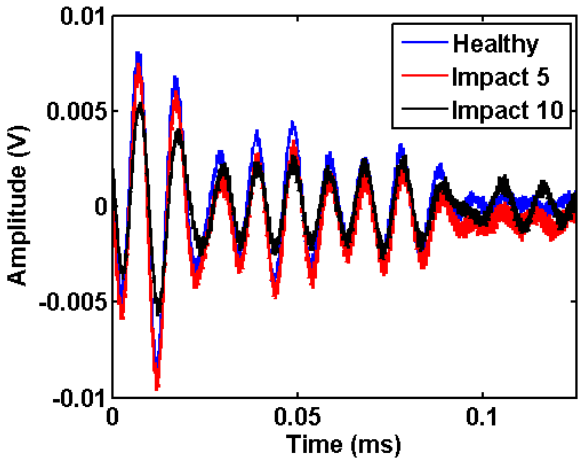

Figure 49. Original sensing signals from healthy state, impacts 5 and 10

5.4. Results and Discussion

To monitor the condition of the composite sandwich wing, nine statistical features of the MFC sensor signals in the time and frequency domains are extracted to represent the characteristics of damage. At each damage state, every observation provides one feature vector, denoted as $\{\vec{F_i} | \, i = 1 \ldots 9\}$. Because 100 observations are recorded at each damage state, 100 statistical feature vectors can be obtained. First, five statistical features are extracted from the time domain of the sensor signals. These features are Root-Mean-Square (RMS), variance, Kurtosis, peak value and peak to peak value. Using Fast Fourier Transform (FFT) and Hilbert Transform (HT), the MFC sensor signals are transformed to the frequency domain. The power spectrum energy is calculated as the sum of the frequency amplitude using FFT. The Hilbert spectrum is calculated using HT. The max Power Spectrum Densities (PSD) and max HT amplitude are also considered as statistical features. A detailed definition of each statistical feature is presented in Table 6.

Table 6. Definition of statistical features in time and frequency domains

Name	Definition
RMS	$x_{rms} = \sqrt{\frac{1}{M}\sum_{i=1}^{M}\|x_i\|}$
Variance	$Var_x = \frac{1}{M-1}\sum_{i=1}^{M}(x_i - \bar{x})^2$
Kurtosis	$Kur_x = \frac{1}{M}\sum_{i=1}^{M}x_i^4$
Peak Value	$P_x = \|\max(x)\|$
Peak to Peak Value	$PP_x = \|\max(x)\| + \|\min(x)\|$

PSD	$\varphi(\omega) = \left\| \frac{1}{\sqrt{2\pi}} \sum_{i=-\infty}^{\infty} x_i e^{-i\varpi n} \right\|^2$
Signal Energy	$E = \int_0^F \varphi(f) df$
Max HT Amplitude	$HT_{max} = \max\left(\frac{1}{\pi} \int_{-\infty}^{\infty} \frac{x(\tau)}{\tau - t} d\tau\right)$
HT Area	$A = \int_0^F HT df$

The extracted statistic features are shown in Figure 50. It is noted that these features can provide rough trends of structural degradation. However, these feature trends are not constant and it is difficult to estimate which features are more sensitive to impact damage. In addition, some of these original statistical features repeatedly demonstrate similar sensing information. Briefly stated, advanced techniques are required to extract more robust features and reduce the redundant features.

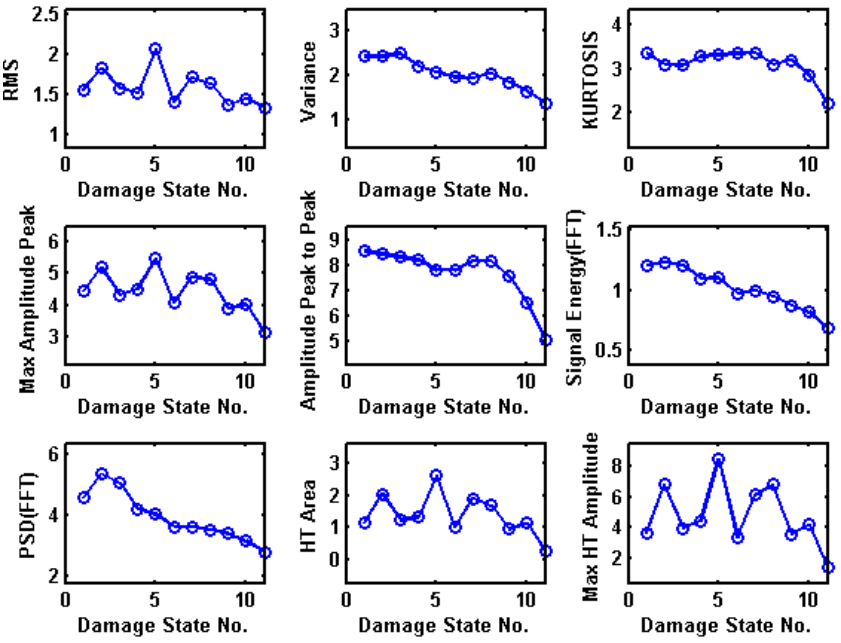

Figure 50. Statistical features extracted from time and frequency domains

For the purpose of comparison, both the KPCA and PCA techniques are applied to the original statistical features $\{\vec{F}_m | \, m = 1 \ldots 9\}$. Every ten feature vectors are combined to build the feature matrix for the PCA and KPCA analysis. The feature matrix can be expressed as $\vec{F}_{mn} | \, m = 1 \ldots 9, n = 1 \ldots 10$, where m is the number of feature in each feature vector and n is the number of observations in each feature matrix.

The key issue in the KPCA algorithm is to transform the input features into a high dimensional feature space using nonlinear mapping. In this paper, the nonlinear mapping is conducted using the kernel function as shown in Equations 44 and 45. The first three principal components using KPCA and PCA methods are extracted at three states: the healthy state, the state following the fifth impact, and the state following the tenth impact. The cluster analysis results are shown in Figure 51 and Figure 52. The traditional PCA algorithm can extract and select features in the original input space, but cannot handle the

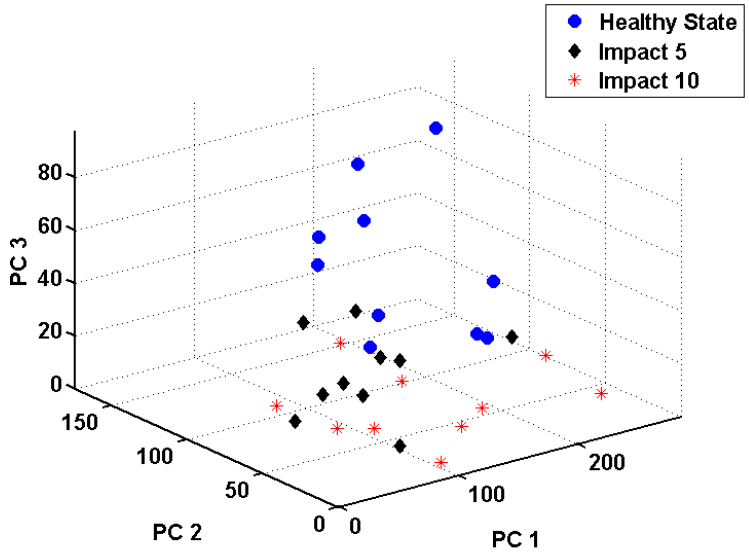

Figure 51. Typical PCA features for healthy state, impacts 5 and 10

nonlinear relationships in the input features well. This indicates the lack of a clear separation between damage states using the PCA method. However, the KPCA representations in Figure 52 show clear separation among the three states. This demonstrates that KPCA can extract the higher order and nonlinear information that is more useful to demonstrate the effects of low velocity impact to the composite wing. Further, more robust damage quantification results can be obtained when the KPCA features are used.

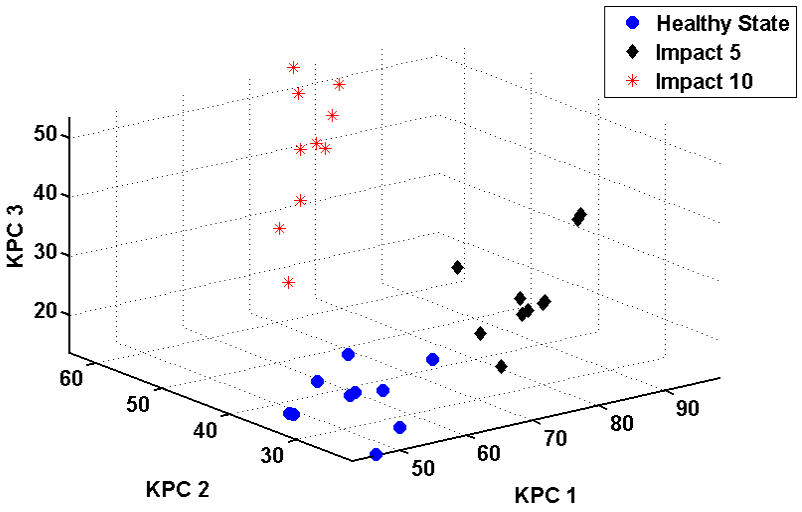

Figure 52. Typical KPCA features for healthy state, impacts 5 and 10

The Mahalanobis distance based damage index, Equation 47, is used to quantify the extent of the low velocity impact damage. Ten KPCA feature sets at each damage state are obtained using the developed algorithm. The average features calculated from these feature sets are used as the input to quantify the damage. As shown in Figure 53, the low velocity damage propagates almost at a constant rate during the first eight impact events. However, the damage propagation is much faster during the last two impacts. This can be explained as follows. During the first eight impacts, the impact head hits a

new section on the wing surface, as shown in Figure 53, and since each impact introduces the same amount of energy into the wing, the propagation rate is consistent. The last two impacts were between multiple previous impact sections. Although there was no visible surface damage shown after the first eight impacts, the wing foam cracked and there were delaminations between the composite skin and foam. When these areas were further impacted the damage severity increased significantly even though the impact energy was still the same. This illustrates the critical nature of repetitive low velocity impact damage on composite wing, which may lead to catastrophic failure.

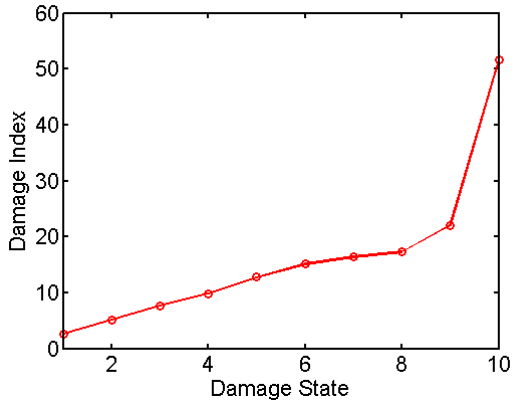

Figure 53. Damage quantification using Mahalanobis distance based damage index

5.5. Conclusions

An impact damage monitoring and quantification methodology using KPCA algorithm is developed in this chapter. Statistical features are extracted from the sensor signals in the time and frequency domains. Choosing an appropriate kernel function, the statistical features are mapped to a high dimensional space for feature clustering. The kernel eigenvalues obtained from the original statistical feature datasets represent the damage propagation caused by impacts, which are considered as new feature datasets for

damage quantification. Redundant features are compressed during the KPCA analysis. A novel Mahalanobis distance based damage index is defined to quantify the impact damage.

Low velocity impact experiments were conducted on a sandwich composite wing to validate the developed methodology. MFC based active sensing was used for damage detection. After each impact, flash thermography images were taken to detect the presence of sub-surface (invisible) damage. A wing autopsy was conducted after the last impact to examine the exact nature of the damage in the composite wing. Multiple types of damage including fiber breakage, foam cracking, delaminations in the composite skin, and delaminations between composite skin and foam core, were detected. By studying the MFC sensor data, the damage quantification results show steady structural degradation after the initial eight impacts, followed by rapid damage progression over the last two impacts.

Chapter 6

APPLICATION OF SHM TECHNIQUES TO ON-ORBIT SATELLITE BOOM STRUCTURES

6.1 Introduction

The integration of composites into spacecraft is challenged by the risk of damage initiation and propagation during storage, launch and service life. Elastically deployable composite booms are being developed for space utility. Matrix cracks are considered a primary form of damage caused by packaging prior to launch. However, while on orbit, most damages are induced by the environmental effects on the polymers. A well-developed structural health monitoring system will provide information for the dynamic control of the satellite and the condition of the deployable mechanisms on the space vehicle. A structural health monitoring methodology, based on the system identification techniques, is proposed to identify the structural degradation in laminated composite booms. Non-destructive evaluation techniques, frequency response analysis and ARX input models are used to approximate the transfer functions between input and output sensing signals. Structural degradation is identified by examining the change of transfer functions at different storage states. A single-input-single-output approach is adopted in this paper. The proposed methodology is validated through experimentation where matrix cracking is gradually induced by packaging the sample.

Advanced carbon/epoxy composites have been widely used for a variety of structural components in spacecraft due to their light weight, dimensional stability, and optimized mechanical properties (Fortescue et al., 2006). On-orbit satellite systems

operate in a harsh environment and the structural degradation of composite components can be caused by various sources such as atomic oxygen, ultraviolet (UV) radiation, proton and electron radiation, vacuum, and thermal cycling (Reilly and Terrance, 2006; Arritt et al., 2007; Arritt et al., 2008). Although the coefficient of the thermal expansion (CTE) of composites is commonly near zero and significantly less than typical aluminum, composites are just as vulnerable to the environmental influences. High vacuum pressure can lead to material outgassing, UV can deteriorate the surface matrix and discolor the surface changing the thermal performance, and debris can shatter supports, as was the case for the Cerise microsatellite that had a catalogued item locally vaporized by impact on its Earth pointing boom (Harland and Lorenz, 2006). Like most space mishaps, the system was recoverable, but difficult to diagnose. The mechanical behaviors of polymeric matrix materials have been comprehensively addressed by Yekani Fard et al. (2011a, 2011b, 2011c, 2012).

Damage in composite satellite structures, such as matrix cracks and matrix-fiber debonding, causes the degradation of structural stiffness and can affect the dynamic response of the satellite system during maneuvers such as slewing or deployments. Structural degradation needs to be monitored to update the dynamic control system of the spacecraft. Developing a SHM system for monitoring the flexible structures of a satellite, such as the composite booms, will allow the satellite guidance, navigation, and control (GN&C) systems to incorporate any quantified stiffness degradation values into future functions. A properly designed SHM system will be able to detect, classify, localize damage and determine if the composite components of the satellite will continue to

perform safely and sufficiently. Price et al. (2003) developed an integrated health monitoring system for real-time sensing of impact damages in aerospace vehicles using piezoelectric Polyvinylidene Fluoride (PVDF) transducers based passive sensing and a self-organizing approach. Prosser et al. (2004) compared a variety of sensor types, such as fiber optic sensors, carbon nanotube sensors, and acoustic emission sensors, and reported the data processing techniques for the sensor placement optimization and the damage identification of composite components in space vehicles. Zagrai et al. (2010) detected and located loose bolts in complex space structures with a large number of bolted joints using the embedded ultrasonic acoustic-elastic method and the integrity of the bolted joint was evaluated by the stress-induced phase shift in the recorded elastic wave signals. However, few on-orbit influences are considered in the previous literature. A SHM system for on-orbit composite components needs to be used not only to determine the status of a satellite structure prior to launch but also for the on-orbit detection of damage. This can be seen in the case of the deployable antenna of the Mars Advanced Radar for Subsurface and Ionosphere Sounding (MARSIS) project on Mars express. The deployable antenna was made with glass fibers and collapsed in a manner to deploy using stored elastic energy. When it was time to deploy on-orbit, the risk was considered unacceptable and it was never released due to the concerns of deployment and how guidance and other functioning instrumentation would be impacted along with the inability to diagnose any conditions after deployment (Harland and Lorenz, 2006).

Although significant research on SHM of composites has been reported in the last decade, most of the published work focuses on the macro scale damage, such as

delamination and impact damage. Well-developed SHM techniques, including acoustic emission methods, have also shown to be effective in detecting macroscale damage in composites. However, the dominant structural degradation mode induced into a flexible composite boom prior to launching is matrix cracking. As shown in Figure 54, the carbon fiber reinforced plastics (CFRP) boom in the stowed configuration and the fully deployed solar sail is developed by the German Aerospace Center (DLR). Both the CFRP booms and solar sail membranes are used as critical structural components of the propulsion system for the Synthetic Aperture Radar (SAR) satellites. When the solar sail membranes and CFRP boom are packed into a small volume, matrix cracking is introduced to the boom structure due to the flattening and wrapping procedure. The detection of matrix cracking in composites requires more sensitive and reliable techniques. However, research in monitoring micro matrix cracks in composites is still in its infancy. In addition, most current non-destructive evaluation (NDE) techniques, such as x-ray, ultrasonic scan, and radiography, are costly, time-consuming, labor-intensive, and do not satisfy the responsive ground-base or on-orbit service. A SHM system that automatically monitors and detects on-orbit degradation of composite components is required for the

(a)  (b) 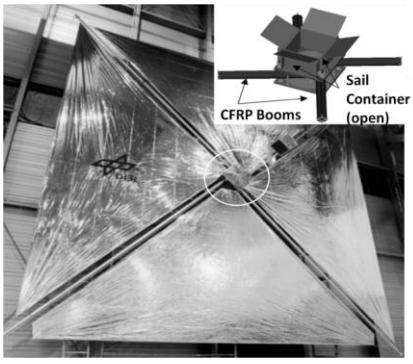

Figure 54. (a) Deployable DLR CFRP boom and (b) Solar sail (Leipold et al., 2003; 2005)

reliable use of composite satellite structures.

System identification techniques have been used for structural evaluation of both metallic and composite structures to interpret data and extract diagnostic features. The extraction of damage-sensitive features from experimental measurements or simulation, and the statistical analysis of these features determine the current state of the system's health. Nonparametric models, such as frequency response methods, and parametric models, such as state-space models, are the two main approaches for system identification techniques. Park et al. (2009) used an inverse method for identifying the damage location and the impact force time history on composite plates using the state-space estimation techniques. The transfer function at any point was constructed by interpolating four neighboring known transfer functions. However, the actual damage induced in the composite samples by the impact loading was not clarified. Different types of structural damage, such as fiber breakage and delamination, can be introduced by different impact velocities and energies. The nature of impact damage introduced into their composite specimens needs to be demonstrated and the method also needs to prove functionality on complicated structures. Sohn et al. (2001) presented a damage feature extraction approach by combining the Auto-Regressive (AR) and Auto-Regressive with eXogenous input (ARX) models and applied the two techniques to fiber optic strain gauge data obtained from two different structural conditions of a surface-effect fast patrol boat. Although the damage features were identified by combining the two models, the procedure needs to be examined with composite structures and under more operational conditions before it can be applied as a SHM system for composite components. Mohanty

et al. (2009) proposed an unsupervised system identification based techniques to estimate the time-series fatigue damage states for metallic materials. To estimate the nonparametric damage state, ultrasonic broadband active sensing and correlation analysis were used. In most cases, the system identification techniques showed acceptable performance for visible damage, such as cracks in metal and delamination in composites.

In this chapter, a system identification-based SHM technique is proposed to quantify the structural degradation of the composite booms used in satellite applications, as shown in Figure 55. Low frequency broadband sweep excitations are applied to the modeled samples using MFC transducers. Structural degradation and changes in dynamic response of the samples are determined from the frequency response of measured actuator and sensor signals. The transfer functions of single-input-single-output (SISO) approach are estimated using the ARX model to identify the damage levels. A damage index is defined to describe the structural degradation condition in the booms. Both local

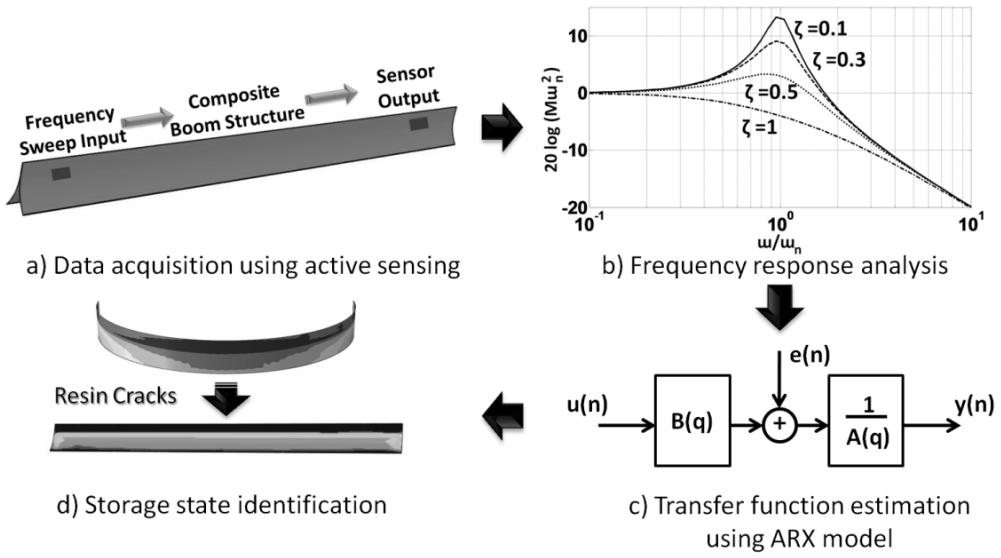

Figure 55. SHM of composite booms based on a system identification approach

and global structural degradation estimations are completed by using the MFC data collected from different positions. The proposed method has been validated experimentally.

6.2 SHM Framework for a Satellite Structure

6.2.1 Frequency Response Method of System Identification

The frequency response method for system identification characterizes the response of the composite boom subject to a sweep excitation. The frequency response is estimated using spectral analysis and can be expressed in a cross-correlation function and auto-correlation function. For time domain input signal,$x(t)$, and output signal, $y(t)$, the spectral densities, $S_{yx}(j\varpi)$ and $S_{xx}(j\varpi)$, of the relevant measured input and output are written as (Klein and Morelli, 2006)

$$S_{yx}(j\varpi) = \tilde{y}(j\varpi)\tilde{x}^*(j\varpi) \tag{48}$$

$$S_{xx}(j\varpi) = \tilde{x}(j\varpi)\tilde{x}^*(j\varpi) \tag{49}$$

where $\tilde{x}(j\varpi)$ and $\tilde{y}(j\varpi)$, are the finite Fourier transforms of the relevant measured input and output, and $\tilde{x}^*(j\varpi)$ is the conjugate of $\tilde{x}(j\varpi)$.

By applying the finite Fourier transform to measured input and output data, an estimate of the frequency response function can be written as

$$G(j\varpi) = \frac{S_{yx}(j\varpi)}{S_{xx}(j\varpi)} = \frac{\tilde{y}(j\varpi)\tilde{x}^*(j\varpi)}{\tilde{x}(j\varpi)\tilde{x}^*(j\varpi)} \tag{50}$$

where the frequency response function, $G(j\varpi)$, is a complex vector. Both input-output amplitude ratio and phase shift are considered. The amplitude ratio, $R(\varpi)$, and phase, $\phi(\varpi)$, can be expressed as

$$R(\varpi) = \sqrt{\{\mathrm{Re}[G(j\varpi)]\}^2 + \{\mathrm{Im}[G(j\varpi)]\}^2} \tag{51}$$

$$\phi(\varpi) = \tan^{-1}\{\frac{\mathrm{Im}[\mathrm{G}(j\varpi)]}{\mathrm{Re}[\mathrm{G}(j\varpi)]}\} \tag{52}$$

The frequency response method constitutes a describing function which linearly characterizes the behavior of the input-to-output MFC transducers. Once the transfer function of the MFC transducers changes due to induced matrix cracking, the Bode plot of input-output sensor measurements will indicate the change of the transfer function and provide guidance for the future construction of a system transfer function model. Further details are explained later in the paper.

6.2.2 Transfer Function Estimation Using ARX Model

In this study, an ARX model is utilized to estimate the transfer function of the composite active sensing system. Traditional autoregressive (AR) and autoregressive moving average (ARMA) models are fitted to the sensing signals (output signals) and do not consider the excitation signals (input signals). ARX model considers the excitation signals as additional information in a time series model. The input-output model can be reasonably estimated using the ARX model and the linear least squares method (Yoshida and Kumar, 1999; Yang and Makis, 2010). As a typical example of the "black box" model, the model is widely used due to its simplicity. Ignoring the estimation error, the ARX model which describes the relationship between input, $x(t)$, and output, $y(t)$, is shown in Equation 53 (Juang, 1994)

$$\begin{aligned} &y(t) + a_1 y(t-1) + \cdots + a_n y(t-n) \\ &\quad = b_1 x(t-1) + \cdots + b_m x(t-m) \end{aligned} \tag{53}$$

where a_i and b_j are the parameters of the ARX model, n is number of poles and m is number of zeros. Once m and n are calculated, the ARX can be written as ARX (m, n) model. The model assumes that the sampling interval is uniform in the time domain. In

order to determine the next output value given by previous observation, it is easier to write Equation 53 as

$$y(t) = -a_1 y(t-1) - \cdots - a_n y(t-n) + b_1 x(t-1) + \cdots + b_m x(t-m) \tag{54}$$

The parameters of the ARX model, a_i and b_j, are calculated from the sensor measurements ,$x(t)$and $y(t)$, using the linear least squares method. For a more compact notation, these adjustable parameters can be written in a vector form

$$\theta = [a_1 \ \cdots \ a_n \, b_1 \ \cdots \ b_m]^T \tag{55}$$

and the previous input-output measurement can be written as

$$\varphi = [-y(t-1) \ \cdots \ -y(t-n) \ \ x(t-1) \ \cdots \ x(t-m)]^T \tag{56}$$

According to Equation 56, the output estimation of the ARX model is

$$y(t) = \varphi^T(t)\theta \tag{57}$$

It is noted that the calculation of the next output measurement from previous data in vector φ depends on all the parameters in vector θ. The calculated value, $\hat{y}(t|\theta)$, is different from the real measurement, $y(t)$.

$$\hat{y}(t|\theta) \ = \varphi^T(t)\theta \tag{58}$$

All the unknown parameters in vector θ are calculated using the least squares method. From the recorded input-output measurement, R^N , the unknown parameters can be calculated by minimizing the error, $E(\theta, R^N)$, between the real output measurement, $y(t)$, and the calculated output, $\hat{y}(t|\theta)$. Here,

$$R^N = [x(1) \ \ y(1) \ \cdots x(N) \ \ y(N)] \tag{59}$$

$$E(\theta, R^N) = \frac{1}{N}\sum_{i=1}^{N}(y(t) - \hat{y}(t|\theta))^2 = \frac{1}{N}\sum_{i=1}^{N}(y(t) - \varphi^T(t)\theta)^2 \tag{60}$$

Set the derivative of $E(\theta, R^N)$ to zero,

$$\frac{d}{d\theta}E(\theta, R^N) = \frac{2}{N}\sum_{i=1}^{N}\varphi(t)(y(t) - \varphi^T(t)\theta) = 0 \tag{61}$$

resulting in,

$$\sum_{i=1}^{N}\varphi(t)y(t) = \sum_{i=1}^{N}\varphi(t)\varphi^T(t)\theta \tag{62}$$

Because $\varphi(t)$ has been defined by the previous input-output measurement, all the parameters for the ARX model can be calculated using Equation 62

$$\theta = \left[\sum_{i=1}^{N}\varphi(t)\varphi^T(t)\right]^{-1}\sum_{i=1}^{N}\varphi(t)y(t) \tag{63}$$

The goal of system identification is to obtain a transfer function that predicts the output using input of the system reliably. From a given set of experimental data, the modeled data, $\hat{y}(t|\theta)$, is compared with the experimental data, $y(t)$, to minimize the error between the two data sets. Once θ is calculated, the transfer function can be obtained from Equation 57.

6.2.3 Structural Degradation Identification Using Damage Index

The accuracy and sensitivity of the defined damage index is critical for identifying matrix cracks in composites. Ideally, a composite structure without damage can be modeled as a linear system. However, composite structures present more nonlinear properties when non-visible damages, such as matrix cracks, are introduced (Polimeno and Meo, 2009; Van Den Abeele1 et al., 2000a, 200b). Although the ARX model can be expressed as shown in Equation 53, an error term, $\varepsilon(t)$, should be introduced to this model for the reconstruction accuracy. The modified ARX model can be expressed as

$$y(t) + a_1 y(t-1) + \cdots + a_n y(t-n) = b_1 x(t-1) + \cdots + b_m x(t-m) + \varepsilon(t) \tag{64}$$

It is assumed that the error between the measurement and estimation obtained by the ARX model is caused mainly by the nonlinear properties of matrix cracking in composites. The estimation error becomes larger when more nonlinearities due to matrix cracks are introduced. A clear definition of estimation error, ε_s, at storage state, *s,* is expressed as:

$$\varepsilon_s = y_s(t) + \sum_{i=1}^{n} a_{i,s} y_s(t-i) - \sum_{j=1}^{m} b_{j,s} x_s(t-j) \tag{65}$$

where $a_{i,s}$ and $b_{j,s}$ are the parameters of the ARX model at storage state, *s*, $y_s(t-i)$ $(i = 0,1,\cdots,n)$ are the sensor output measurements at storage state, *s*, and $x_s(t-j)$ $(j = 1,2,\cdots,m)$ are the sensor output measurements at storage state, *s*. By carefully choosing the order of the ARX model, a damage index can be defined as:

$$DI_s = \sqrt{\frac{[\varepsilon_s - \varepsilon_0]^2}{{\varepsilon_0}^2}} \tag{66}$$

where ε_0 is the estimation error for the referred initial storage level. When the healthy state of the structures is known, ε_s is the s^{th} storage state with respect to the healthy state (*s*=0). However, when the healthy state is unknown, the defined damage index, DI_s, can still be used to compare the later storage state with the reference storage level (the first available storage state).

6.3 Experimental Setup

To validate the system identification based SHM framework, a flattening and wrapping experiment was performed on composite booms, which were supplied by the

Air Force Research Laboratory, Space Vehicles Directorate (AFRL/RVSV). The materials used for the composite booms are CFRP in uni-directional tape and plain weave fabric forms, both using Hexcel® IM7 fibers and M72 resin. A boom is composed of two flanges. The cross section of the boom is shown in Figure 56. The stacking sequence of each flange is [0° tape/0° tape/ ±45° weave/ 0° tape/ 0° tape] (0° is the long axis of the boom). These two laminates overlap at the ridge to form a $[0°/ 0°/ \pm 45°/ 0°/ 0°]_s$ stacking sequence. The boom specimen was instrumented with four MFC transducers (Smart Material Corp., Model: M 2814 P1), as seen in Figure 57. In order to obtain proper bonding conditions between the boom and the sensors, the sample surface was prepared with abrasive paper and cleaned with cotton tipped applicator. Stewart-MacDonald super glue (Model: 20-X) was used as the adhesive. Outgassing properties of this particular adhesive are not critical at the stage of research, but consideration should be addressed when applied to systems containing optical payloads where outgassing is a concern.

Figure 56. Cross section of AFRL composite boom

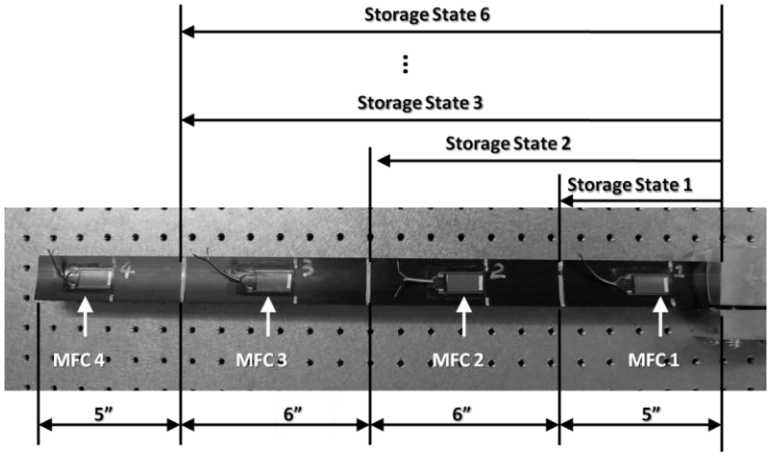

Figure 57. Composite boom specimen

The primary source of degradation to the boom structure occurs during the flattening and wrapping process of the boom around a hub that is used to store the boom prior to deployment. The extent of structural degradation, due to wrapping the boom around the hub, can be critical in the system response depending on the size of the deployable relative to the system. As the stiffness changes, due to matrix microcracking, the system's response will be affected. The structural degradation incurred by storing the structure has been simulated experimentally using a wrapping fixture, as shown in Figure 58. The wrapping fixture consists of a 14″ diameter hub around which the boom sample is wound. This fixture was constructed to test 24″ samples. The boom was clamped as shown in Figure 58 (a) with a 2″ long clamping surface, flattening the clamped end of the boom to the hub. The boom was then wrapped taut around the center hub and clamped at the preset location. The rate of wrapping was approximately 1 inch per second, which was necessary to ensure the boom flattened properly and to maintain as little gap as possible from the center hub. Similar wrapping and deploying rates were used by the CFRP boom and solar sail membrane of the SAR satellites developed by DLR [10].

(a)

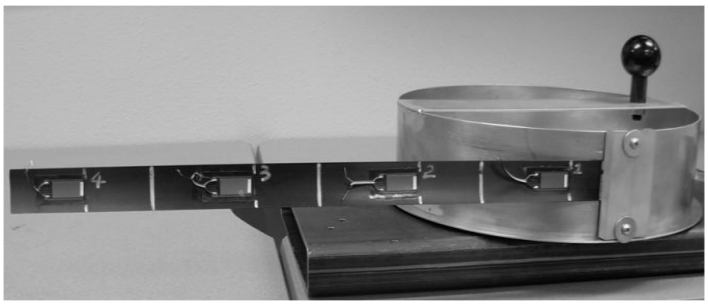

(b)

Figure 58. Composite boom in the wrapping machine at (a) Initial position of composite and (b) Final wrapped position

The storage states were generated six times by wrapping the boom specimens to different arc lengths, as shown in Figure 59. Before any damage was introduced to the boom specimen, vibration based modal analysis test and MFC based active sensing baseline data were collected. State 1 was wrapping the specimen around the hub to introduce matrix cracks up to the section indicated (arc length 5”). The boom specimen was clamped at the preset location for 30 seconds before being deployed to its initial position. Both modal analysis and MFC active sensing data were collected after the deployment. In the second step, both states 1 and 2 were used (arc length 11”) and in step 3 to 6, states 1, 2 and 3 were all used (arc length 17”) to introduce matrix cracks to the boom structure. The sensor data collecting procedure used for state 2-6 was the same as used for state 1. At the end of each state the boom specimen was fully deployed to the original position. Both modal analysis and active sensing were conducted.

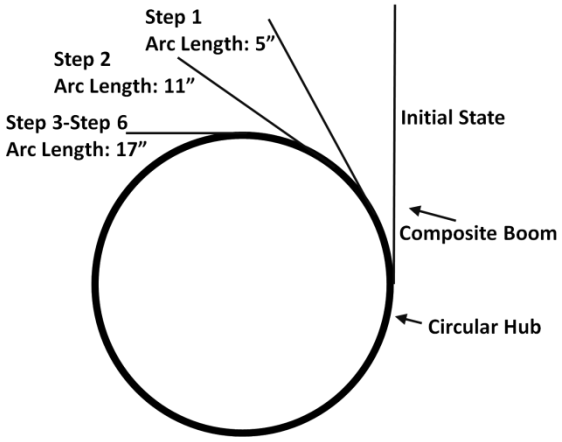

Figure 59. Six storage states for the composite boom flattening/wrapping test

Current NDE techniques, such as flash thermography and ultrasonic scan, can hardly detect matrix cracking in composites. However, matrix cracking and structural stiffness degradation can be detected by the shift of resonant modes using vibration modal analysis. In order to validate the matrix cracking induced by flattening and wrapping of the boom, the first three resonant modes were measured experimentally through a scanning head laser vibrometer coupled with a vibration shaker. The experimental setup of vibration modal analysis is shown in Figure 60. Three steps were used to ensure the laser points were in the exact locations during each scan. First, the length from the free end of the boom to the custom made fixture was the same in each scan. Then, the sample was clamped at the same position on the shaker according to the marks drawn on the shaker fixture. Finally, the vibrometer scan head was fixed and the position of boom on the shaker was adjusted slightly so that each scan was started from the same point, as shown in Figure 60. The shift of first resonant mode can be seen in Figure 61. The first resonant mode shows the clearest shift after matrix cracks are induced into the sample. After flattening and wrapping the sample five times, the first

resonant mode stops decreasing, which means matrix cracking damage ceases to increase in the composite boom sample.

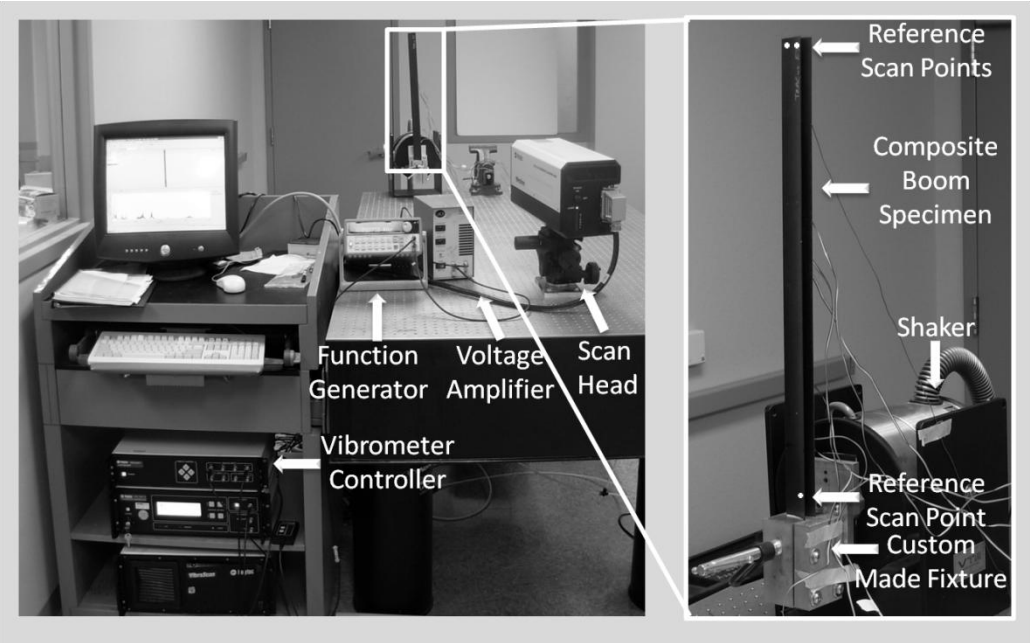

Figure 60. Experimental setup of vibration modal analysis

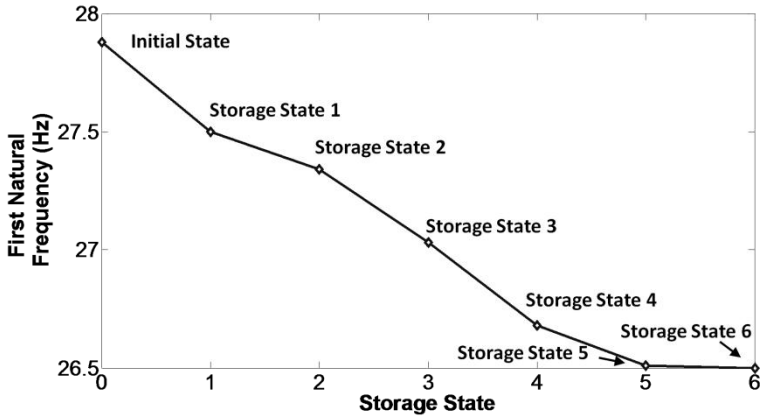

Figure 61. Resonant mode shift

A 48 channel DAQ was used for active sensing using the MFC transducers. A broadband sweep signal with frequency varying from 10 Hz to 1 kHz is used for active sensing of the MFCs and the excitation signal collected from MFC 1 is shown in Figure

62 (a). A representative sensor signal from MFC 4 at the initial condition is shown in Figure 62 (b). The power spectral density plots of both the input and output signals at the healthy and six storage states are shown in Figure 63. With constant input signals, the differences of the power spectral density at different storage states are not clear. The frequency response method and the ARX model are used for more sensitive and robust structural degradation identification.

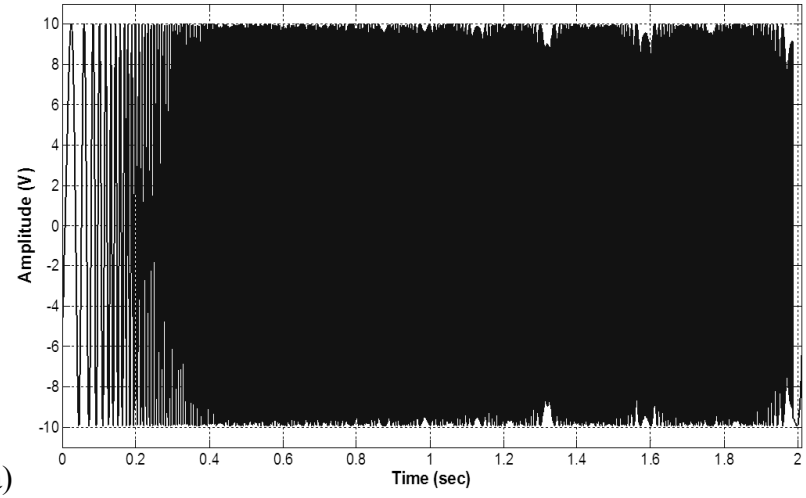

(a)

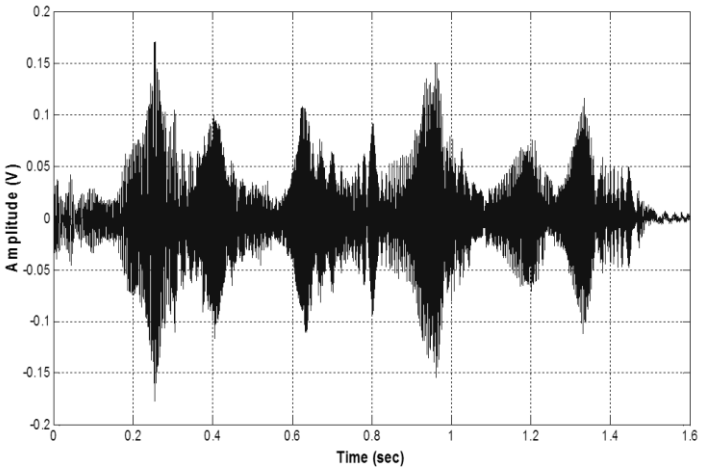

(b)

Figure 62. (a) Broadband chirp input signal for MFC 1; (b) Measured output signal for MFC 4

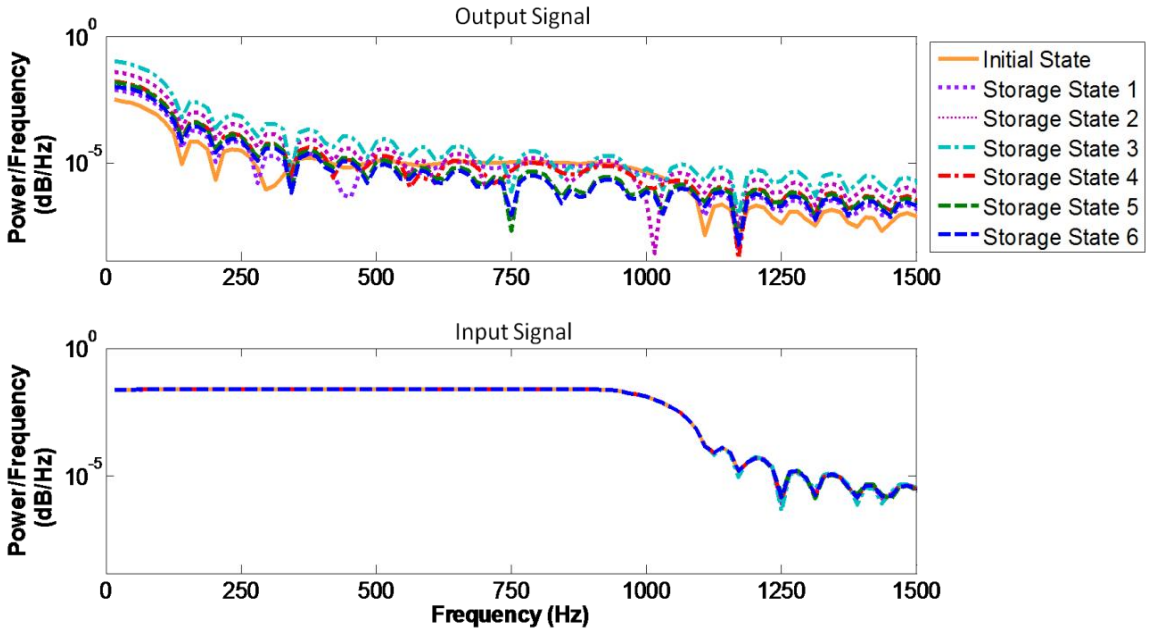

Figure 63. Power spectral density of input MFC 1 and output MFC 4 signals at different storage states

6.4 Results and Discussion

6.4.1 Frequency Response Method of Input-Output MFC Transducers

The frequency response method can be used to analyze the input/output relationship and to non-parametrically understand the key aspects of the system before moving to the more complex parametric modeling stages. The information obtained is the basis for identifying parametric transfer function models. In this paper, a SISO frequency response method is used to analyze the change of transfer functions at different storage states. The input signals are collected from MFC 1 and output signals are collected from MFC 4. The sensor input/output signals cover the entire damage area and can be used for global damage characterization. The plots for amplitude and phase versus frequency, which can be calculated using Equation 48-52, are showed in Figure 64.

In Equation 50 the frequency response is determined from the ratio of the cross-correlation spectrum estimate, $S_{yx}(j\varpi)$, and auto-correlation spectrum estimate, $S_{xx}(j\varpi)$. As described before, the amplitude change of the frequency response at a relatively low frequency range (from 10 Hz to 200 Hz) is mainly caused by the presence of nonlinear properties when matrix cracks are introduced. The understanding of nonlinearity in damaged composite structures helps to choose a proper model for the transfer function estimation and design the damage index based on the estimated damage index.

The frequency response method provides an approach to select frequency ranges for the input/output pair to include only relevant data. As shown in Figure 64, the amplitude has a clear response at a low frequency range from 10 Hz to 200 Hz. The phase also has obvious responses in the same frequency range. This quick analysis helps to choose the frequency range, which provides useful data for the transfer function estimation.

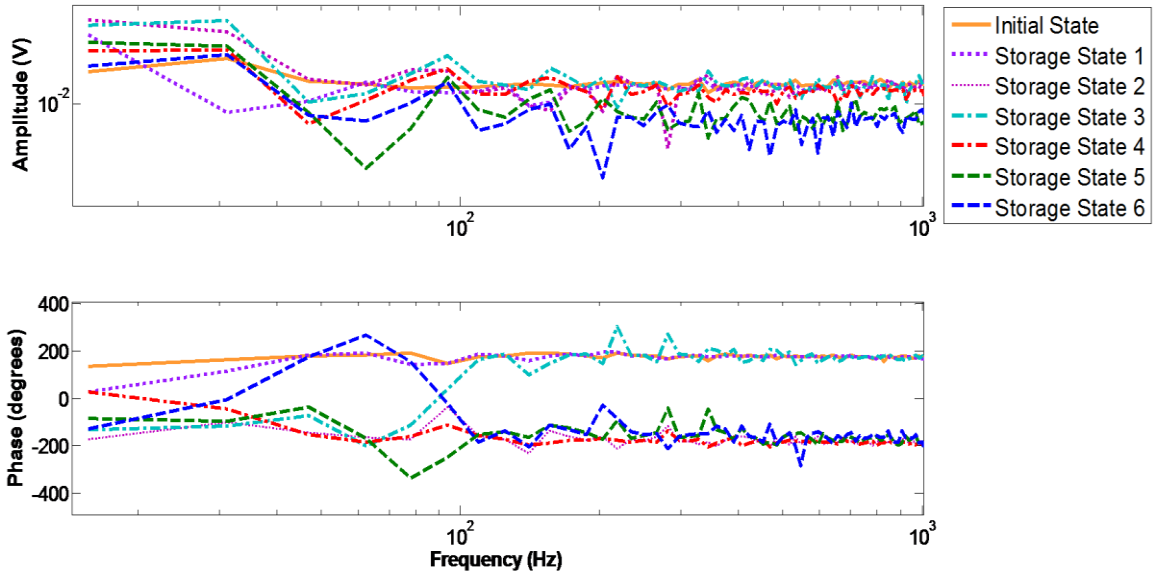

Figure 64. Frequency response of input/output signal measured from MFCs 1 and 4

A key aspect for the frequency response method is the direct and accurate identification of time delays. The linear relationship between the time delay, τ, and frequency response phase shift with frequency, ω (rad/s), is expressed as:

$$\delta = -\tau\omega \qquad (2)$$

where δ is the angle of phase shift at frequency, ω . From the frequency response plot shown in Figure 64, the phase shift after storage state 2 has a clear change in the frequency range of 10 Hz to 100 Hz, which indicates the change of time delay due to induced damage. It can be used as a feature to quickly demonstrate the existence of damage in the composite booms. This also indicates that the time delays are more sensitive in the specific frequency range as more damage is introduced. In the selected sensing frequency range, the velocities of the elastic waves are more sensitive to the change of structural stiffness which is caused by matrix cracking. The time delay feature is useful for transfer function estimation.

6.4.2 Transfer Function Estimation and Order Selection of ARX Model

By carefully choosing the order of the ARX model, SISO transfer functions can be estimated accurately and efficiently. As shown in Equation 65, the order of the ARX model is the sum of the order of output, *n,* and the order of input, *m*. The value of *m* and *n* can be different. The criterion of selecting the proper order number is to get the most reasonable estimation with the smallest order number. In order to find the optimized order number, a set of estimations is needed. Experimental measurements from MFC 1 and MFC 4 at the healthy state are used as input/output pair for the order analysis. The vertical axis in Figure 65, which is called the unexplained output variance, is the ARX

model estimation error for the number of orders shown in the horizontal axis. As the order number increases, the estimation error decreases. The sum of *m* and *n* is the main influence of the estimation error, but each value of *m* and *n* is also considered in order to get the minimum order number. Although the estimation accuracy can be improved with a high-order ARX model, the calculation cost increases dramatically. Ideally, by choosing an ARX model with an infinite order number, the estimation error can be completely removed. However, at the same time, the calculation cost will be infinitely high. After the order number increases up to 40, the slope of estimation error decreases dramatically. In this paper, the order of the ARX model is chosen as 40. The input order, m, and output order, n, need to be chosen. The goal is to minimize the sum of m and n and an ARX (28,12) is used for the ARX model.

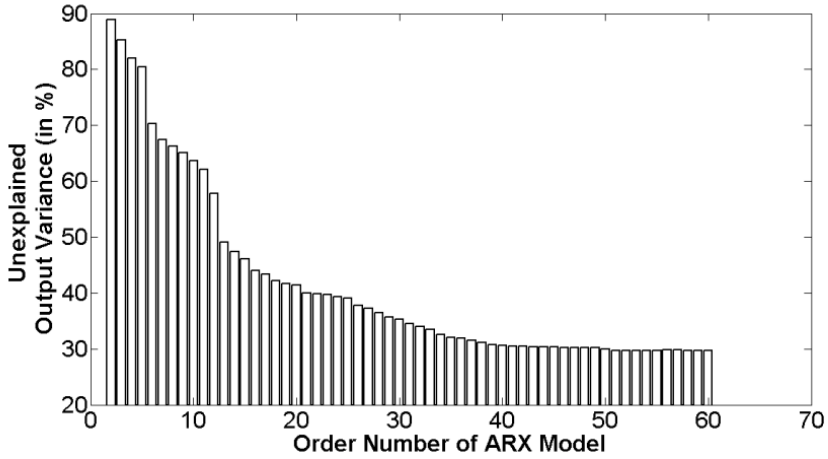

Figure 65. Estimation error with different order number

To check the estimation accuracy of the chosen model, one pair of experimental input/output signal collected from MFC 1 and 4 is used to train and validate the ARX (28, 12) model. The first half of the signal in the time domain is used to train the model and

the second half of the measured output is compared with the simulated output. The comparison of simulated output signal and experimental output signal can be seen in Figure 66. The experimental output signal can be accurately simulated by an ARX (28, 12) model.

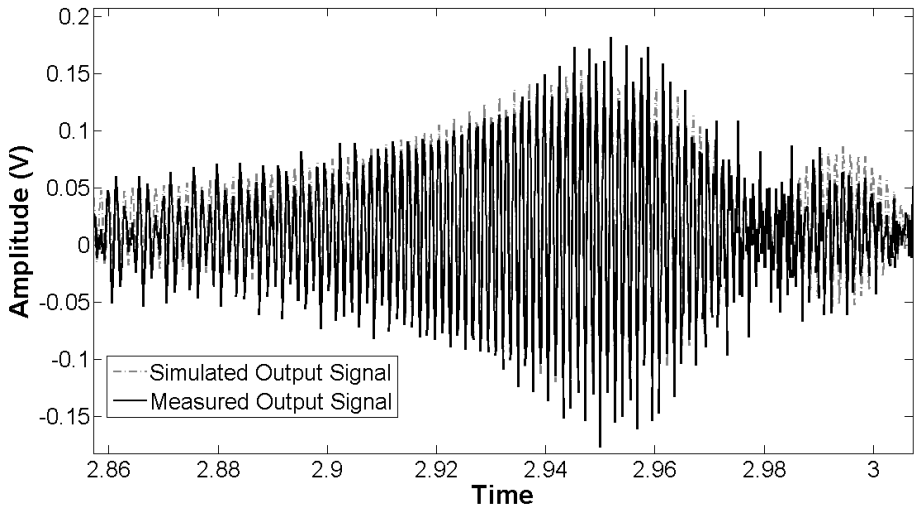

Figure 66. Comparison of simulated and experimental signals

6.4.3 Storage State Identification Using Damage Index

To evaluate the storage state of the entire composite boom sample subject to flattening and wrapping around the circular hub, both global damage estimation and local damage estimation are carried out. Global damage estimation uses MFCs 1 and 4, which cover the entire boom. The damage index obtained from global damage estimation shows the average damage condition along the entire boom. In Figure 67, the estimation starts from the healthy state at which the damage index is zero. However, as the flattening and wrapping induces matrix cracking into the boom, the damage index grows gradually. Global structural degradation estimation provides a clear trend of damage growth. It is noted that the damage caused by matrix cracking is introduced into the boom structure

gradually in the first five steps. However, an equilibrium state was detected in step 6. The feature trend obtained from damage index analysis can be validated by the vibration modal shift analysis, which is shown in Figure 61.

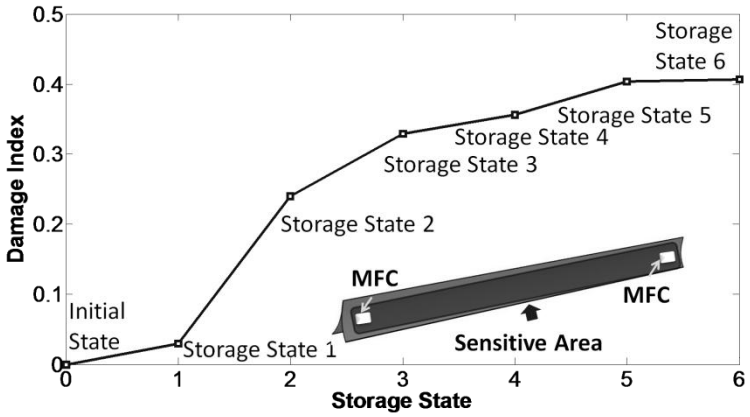

Figure 67. Global storage state estimation

More damage accumulates in the region between MFCs 1and 2, as this area has been wrapped six times during the experiment. The global structural degradation estimation cannot highlight such local storage states. In order to concentrate on the hotspot between MFC transducers, local damage estimation analysis is used. The local storage state estimation for the region between MFCs 1 and 2 is shown in Figure 68. This region is close to the clamping area of the boom specimen. The damage was induced since the step 1. In the first three steps, it is noted that the damage index has a clear increase which indicates the matrix cracking propagation during multiple flattening and wrapping procedures. However, the damage index of this region reaches an equilibrium state after step 4. Compared with the global estimation results in Figure 68Figure 70, the local storage state estimation is more sensitive to the matrix cracking damage. The reason is that the first two storage states contain both healthy and damaged sections in the

monitored area. This increases the estimation error, ε_0, at the initial state. The sensitivity of the damage index decreases as long as the reference becomes larger. Generally speaking, the damage index should provide more sensitivity for local storage state estimation.

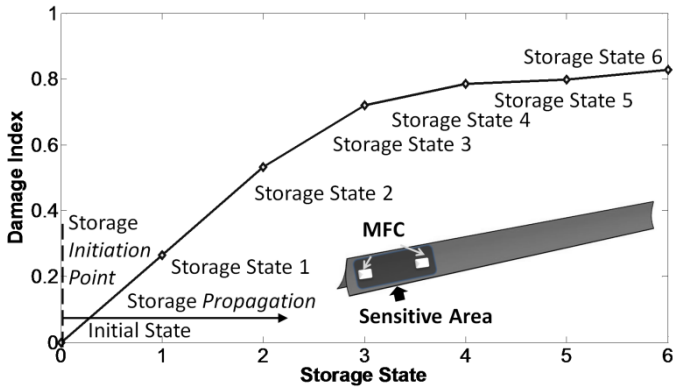

Figure 68. Local storage state estimation near MFCs 1 and 2

The local storage state estimation for the section between MFCs 2 and 3 is shown in Figure 69. As the region was not used in step 1, the damage index keeps constant in this step. It is noted that the matrix cracking originated in the section between MFCs 2 and 3 in step 2, 3, and 4. The clear feature trend can be seen in Figure 69. A similar trend for the damage parameters in the region between MFCs 2 and 3 can be seen as observed from the region between MFCs 1 and 2. An equilibrium state in the local section was achieved after flattening and wrapping the boom specimen three times and the local damage index does not show significant increase in step 5 and 6. For the region between MFCs 3 and 4, in step 1 and 2, the local damage index stays near zero as no severe matrix cracking was introduced, which also indicates a healthy local structural condition, as shown in Figure 70. The fist local matrix cracking was induced in step 3, and the damage

index features keep increasing in step 3, 4 and 5. However, because the boom specimen reaches an equilibrium condition, the damage index does not increase significantly in step 6. Because all the three local regions research the equilibrium state in step 6, the global damage index in this step also indicates equilibrium in this step.

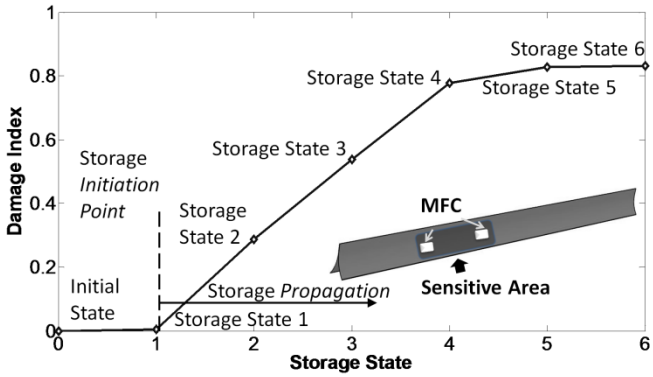

Figure 69. Local storage state estimation between MFCs 2 and 3

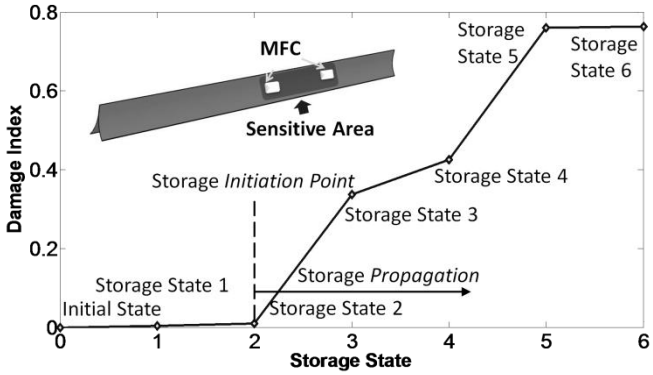

Figure 70. Local storage state estimation between MFCs 3 and 4

6.5 Concluding Remarks

The system identification techniques based structural health monitoring approach is proposed to investigate damage caused by matrix cracking in composite booms subject to flattening and wrapping around a circular hub. Both the frequency response method and Auto-Regressive with eXogenous input model are used to perform single-input-

single-output transfer function estimation and storage state identification. A flexible MFC actuator excites the boom specimen and response is captured by three MFC sensors using low frequency sweep signals to provide experimental input/output data. The frequency response method is used to non-parametrically analyze the relationship between input/output sensor signals and select a relevant frequency range. It also provides useful information for the transfer function analysis using the Auto-Regressive with eXogenous input model. The order of the Auto-Regressive with eXogenous input model is decided by considering both the estimation accuracy of the model and the calculation cost, and the Auto-Regressive with eXogenous input (28, 12) model is chosen. The order selection of Auto-Regressive with eXogenous input model is validated by comparing the simulated and experimental output signals. The damage index estimation using the residual error of the Auto-Regressive with eXogenous input model provides a clear trend of global damage growth because the composites will present nonlinear structural properties when matrix cracks are introduced. An equilibrium state for the composite boom was achieved after flattening and wrapping the boom specimens five times. Local storage state estimation is completed between each MFC sensor. The newly defined damage index is more sensitive in a localized region, but still provides decent global state estimation for the entire length of the composite booms. Results show that storage state estimation using an Auto-Regressive with eXogenous input model correlate with the trends and rate of decay seen from first natural mode shifts using vibration modal analysis techniques. This type of integrated setup is a more feasible method of acquiring dynamic characteristics on orbit as the size, weight, and power requirements are significantly less. For future

research, the detection of the equilibrium state can be used for the prelaunch quality assurance testing to ensure that a boom structure at equilibrium is inspected before launch. Further research is also needed for qualifying installation methods and hardware for space environment and analyzing the effect of space conditions on sensing performance.

Chapter 7

SUMMARY AND FUTURE DIRECTION

The research work presented in this dissertation is focused on the development of a general and comprehensive framework for SHM and prognosis of complex carbon fiber reinforced composite structures. The research objective is to detect, localize, and quantify the damage and to estimate the RUL of structures. The proposed framework aims to reduce labor costs by automating the process and enabling *in-situ* SHM. The methods developed have been tested on flat plates, stiffened panels, UAV wings and deployable satellite boom structures. This dissertation addresses the following issues:

1. Damage detection using Lamb wave techniques and time-frequency analysis approaches
2. Damage localization in flat and stiffened composite panels using GW techniques
3. Prognosis and RUL estimation of composites under uniaxial and biaxial fatigue loading
4. Impact monitoring and quantification on UAV composite wings
5. Application of SHM to deployable composite boom structures

The following sections summarize the work presented in this dissertation and suggest future research directions to further extend the application of SHM to real engineering composite structures, and eventually provide applicable techniques for aerospace engineering.

7.1. Damage Detection

A robust delamination detection using GW techniques and MPD algorithm based time-frequency analysis is presented. Lamb wave mode conversions were used to detect delaminations of different sizes in composite components with various mechanical properties and geometries. The MPD algorithm provides good time-frequency resolution and is capable of filtering noise from sensor signals. The computational efficiency was increased by reducing the MPD atom dictionary. The developed algorithm was experimentally validated using composite laminates and piezoelectric transducers in pitch-catch mode. The results obtained indicate that the methodology is capable of differentiating between multiple Lamb wave modes, including the symmetric, anti-symmetric, reflected, and converted modes. The use of the MPD technique resulted in significantly improved time frequency resolutions of the converted mode, which was then used to detect the existence of damage. The developed detection methodology was further tested using stiffened composite panels. A two-step strategy using pulse-echo and pitch-catch schemes was developed for detection of delaminations in stiffened composite panels. The pulse-echo scheme was able to rapidly detect the existence of delamination in the composite panels through identification of the converted modes caused by delaminations. The geometrically complex structure was then interrogated using a single PZT ring sensor. The pitch-catch scheme was able to detect delamination in the area between the PZT actuator and sensors. By studying the signal energy of the converted mode, the severity of the signal was also estimated.

For damage detection, Lamb wave signals recorded from the healthy panels are required in order to help define a reference state for the identification of the converted modes caused by delaminations. However, these reference signals may not always be available for the application. Therefore, developing unsupervised damage detection approaches for composite structures is one extension of the methods developed in this dissertation. Sandwich composite structures have also been widely used in aerospace applications, but currently these methods are still not fully mature to be used for the damage detection. A modification of the developed detection method for sandwich composite structures can result in significant impact on real time aerospace structure applications, such as airplanes and spacecrafts.

7.2. Damage Localization

Once the presence of damage is detected in composite structures, the next step is to determine its location of damage in order to provide necessary damage assessment and service. A localization method, which estimates the damage position by solving an optimization function subject to three nonlinear objective equations, was developed. This methodology required information of the sensor position, and the difference of ToFs of the converted modes caused by delamination between the master sensor and slave sensors. By comparing the sensor data with the baseline data collected from the healthy samples, converted modes resulting from the seeded delamination were identified. Using the MPD algorithm, the guided wave signals were represented in the time-frequency domain, and the difference of the ToF of the converted modes between master and slave sensors were calculated. The group velocities from the delamination to the two nearby PZT sensors

were assumed to be the same. Redundant sensors were placed on the surface of composite samples. Probabilistic confidence range estimation provides a 95% confidence range for the estimated delamination positions.

For future research, environmental effects should be taken into consideration before the application of localization method in real structures. The difference between ToFs of two nearby sensors can vary significantly due to temperature change; as a result, the environmental effects can severely decrease the accuracy of the algorithm. Another route for improvement is to incorporate the dispersive effects of GW into the MPD atom library. In this case, the signal decomposition accuracy will be significantly improved which will result in more accurate ToF calculation and damage position estimation. Increases in computational efficiency will also benefit from the implementation of an adaptive version of the MPD algorithm.

7.3. Damage Prognosis and RUL Estimation

In this dissertation, an integrated prognosis algorithm was developed to forecast damage states and estimate RUL of composite test structures. The prognosis model combined two modules: on-line damage state estimation and off-line damage state and RUL prediction. A damage index formulation was evaluated and used to extract fatigue damage states from real-time strain gage measurements. Based on the on-line estimated damage states, the second stage Gaussian process predictive model was used to forecasts future damage states and the corresponding remaining useful life. A good correlation exists between the predicted damage states and actual damage states. The accuracy of predicted states and RUL improved at later stages of fatigue life as more on-line

information or states became available to the predictive model. The prognosis model was validated for both uniaxial tensile fatigue and biaxial fatigue tests with composite specimens manufactured in-house.

The following several topics need to be addressed in the future research. Due to the unique fabrication procedures for CFRP composites, the material properties and structural performance may vary with slight fiber orientation changes. Therefore, before *in-situ* prognosis and RUL estimation can be achieved, advanced robust sensing techniques, physics based modeling, and prognosis mathematical algorithms need to be improved. The advanced sensing techniques should be robust to various loading conditions and environmental impacts. Physics based modeling can improve the current knowledge of composites structures, especially in the case of fracture and fatigue. Improved prognosis mathematical models can accurately study the degradation trend from previous structural information and more accurately predict future structural condition states. By combining these three aspects, future prognosis techniques will not only increase structural lifespan and reduce maintenance costs, but also result in "smart" composite structures.

7.4. Application of SHM to Aerospace and Space Vehicles

Since aerospace and space vehicles represent some of the most advanced technologies in the world, integrating applicable SHM techniques in composites used in airplanes and spacecrafts will be beneficial in achieving the goal of overall structural integrity. This dissertation addressed the monitoring and quantification of impacts on UAV composite wings using the KPCA algorithm. Statistical features were extracted

from the sensor signals in the time and frequency domains, and were mapped to a high dimensional space for feature clustering through use of an appropriate kernel function. The kernel eigenvalues obtained from the original statistical feature datasets represented the damage propagation caused by impacts, which were considered as new feature datasets for damage quantification. Redundant features were compressed during the KPCA analysis. A novel Mahalanobis distance based damage index was defined to quantify impact damage. Low velocity impact experiments were conducted on a sandwich composite wing to validate the developed methodology. MFC based active sensing was used for damage detection. After each impact, flash thermography images were taken to detect the presence of sub-surface (invisible) damage. A wing autopsy was conducted after the last impact to examine the exact nature of the damage in the composite wing. Multiple types of damage including fiber breakage, foam cracking, delaminations in the composite skin, and delaminations between composite skin and foam core, were detected. By studying the MFC sensor data, the damage quantification results showed steady structural degradation after the initial eight impacts, followed by rapid damage progression over the last two impacts.

The investigation of SHM on satellite used deployable composite boom structures is a valuable endeavor for the future in space applications. In this dissertation, the system identification techniques based SHM approach was proposed to investigate damage caused by matrix cracking in composite booms subject to flattening and wrapping around a circular hub. Both the frequency response method and ARX input model were used to perform SISO transfer function estimation and storage state identification. A flexible

MFC actuator excites the boom specimen, and the response was captured by three MFC sensors using low frequency sweep signals to provide experimental input/output data. The frequency response method was used to non-parametrically analyze the relationship between input and output sensor signals and select a relevant frequency range. This also provided useful information for the transfer function analysis using the ARX model. The order of the ARX model was decided by considering both the estimation accuracy of the model and the calculation cost. The order selection of ARX model was validated by comparing the simulated and experimental output signals. The damage index estimation using the residual error of the ARX input model provided a clear trend of global damage growth because the composites presented nonlinear structural properties when matrix cracks were introduced. An equilibrium state for the composite boom was achieved after flattening and wrapping the boom specimens five times. Local storage state estimation was completed between each MFC sensor. The newly defined damage index was more sensitive in a localized region, but still provided reasonable global state estimation for the entire length of the composite boom. Results showed that storage state estimation correlated with the trends and rate of decay seen from first natural mode shifts using vibration modal analysis techniques. This type of integrated setup was a feasible method of acquiring dynamic characteristics on orbit as the size, weight, and power requirements were significantly less than traditional methods.

More fundamental research is required for the future integration of SHM in aerospace and spacecraft vehicles. The uniqueness of aerospace engineering is the first key issue. For example, the composite wings and fuselages for airplanes, such as the

Boeing Dreamliner and Airbus A380, have complicated lay-up sequences, coatings, shapes and geometries. To design efficient SHM systems to cover such large structures with high accuracy and low costs is a large challenge. Vibration and noise can also introduce a significant amount of error in both the sensor data and extracted damage features. Other issues including temperature effects, lighting, power supply, and risk assessment should be considered as a system instead of as an independent factor.

Finally, environmental factors also need to be considered in the development of advanced structural materials, designs, and sensing systems for SHM. Radiation, temperature control, and power supply are the three most obvious environmental issues. Research of SHM for the next generation of spacecrafts should carefully study these influences and fully demonstrate their impact before implementation.

REFERENCES

Adewuyi, A.P., Wu, Z. S., 2010, "Modal macro-strain flexibility methods for damage localization in flexural structures using long-gage FBG sensors," Structural Control Health Monitoring, Vol. 18, No. 3, pp. 341-360.

Aktas, E., Seaver, M., Nichols, J.M., Trickey, S.T., Davis, W.R., "The influence of low energy impacts on the static and dynamic response of a foam core composite wing," Journal of Intelligent Material Systems and Structures, Vol. 20, No. 11, pp.1351-1361, 2009.

Amaro, A.M., Reis, P.N.B., de Moura, M.F.S.F., Santos, J.B., "Damage detection on laminated composite materials using several NDT techniques," Insight - Non-Destructive Testing and Condition Monitoring, Vol. 54, No. 1, pp. 14-20(7), 2012.

Arritt, B., Buckley, S.J., Ganley, J.M., Welsh, J.S., Henderson, B.K., Lyall, M.E., Williams, A.D., Prebble, J.C., DiPalma, J., Mehle, G., Roopnarine, "Development of a satellite structural architecture for operationally responsive space", SPIE Smart Structures and Materials and Nondestructive Evaluation and Health Monitoring, San Diego, CA, March 2008.

Arritt, B., Kumar, A., Buckley, S.J., Hannum, R., Welsh, J.S., Beard, S., Qin, X., Wegner, P., "Responsive satellites and the need for structural health monitoring", SPIE Smart Structures and Materials and Nondestructive Evaluation and Health Monitoring, San Diego, CA, March 2007.

Aymerich, F., Staszewskib, W.J., "Impact damage detection in composite laminates using nonlinear acoustics," Composites Part A: Applied Science and Manufacturing, Vol. 41, No. 9, pp. 1084 – 1092, 2010.

Balmès, É., Basseville, M., Bourquin, F., Mevel, L., Nasser, H., Treyssede, F., "Merging sensor data from multiple temperature scenarios for vibration monitoring of civil structures," Structural Health Monitoring, Vol. 7, No. 2, pp.129-142, 2008.

Boerstra, G.K., 'A descriptive model for the fatigue behavior of fiber reinforced plastics', AE-Rotortechniek report no. D0003301, October 2005

Bond, I.P. and Farrow, I.R., 'Fatigue life prediction under complex loading for XAS/914 CFRP incorporating a mechanical fastner', International Journal of Fatigue, Vol. 22, pp. 633–644, 2000.

Büche, D., Schraudolph, N. N., and Koumoutsakos, P., 'Accelerating evolutionary algorithms with gaussian process fitness function models,' IEEE Transactions on Systems, Man, and Cybernetics, (Special Issue on Knowledge Extraction and Incorporation in Evolutionary Computation—Part C), vol. 35, no. 2, pp. 183–194, 2005.

Cao, B., Shen, D., Sun, J.T., Yang, Q., Chen, Z., 2007, "Feature selection in a kernel space," Proceedings of the 24th international conference on Machine learning, pp. 121-128, June 20-24 Corvalis, Oregon.

Coverley, P.T., Staszewski, W.J., 2003, "Impact damage location in composite structures using optimized sensor triangulation procedure," Smart Materials and Structures, Vol. 12 (5), pp. 795-803.

Das, S., Kyriakides, I., Chattopadhyay, A., Papandreou-Suppappola, A., Monte Carlo matching pursuit decomposition method for damage quantification in composite structures, Journal of Intelligent Material System and Structures, Vol. 20, pp 647-658, 2009.

Degrieck, J. and Van Paepegem, W, 'Fatigue Damage Modeling of Fiber-Reinforced Composite Materials: Review,' Applied Mechanics Review, Vol. 54, Issue 4, pp. 279-300, Jul. 2001.

Doebling, S., Farrar, C.R., Prime, M., A summary review of vibration-based damage identification methods. Shock and Vibration Digest, 1998.

Epaarachchi, J. A., 'A study on estimation of damage accumulation of glass fibre reinforced plastic (GFRP) composites under a block loading situation', Composite Structures, Vol. 75, pp. 88–92, 2006.

Farrar, C.R., and Lieven, N.A., "Damage prognosis: the future structural health monitoring," Philosophical Transactions of Royal Society A., Vol. 365, No. 1851, pp. 623-632, 2007.

Farrar, C.R., Sohn, H., Hemez, F.M., Anderson, M.C., Bement, M.T., Corwell, P.J., Doebling, S.W., Schultze, J.F., Lieven, N., Robertson, A.N., "Damage prognosis: current status and future needs," Report LA-14051-MS, Los Alamos National Laboratory, Los Alamos, NM, USA, 2003.

Filis, P.A., Farrow, I.R., and Bond, I.P., 'Classical fatigue analysis and load cycle mix-event damage accumulation in fiber reinforced laminates', International Journal of Fatigue, Vol. 26, Issue 6, pp. 565–573, Jun. 2004.

Fortescue. P., Stark, J., Swinerd, G., "Spacecraft systems engineering", Proceedings of the 4th Responsive Space Conference, April 2006.

Frieden, J., Cugnoni, J., Botsis, J., Gmür, T., "Low energy impact damage monitoring of composites using dynamic strain signals from FBG sensors – Part I: Impact detection and localization", Composite Structures, Vol. 94, No. 2, pp. 438–445, 2012.

Giurgiutiu, V., 2005, "Tuned Lamb wave excitation and detection with piezoelectric wafer active sensors for structural health monitoring," Journal of Intelligent Material Systems and Structures, 16: 291-305.

Gobbato, M., Conte, J.P., Kosmatka, J.B., Oliver, J.A., Farrar, C.R. 'Damage Prognosis of Adhesively-Bonded Joints in Laminated Composite Structural Components of Unmanned Aerial Vehicles', COMPDYN 2009 ECCOMAS Thematic Conference on Computational Methods in Structural Dynamics and Earthquake Engineering, Rhodes, Greece, 2009.

Gobbato, M., Conte, J.P., Kosmatka, 'Reliability-Based Framework for Damage Prognosis of Composite Unmanned Aerial Vehicles Structural Components', Proc. Inaugural International Conf. of the Engineering Mechanics Institute, Minneapolis, MN, 2008.

Gorman, M. R. and Ziola, S. M., "Plate waves produced by transverse matrix cracking," Ultrasonics, Vol. 29, 1991, pp. 245-251.

Harland, D., Lorenz, R., "Space Systems Failures: Disasters and Rescues of Satellites, Rockets and Space Probes", Praxis, UK, 2006.

Hiche, C., Coelho, C., Chattopadhyay, A., and Seaver, M., 2010, "Impact localization on complex structures using FBG strain amplitude information," Proceeding of SPIE, Smart Structures and Materials/NDE, March 8-12nd, San Diego, CA, USA.

Hiche, C., Ceolho, C., Chattopadhyay, A., "A strain amplitude-based algorithm for impact localization on composite laminates," Journal of Intelligent Material Systems and Structures, Vol. 22, No. 17, pp. 2061-2067, 2011.

Huang, M., Jiang, L., Liaw, P.K., Brooks, C.R., Seeley, R., and Klarstrom, D.L., "Using acoustic emission in fatigue and fracture material research", Journal of Materials-e, Vol. 50, No. 11, 1998.

Inman, D.J., Farrar, C.R., Vicente, L.J., Valder, S.J., "Damage prognosis: For aerospace, civil and mechanical systems," Wiley, Chichester, UK, 2005.

Juang, J.-N., "Applied system identification", Prentice-Hall, Upper Saddle River, NJ, 1994.

Kessler, S.S., Spearing, S.M., and Soutis, C., 2002, "Damage detection in composite materials using Lamb wave methods," Smart Materials and Structures, 11: 269–278.

Kim, S.B., Sohn, H., 2007, "Instantaneous reference-free crack detection based on polarization characteristics of piezoelectric materials," Smart Materials and Structures, 16: 2375–2387.

Klein, V., Morelli, E.A., "Aircraft system identification: theory and practice", Reston, VA : American Institute of Aeronautics and Astronautics, 2006.

Leipold, M., Eiden, M., Garder, C.E., Herbeck, L., Kassing, D., Niederstadt, T., Kruger, T., Pagel, G., Rezazad, M., Rozemeijer, H., Seboldt, W., Schoppinger, C., Sickinger, C., Unckenbold., W., "Solar sail technology development and demonstration", Acta Astronautica, Vol. 52. pp. 317-326, 2003.

Leipold, M., Runge, H., Sickinger, C., "Large sar membrane antennas with lightweight deployable booms", 28th ESA Antenna Workshop on Space Antenna Systems and Technologies, ESA/ESTEC, May 31 - June 03, 2005.

Liu, Y., Mohanty, S., Chattopadhyay, A., "A Gaussian process based prognostics framework for composite structures," Proceeding of SPIE, Smart Structures and Materials & Nondestructive Evaluation and Health Monitoring, March 8-12, San Diego, CA, USA, 2009.

Liu, Y., Mohanty, S., Chattopadhyay, A., "Condition Based Structural Health Monitoring and Prognosis of Composite Structures under Uniaxial and Biaxial Loading," Journal of Nondestructive Evaluation, Vol. 29, No. 3, pp. 181-188, 2010.

Liu, Y., Yekani Fard, M., Kim, S.B., Chattopadhyay, A., Doyle, D., "Structural health monitoring and damage detection in composite panels with multiple stiffeners," 52 AIAA/ASME/ASCE/AHS/ASC, Structures, Structural Dynamics, and Materials Conference (SDM), April 4-7, Denver, CO, USA, 2011.

Liu, Y., Yekani Fard, M., Kim, S.B., Chattopadhyay, A., Doyle, D., "Damage detection in composite structures using lamb wave analysis and time-frequency approach,"

Proceeding of SPIE, Smart Structures and Materials/NDE, March 6-10, San Diego, CA, USA, 2011.

Liu, Y., Kim, S. B., Chattopadhyay, A., Doyle, D., "Damage localization in complex composite panels using guided wave based structural health monitoring system," Proceedings of the ASME 2011 Conference on Smart Materials, Adaptive Structures and Intelligent Systems (SMASIS), September 18-21, Phoenix, AZ, USA, 2011.

Liu, Y., Kim, S.B., Chattopadhyay, A., Doyle, D., "Application of System Identification Techniques to Health Monitoring of On-Orbit Satellite Boom Structures," Journal of Spacecraft and Rockets, Vol.48, No.4, pp. 589-598, 2011.

Liu, Y., Yekani Fard, M., Chattopadhyay, A., Doyle, D., 2012, "Damage Assessment of CFRP Composites Using Time-Frequency Approach," Journal of Intelligent Material Systems and Structures, Vol. 23, No. 4, pp. 397 – 413, 2012.

Liu, Y., Yekani Fard, M., Rajadas, A., Yekani Fard, M., Chattopadhyay, A., "Autonomous sensing of composites with carbon nanotubes for structural health monitoring," Proceeding of SPIE, Smart Structures and Materials/NDE, March 11-15, San Diego, CA, USA, 2012.

MacKay, D. J. C., 'Introduction to gaussian processes,' in Neural Networks and Machine Learning. ser. NATO Advanced Study Institute, C. M. Bishop, Ed. Berlin, Germany: Springer-Verlag, vol. 168, pp. 133–165, 1998.

Mallat, S., Zhang, Z., "Matching pursuits with time-frequency dictionaries," IEEE Transactions on Signal Processing, Vol. 41, No. 12, pp. 3497-3415, 1993.

Matt, H., Bartoli, I., Lanza di Scalea, F., "Ultrasonic guided wave monitoring of composite wing skin-to-spar bonded joints in aerospace structures," Journal of the Acoustical Society of America, Vol. 118, No. 4, pp. 2240-2252, 2005.

Meo, M., Zumpano G., Pigott, M., and Marengo, G., 2005, "Impact indentification on a sandwich plate from wave propagation responses," Composite Structures, Vol. 71, pp. 302-306.

Meo, M., Zumpano, G., 2005, "Nonlinear elastic wave spectroscopy identification of impact damage on a sandwich plate," Composite Structures, Vol. 71, No. 3-4, pp. 469-474.

Mohanty, S.., Das, S., Chattopadhyay, A., and Peralta, P., 'Gaussian Process Time Series Model for Life Prognosis of Metallic Structure', Journal of Intelligent Material Systems and Structures, Vol. 20, No. 8, pp. 887-896, 2009.

Mohanty, S., Chattopadhyay, A., Wei, J., Pelralta, P., "Unsupervised time-series fatigue damage state estimation of Complex structure using ultrasound based narrowband and broadband active sensing", Structural Durability & Health Monitoring, Vol. 5, No. 3, pp. 227-250, 2009.

Mohanty, S., Chattopadhyay, A., Wei, J and Peralta, P., "Real time Damage State Estimation and Condition Based Residual Useful Life Estimation of a Metallic Specimen under Biaxial Loading," Structural Durability & Health Monitoring Journal, Vol. 5, No. 1, pp. 33-56, 2009.

Mohanty, S., Chattopadhyay, A., Wei, J and Peralta, P., "Unsupervised time-series damage state estimation of complex structure using ultrasound broadband based active sensing," Structural Durability & Health Monitoring Journal, Vol.130, No.1, pp.101-124, 2010.

Moll, J., Schulte, R.T., Hartmann, B., Fritzen, C-P, and O Nelles, 2010, "Multi-site damage localization in anisotropic plate-like structures using an active guided wave structural health monitoring system,'' Smart Materials and Structures, Vol. 19, pp. 04502-04517.

Montalvão, D., Maia, N.M.M., and Ribeiro, A.M.R., "A review of vibration-based structural health monitoring with special emphasis on composite materials," The Shock and Vibration Digest, Vol. 38, No. 4, pp. 295-324, 2006.

Mujica, L.E., Rodellar, J., Fernandez, A., Guemes, A., 2011, "Q-statistic and T2-statistic PCA-based measures for damage assessment in structures," Structural Health Monitoring, 10(5): 539-553.

Papoulis, A., Pillai, S.U., "Probability, random variables and stochastic processes (4 ed.)," New York, McGraw-Hill, 2002.

Park, J., Ha. S., Chang, F.K., "Monitoring impact events using a system-identification method", AIAA Journal, Vol. 47, No. 9, September, 2009.

Park, G., Sohn, H., Farrar, C., and Inman, D., "Overview of piezoelectric impedance-based health monitoring and path forward," Shock and Vibration Digest, Vol. 35, No.6, pp. 451-463, 2003.

Park, G., Farrar, C.R., Rutherford, A.C., Robertson, A.N., "Piezoelectric active sensor self-diagnostics using electrical admittance measurements," Journal of Vibration and Acoustics, Vol. 128, No. 4, pp. 469(8), 2006.

Philippidis ,T.P. and Passipoularidis, V.A., 'Residual strength after fatigue in composites: theory vs. experiment,' International Journal of Fatigue, Vol. 29, Issue 12, pp. 2104–2116, Dec. 2007.

Polimeno, U., Meo, M., "Detecting barely visible impact damage detection on aircraft composites structures", Composite Structures, Vol. 91, No. 4, pp. 398-402, December 2009.

Price, D.C., Scott, D.A., Edwards, G.C., Batten, A., Farmer, A.J., Hedley, M., Johnson, M.E., Lewis, C.J., Poulton, G.T., Prokopenko, M., Valencia, P., Wang, P., "An integrated health monitoring system for an ageless aerospace vehicle", Proceedings of the 4th International Workshop on Structural Health Monitoring, Stanford, CA, pp.310-318, September 2003.

Prosser, W.H., Allison, S.G., Woodard, S.E., Wincheski, R.A., Cooper, E.G., Price, D.C., Hedley, M., Prokopenko, M., Scott, D.A., Tessler, A., Spangler, J.L., "Structure health monitoring for future space vehicles", Proceedings of the 2nd Australasian workshop on structural health monitoring, Monash University, Melbourne, Australia, 16–17 December, 2004.

Qian, S., and Chen, D., Signal representation via adaptive normalized Gaussian functions, Signal Processing, Vol. 36, pp. 1-11, 1994.

Raghavan, A., Cesnik, C.E.S., 2007, "Review of guided-wave structural health monitoring," Shock and Vibration Digest, 39: 91-114.

Rao, S.S., 1996, "Engineering optimization-theory and practice," Wiley, New York.

Reilly, J., and Terrance, Y., "Autonomous operations for responsive spacecraft", Proceedings of the 4th Responsive Space Conference, April 2006.

Reynolds, W.D., Coelho, C., Kim, S.B., Chattopadhyay, A., Arnold, S.M., "Active damage localization in anisotropic materials using guided waves," 50th AIAA/ASME/ASCE/AHS/ASC, Structures, Structural Dynamics, and Materials Conference (SDM), May 4-7, Palm Springs, CA, USA.

Ruggiero, E.J., Park, G., Inman, D.J., "Multi-input multi-output vibration testing of an inflatable torus," Mechanical Systems and Signal Processing, Vol. 18, No.5, pp. 1187–1201, 2004.

Salamone, S., Bartoli, I., Rhymer, J., Lanza di Scalea, F., and Kim, H., 2011, "Validation of the piezoelectric rosette technique for locating impacts in complex aerospace panels," Proceeding of SPIE, Smart Structures and Materials/NDE, March 6-10, San Diego, CA, USA.

Scholkopf, B., Smola, A., Muller, K.R., 1999, "Kernel principal component analysis," In B. Scholkopf, C. J. C. Burges, & A. J. Smola (Eds.), Advances in kernel methods—Support vector learning 327–352, Cambridge, MA: MIT Press.

Seaver, M., Aktas, E., Trickey, S.T., 2010, "Quantitative detection of low energy impact damage in a sandwich composite wing," Journal of Intelligent Material Systems and Structures, 21(3): 291-308.

Sodano, H.A., Inman, D.J., Park, G., "Comparison of piezoelectric energy harvesting devices for recharging batteries," Journal of Intelligent Material Systems and Structures, Vol. 16, No. 10, pp. 799-807, 2005.

Sohn, H., 2007, "Effects of environmental and operational variability on structural health monitoring," Philosophical Transactions of the Royal Society A, 365(1851):539-560.

Sohn, H., Farrar, C., Hunter, N., Worden, K., 2001a, "Structural health monitoring using statistical pattern recognition techniques," ASME Journal of Dynamic Systems, Measurement and Control: Special Issue on Identification of Mechanical Systems, 123(4):706–711.

Sohn, H., Park, H., Law, K.H., and Farrar C., 2005, "Instantaneous online monitoring of unmanned aerial vehicles without baseline signals," In Processing of 23rd International Modal Analysis Conference, Orlando, Florid.

Sohn, H., Farrar, C.R., Hunter, N.F., Worden, K., "Structural health monitoring using statistical pattern recognition techniques", Journal of Dynamic Systems, Measurement, and Control, Vol. 123, Issue 4, pp. 706-711, December, 2001.

Sohn, H., and Farrar, C.R., "Damage diagnosis using time series analysis of vibration signals," Smart Materials and Structures, Vol. 10, No. 3, pp. 446(10), 2001.

Soma Sekhar, B.V., Balasubramaniam, K., Krishnamurthy, C.V., "Structural health monitoring of fiber-reinforced composite plates for low-velocity impact damage using ultrasonic lamb wave tomography," Structural Health Monitoring, Vol. 5, No. 3, pp. 243-253, 2006.

Staszewski, W.J., Mahzan, S., Traynor, R., 2009, "Health monitoring of aerospace composite structures – active and passive approach," Composite Science and Technology, 69: 1678-1685.

Su, Z.Q., Ye, L., and Lu, Y., "Guided Lamb waves for identification of damage in composite structures: A review," Journal of Sound and Vibration, Vol. 295, No. 3, pp.753-780, 2006.

Takeda, N., Okabe, Y., Kuwahara, J., Kojima, S., Ogisu, T., "Development of smart composite structures with small-diameter fiber Bragg grating sensors for damage detection: Quantitative evaluation of delamination length in CFRP laminates using Lamb wave sensing," Composites Science and Technology, Vol. 65, No. 15–16, pp. 2575–2587, 2005.

Tang, H.Y., Winkelmann, C., Lestari, W., and La Saponara, V., 2011, "Composite structural health monitoring through use of embedded PZT sensors," Journal of Intelligent Material Systems and Structures, 22: 739-755.

Van Den Abeele1, K.E.-A., Johnson, P.A., Sutin, A., "Nonlinear elastic wave spectroscopy techniques to discern material damage, Part I: nonlinear wave modulation spectroscopy", Research in Nondestructive Evaluation, Vol. 12, No. 1, pp.17-30, September, 2000.

Van Den Abeele1, K.E.-A., Carmeliet1, J., Ten Cate, J.A., Johnson, P.A., "Nonlinear elastic wave spectroscopy techniques to discern material damage, Part II: single mode nonlinear resonance acoustic spectroscopy", Research in Nondestructive Evaluation, Vol. 12, No. 1, pp.31-42, September, 2000.

Vizzini, A.J., Liu, Y., Chattopadhyay, A., "Damage localization in a stiffened composite panel using lamb wave based tomography approach," Proceedings of the ASME 2011 Conference on Smart Materials, Adaptive Structures and Intelligent Systems (SMASIS), September 18-21, Phoenix, AZ, USA, 2011.

Wang, L., and Yuan, F.G., 2006, "Active damage localization technique based on energy propagation of Lamb waves," Smart Structures and Systems, Vol. 3, No. 2, pp. 201-217.

Wilkie, W.K., Bryant, R.G., High, J.W., Fox, R.L., Hellbaum, R.F., Jalink, A., Little, B.D., and Mirick, P.H., "Low-cost piezocomposite actuator for structural control applications," Proceedings of 7th SPIE International Symposium on Smart Structures and Materials, Newport Beach, CA, March 5-9, 2000.

Yang, M., Makis, V. "ARX model-based gearbox fault detection and localization under varying load conditions", Journal of Sound and Vibration, , Vol. 329, Issue 24, pp. 5209-5221, 2010.

Yashiro, S. Takeda, N., Okabe, T., Sekine, H., "A new approach to predicting multiple damage states in composite laminates with embedded FBG sensors," Composites Science and Technology, Vol.65, No. 3–4, pp. 659–667, 2005.

Yekani Fard, M., Liu, Y., and Chattopadhyay, A., "Characterization of epoxy resin including strain rate effects using digital image correlation system," Journal of Aerospace Engineering, 2011, In press (doi org/10.1061/(ASCE)AS.1943-5525.0000127).

Yekani Fard, M., Liu, Y., and Chattopadhyay, A., "A simplified approach for flexural behavior of epoxy resin materials," Journal of Strain Analysis for Engineering Design, Vol. 47, No.1, pp. 18 – 31, 2011.

Yekani Fard, M., Liu, Y., and Chattopadhyay, A., 2012, "Analytical solution for flexural response of epoxy resin materials," Journal of Aerospace Engineering, In Press (doi: 10.1061 / (ASCE) AS. 1943-5525.0000133).

Yekani Fard, M., "Nonlinear inelastic mechanical behavior of epoxy resin polymeric materials", PhD Thesis, Arizona State University, 2011.

Yoshida, H., Kumar, S., "ARX and AFMM model-based on-line real-time data base diagnosis of sudden fault in AHU of VAV system", Energy Conversion and Management, Vol. 40, Issue 11, pp. 1191-1206, 1999.

Zagrai, A., Doyle, D., Gigineishvili, V., Brown, J., Gardenier, H., Arritt, B., "Piezoelectric wafer active sensor structural health monitoring of space structures", Journal of Intelligent Material Systems and Structures , Vol. 21, No. 9,pp. 921-940, 2010.

Zhao, X., Gao, H., Zhang, G., Ayhan, B., Yan, F., Kwan, C.,Rose, J., 2007, "Active health monitoring of an aircraft wing with embedded piezoelectric sensor/actuator

network: I. Defect detection, localization and growth monitoring," Smart Materials and Structures, 16: 1208–1217.